MEASUREMENTS IN A TURBULENT

COUNTERFLOW FLAME

By

ADEL MOHAMED MAHMOUD HUSSIEN

A thesis submitted for
The Degree of Doctor of Philosophy
of the University of London
and
The Diploma of Imperial College

August 1989

Department of Mechanical Engineering
Imperial College of Science,Technology
and Medicine

London SW7 2BX

To

My Family

Abstract

The thesis describes the interaction between two opposed turbulent natural gas and air premixed flames. These flames have been generated by using two vertical orientated and axially aligned opposing burners. The aim of the research is to study the interaction between two opposed premixed jets, by measurements of the mean species concentration, temperature, and ion-current. The results include axial and radial profiles for the temperature and ionization measurements. Primary investigations have been done in a single flame by measurement of the axial temperature distribution and by the aid of photographs, in order to delineate the operating conditions.

The final data were obtained with the use of a quartz microprobe, fine wire thermocouple, and an ionization probe for species concentration, temperature, and ion-current measurements respectively. The laser sheet technique was used for flow visualization. The effect of Reynolds number, equivalence ratio, and burners separation on the flame core, flame thickness and flame length were also obtained.

Extinction has been studied for different conditions, fuel and air were introduced from both burners, fuel and nitrogen were introduced from both and fuel and nitrogen were introduced from the lower burner

while air was introduced from the upper one. This study concerned the effect of burner separation distance, equivalence ratio, and fuel-nitrogen ratio on the burner exit velocity required to achieve extinction.

Particular attention has been paid to the supply system in order to ensure that the same flow rate and fuel/air mixture are supplied to each burner. Co-flowing air was used in order to reduce buoyancy effects. Hydrogen was used as a stabilising gas and the upper burner was cooled by a water jacket to ensure no preheating for the upper flow.

Acknowledgement

It gives me great pleasure to express my gratitude to all persons who have helped me during my research activities at Imperial College during the period of June 1986 toAugust 1989.

First and foremost, I wish to acknowledge with gratitude, the help, guidance, advice and constructive criticism provided by my supervisor Dr. F.C.Lockwood which greatly aided the progress and completion of this work. I have derived considerable benefit from working under his supervision and I consider myself lucky to have been his student.

I have benefitted greatly from the assistance of, valuable advice, and discussions with, Dr. M.Ismail, Dr.A.Ahmed and Dr.M.Hassan. I greatfully acknowledge their contributions to this work.

I am deeply indebted to the assistance of Mr.I.Drummond and Dr.S.Godoy. They have been available to advice and assist me throughout experimental programme.

My thanks go to Dr.P.Costen, Mr.J.Miller, Mr.M.Yehia for their valuable discussions.

I would like to thank Mr.B.Crew and his technical staff for their technical support. I would like also to thank Miss C.Barron for the secretarial assistance she has provided to me. Many thanks also to Mech. Eng. librarians staff who willingly assisted me.

I am greatful to the Science and Engineering Research Council (grant GR/D/39450) for financial support of this work.

I would like to express my profound thanks to my parents for their interest in and encouragement of my education throughout my life.

I would like to express my gratitude to my wife, Nahed, for being patient and tolerant throughout the course of my studies.

Contents

List of Tables

List of Panels

List of Figures

Nomenclature

a	area
a_b	bulk strain rate
a_t	turbulent strain rate
a_T	total strain rate
A	constant, element surface area, air
C_w	specific heat of the wire
d	wire diameter
d_b	thermocouple bead diameter
D	nozzle diameter
F	fuel
h	convective heat transfer coefficient
H	burner separation distance
I	ion current
k	wire thermal conductivity
l	length of the wire
L	distance between the sensors, integral length scale
L	separation distance (stagnation point flow)
Le	Lewis number
L_i	height of the inner core
L_b	length of the burning part of a flame
L_g	length of the faint luminous zone of a flame
m	mass flow rate
m_a	mass flow rate of air
m_g	mass flow rate of gas
m_{H2}	mass flow rate of hydrogen
M	molecular weight
p	pressure

p_{at} atmospheric pressure

Re Reynolds number

t time

T_{ad} adiabatic flame temperature

T_f flame temperature

T_g true gas temperature

T_s surrounding temperature

T_t indicated thermocouple temperature

u local flow velocity

u' turbulent velocity fluctuation

v element volume

v_{fm} local flame front speed

V jet exit velocity

V_p potential voltage

V volume flow rate

V_a volume flow rate of air

$V_{a,at}$ volume flow rate of air at atmospheric conditions

V_g volume flow rate of gas

$V_{g,at}$ volume flow rate of gas at atmospheric conditions

V_T total volume flow rate

Greek Sympols

ΔY^* distance between the flame and the stagnation surface

Ω fuel concentration in the mixture

Ω^* fuel concentration at extinction

Ω_L fuel concentration of the lower burner

Ω_u fuel concentration of the upper burner

δ_T length of the bright luminous zone of a flame

ε emissivity of the wire

ρ local mean density

ρ' fluctuating density

ρ_a air density

$\rho_{a,at}$ air density at atmospheric conditions

ρ_g gas density

$\rho_{g,at}$ gas density at atmospheric conditions

ρ_m mixture density

ρ_u unburned mixture mean density

ρ_w density of the wire

σ Stefan-Boltzman constant = 4.93×10^{-8} kcal/hr m^2 $^oK^4$

υ kinematic viscosity

τ time

ω angular velocity

μ viscosity

μ_m mixture viscosity

Φ equivalence ratio

Subscripts

a air

g	gas
m	mass
r	radius
st	stoichiometric
v	volume

CHAPTER 1

INTRODUCTION

1.1 Preliminary Remarks

In practice virtually all engineering combusting flows (flames) are turbulent. Generally, flames are divided into two classes: those where fuel and oxidant are mixed before being injected into the combustion chamber so producing 'premixed' flames, and those where fuel and oxidant enter the combustion zone in separate streams to produce 'diffusion' flames. In the latter case, it can very often be assumed to a close approximation that the rate of combustion depends solely on the rate at which the two streams mix together, the mixing process occurs via a diffusional phenomenon. Although in practice most flames are confined, (furnaces and boilers), experimentalists use unconfined flames in their studies for ease of probing.

The analysis of turbulent combusting flows presents a very complicated and challenging task for engineers and scientists. It is an integrated phenomenon involving the subject areas of: fluid mechanics, chemical kinetics, turbulence, chemistry-turbulence interaction, thermodynamics, and heat transfer. It is clear that the physical understanding and quantitative analysis of turbulent flames can only be

advanced by a comprehensive and combined effort by experimentalists and theoreticians.

Combustion problems of practical interest occur primarily in turbulent flow fields and involve complex flame-flow interactions, Williams (1984). Because of the resulting complexities of turbulent combustion, many experimental and analytical studies have preferred to consider laminar premixed or diffusion flames. However, it is important to stress that there exist circumstances where the behaviour of turbulent flames may be predicted by modelling them as collections of stretched 'laminar flamelets'. The success of such models will then depend on how accurately the flow conditions experienced by the individual flamelets within the turbulent field can be simulated.

Under the influence of turbulent fluctuations, the flamelets undergo distortion and stretching. The concept of flame stretch was introduced by Karlovitz (1953) as a measure of the rate of change of the flame surface area. A more general definition of the flame stretch, as a function of flame speed and temperature, was later introduced by Matalon (1983). There have been many theoretical and experimental studies on the flame stretching phenomenon. Some of these employ the case of stagnation point flow, Fig. (1.1), or counterflow streams, Fig. (1.2). For example, Tsuji and Yamaoka (1982), Lewis et al (1984), Sohrab and Law

(1984), Puri and Seshadri (1986), Rogg (1988), Kostiuk et al (1988) and Egolfopoulos et al (1989). The choice of stagnation point flow or opposed jet flows for these studies was motivated by the relative simplicity of analytical analysis and ease of experimental control of the rate of stretch.

In addition to flame stretch, the interactions between flamelets also have significant effect on turbulent flame behaviour. The interactive combustion of multiple flames was recently considered by Sohrab et al (1984,1986). It was found that thermal and concentration interaction between flamelets alter their behavior profoundly. For example, in close proximity to a sufficiently strong flame, all compositions of a mixture will support combustion. Also, when the stretch rates exceed the critical values corresponding to extinction, flamelets can seek shelter and burn within the products of combustion of adjacent flamelets. Moreover, in addition to the purely premixed and diffusion flames, intermediary partially premixed reaction zones may occur depending on the composition of the interacting flamelets.

1.2. Previous Work

This section reviews the relevant literature and is included to provide the background necessary for introducing the aims and purposes of the present contribution. In sub-section (1.2.1), the previous

work on free jet premixed flames is considered, followed by that in stagnation point flow in sub-section (1.2.2). The section ends by considering the previous work on counterflow flames.

1.2.1 Investigation in a single flame

Ievlev (1957) studied the individual stages of the combustion process of a turbulent premixed flame. The burner diameter was 30 mm and the feed velocity varried between 10 and 30 m/sec. Visual examination of a burning free jet showed separate zones or regions which together make up the total length of the jet, Fig. (1.3). These zones are: (1) that extending from the burner exit to the point where the axial stream ignited (L_i), i.e., the nucleus along which the flame spreaded from the periphery to the centre and covered the entire cross section of the jet; (2) the zone of bright luminescence (δ_T) between the surface of the nucleus and the outer cone which determines the turbulent front of the flame; and (3) the zone of faint luminescence (L_g) in which combustion is completed. The overall length of the burning jet, L, is

$$L = L_i + L_b$$

where: $$L_b = \delta_T + L_g$$

He also reported that the quantity (L_i) was largely connected with the aerodynamic organization of the process and with the tube dimensions. Consequently, the simplest way to change the overall flame length was to change (L_i). From the field of the (K) value (ratio between CO_2 concentration and CO_2 maximum), which described the process of combustion of the initial gas mixture, he could determine the specific features of each individual zone and of the overall combustion process.

Suzuki et al (1979) estimated the most probable direction and velocity (v_{fm}) of local flame front movements in a turbulent premixed flame. The flame front velocity was measured by analyzing the ion-currents collected simultaneously by two identical sensors of an electrostatic probe. By comparing a pair of ion-current records, the time (τ) from when an ion-current peak was detected by one sensor to the time when almost the same peak was detected by the other sensor, and knowing the distance between the two sensors (L), the flame front velocity could very simply be determined from:

$$v_{fm} = L / \tau$$

They found that near the reactants side of the turbulent flame zone, the velocity (v_{fm}) was smaller than the mean velocity of the unburned mixture at the burner port and the flame front most probably moved downstream in the direction gradually approaching the burner exit. Their results also showed that across the turbulent flame zone from the unburned mixture side to the burned gas side, v_{fm} increased gradually and the most probable direction of v_{fm} turned away from the burner exit.

Kilham and Kirmani (1979) measured the turbulence intensity, mean velocity and integral length scale of a turbulent premixed flame using a cylindrical burner with fully developed pipe flow at the jet exit (L>30D), where L is the pipe length. They found that in the case of an air jet, a constant value of mean axial velocity appeared which confirmed the existence of a potential core. The turbulence intensity showed a gradual rise up to an axial distance of 3 times the burner diameter, followed by a steeper increase where the interaction between the expanding jet and the surrounding air occurs.

In the case of a premixed methane-air flame results showed that the relative turbulence intensity appeared to fluctuate somewhat randomly between 4 and 5%. Values of the length scale on the jet centre line were calculated from the autocorrelation function of the hot-wire

anemometer measurements. Results of these measurements indicated that the integral length scale increased almost linearly with the axial distance and its value was independent of the flow velocity.

Yoshida and Gunther (1981) studied the structure of the flame zone in a turbulent premixed flame by measuring the temperature and the mean ion-current. Lean mixtures of natural gas and air were used and all flames were stabilized by a small annular hydrogen pilot. The ion-current was found to be proportional to the mean turbulent reaction rate. They also found that on the unburned side of the flame zone, the mean ion-current increased in parallel with the mean temperature but reached a maximum before the mean temperature attained the plateau temperature, and subsequently decreased in the burned gas region. In the burned gas region where the mean temperature retained its high value, some ionization was observed, which could be attributed to an equilibrium state of the reaction kinetics of recombination. Their results showed also that the maximum value of the ion-current decreased with distance from the burner exit because in the downstream region of the flame zone, the thickness of the flame zone increases and that the reaction density decreases.

Boukhalfa and Gokalp (1988) investigated the density field of an open turbulent premixed methane-air flame. The cold flow

turbulence structure was that of fully developed pipe flow at the jet exit. Flame height and average flame thickness were deduced from centre line and transverse profiles of the mean density. The total flame height was defined as the distance from the burner exit (z) where (ρ_u/ρ) is maximum, while the inner core height corresponding to the distance (z) where (ρ'/ρ_u) is maximum.

where : ρ_u = unburned mixture mean density

ρ = local mean density

ρ' = fluctuating density

Their results showed that the total flame height and the inner core height increased with the Reynolds number for a given equivalence ratio. Also the turbulent flame thickness was found to increase linearly with the distance from the burner exit.

Katsuki et al (1988) measured the mean and fluctuating components of velocity and temperature in premixed, pilot-stabilized flames. Their results showed that the spreading angles of the flames were larger than those of non-combusting cases because of the thermal expansion of the burned gases and the flame propagation. They also found that, although the velocity difference across the pilot flame contributed to the development of a noncombusting mixing layer, it did not always

promote flame spread in a combusting flow.

They concluded that, due to expansion of burned gases, flame propagation into the high velocity reactant stream was associated with the emergence of a local maximum in the streamwise velocity profile. Also for flames stabilized with a pilot flame, it was found that a pilot flame having a higher velocity than that of the mixture would allow either flame propagation into the mixture stream or wider flame spread. It was also concluded that the initial turbulence in the reactant flows strongly promoted the mixing of the pilot jet with the mixture and accelerated the flame spread rate.

1.2.2 Investigation of stagnation point flames

Stagnation point flow is achieved by impinging a jet onto a stagnation surface, Fig. (1.1). This flow is usually used to generate a flat, thin and stable flame, parallel to the stagnation surface. This flow configuration has been examined by many investigators, for example, Fang et al (1971), Law et al (1981), Law and Sivashinsky (1982), Pindera and Talbot (1988) and Daneshyar et al (1982). In their efforts to study the effect of nature of the surface (in particular its temperature), strain rate, mixture concentration, velocity and temperature on the extinction limits, flame location (distance between the luminous zone and the stagnation

surface), and maximum flame temperature. Extinction in the case of stagnation point flow occurs when the flame is at a finite distance from the stagnation surface.

Surface temperature

The extinction limits were found to be extremely sensitive to the nature of the surface temperature. Measurements of the extinction limits of lean propane-air flames in a stagnation point flow of a flat surface as a function of the surface temperature have been made by Law et al (1981). Results showed that the fuel concentration required to achieve extinction (Ω^*) decreased by increasing the surface temperature. In the rich propane-air flames, Ishizuka et al (1982) showed that (Ω^*) increased almost linearly with the surface temperature. They also showed that the heat loss downstream of the flame (due to the temperature difference between the flame and the stagnation surface) could be controlled by varying the flow rate of the cooling water through the plate and/or by varying the temperature of the inlet water. At extinction, the flame location and the maximum flame temperatures were not affected by the surface temperature.

Mixture temperature

Preheating the gas mixture increases the flame temperature by an almost equal amount and significantly extends the extinction limits, but at extinction the maximum flame temperature changes little with preheating, Law et al (1981). Dugger and Heimel (1952) reported that increasing the mixture temperature increases the mass burning rate. Thus, Law et al (1981) found that with preheating the mixture, the flame moved towards the burner, indicating an increase in the mass burning rate. They also found that, for lean propane-air flames, increasing the mixture temperature decreased the fuel concentration required to achieve extinction (Ω^*). In rich flames, Ishizuka et al (1982) found that the value of (Ω^*) increased almost linearly with the mixture temperature. It was found that the fuel concentration required to achieve extinction is more sensitive to an increase in the mixture temperature than an increase in the surface temperature. This ratio was almost 14 times (lean limit) and 5 times (rich limit) for an increase of 100 °C in both cases.

Fuel concentration

Measurements by Fang et al (1971) in a premixed carbon monoxide-air flame in a stagnation point flow showed that extinction could be achieved in the range of carbon monoxide concentrations

between 15.6% and 20.7% in the mixture. At lower concentrations the flame could not be lifted from the burner without being extinguished, and at higher concentrations such high flow velocities were required that turbulent conditions prevailed along the stagnation surface before extinction could be achieved. Law et al (1981) studied the effect of mixture concentration on the extinction limits of lean propane and air mixtures in a stagnation point flow. They found that by decreasing the fuel concentration, the flame moved closer to the surface whereas the flame temperature decreases. Ishizuka et al (1982) concluded that, at extinction, the rich flames were located closer to the surface than the lean flames.

Velocity profile

Daneshyar et al (1982) measured the velocity profiles in a stagnation point premixed flame. Their results showed that the radial velocity profile in the plane of the flame were linear (du_r/dr= constant) with radial distance. The axial profiles of the radial component were approximately constant except for a slight increase across the reaction zone. The axial profiles of the axial component indicated a linear decrease towards the flame with a round off minimum due to the preheat zone, followed by a step increase across the flame, and a linear decrease towards zero on the stagnation surface.

The same authors also studied the effect of strain fields on the burning rate in a stagnation point premixed flame. The strain rate was obtained from the gradient of (du_r /dr) measured at the flame position. They found that straining reduced the burning velocity and caused flame extinction. They also concluded that if the strain rate is sufficiently large, a large part of the flame surface may be extinguished and the burning velocity of the remaining flame reduced.

Law et al (1981) and Ishizuka et al (1982) did not measure the velocity profiles in their study of stagnation point flow. They considered the velocity gradient as:

$$\text{velocity gradient} = V_o / 2H$$

where:

V_o = nozzle exit velocity

H = separation distance

They found that at extinction, the maximum flame temperatures and the flame locations were not affected by the velocity gradient.

1.2.3 Studies of counterflow flames

Counterflow flames are generally generated by impinging two opposed flames, Fig. (1.2). Investigations in counterflow flames in order to study their interaction have been performed by many investigators, for example, Sato (1982), Ishizuka et al (1982), Tsuji and Yamaoka (1982), Sohrab and Law (1984), Puri and Seshadri(1986), Chen et al (1987), Lin and Sohrab (1987), Kostiuk et al (1988) and Kobayashi et al (1989). The opposed jets in their studies were not always identical. The identical jets case has been studied by, for example, Lin et al (1986), Chen et al (1987) and Kostiuk et al (1988). Sohrab et al (1984) investigated the interaction between two counterflow premixed flames of different fuel concentrations. Puri et al (1987) performed their experiments with methane introduced from the bottom duct and air introduced from the top duct. Lin and Sohrab (1987) studied the extinction characteristics of counterflow diffusion flames under opposing rigid-body rotation.

Sohrab et al (1984) investigated the interaction between two counterflow premixed flames of different stoichiometries. Their results showed that the extinction limits can be significantly modified in the presence of interaction between the flames such that a mixture much beyond the flammability limit can still burn if it is supported by a stronger flame. Fig. (1.4), Sohrab et al (1984), shows the extinction limit for two

lean premixed methane-air flames. Measurements of the temperature profiles showed asymmetric profile due to the difference in the concentration condition for the two flames. A symmetric profile was found for the case when the same concentrations were used by the two burners. In the case of extinction, a flat temperature profile regions downstream of the two flames was found, due to the lack of interaction between the two flames.

Liu et al (1986) measured the axial and radial temperature profiles of two symmetic counterflow premixed laminar flames. Their experiments involved twin-flames of methane-air stabilized in the stagnation flow between two impinging cylindrical jets of uniform velocity and identical composition. Exhaust suction on the lower burner has been used and it was adjusted so that the flames are symmetrically located between the burners. This corresponded to the condition where the influence of buoyancy of the hot products was just balanced by the exhaust suction. In fact, this suction led to a downstream bend around peripheries which affected their radial measurements.

They found that the minimum temperature occurred at the stagnation plane, and that the influence of radiant loss on the flame appeared to be indirect. This was because the reaction zone was too thin to radiate appreciably. It was also found that, for widely separated premixed

flames, > 4 mm, the radiant heat loss could strickly not be neglected. For the case of lean flames near extinction, the merging of the reaction zones resulted in an adiabatic condition and the neglect of radiation was fully justified. Their results were also interesting in view of the fact that the emitting gases downstream of the rich flames contained products of excess fuel in addition to CO_2 and H_2O.

Puri et al (1987) studied the structure of a diffusion flame stabilized between counterflowing streams of methane and air. Experiments were performed to measure the temperature and species concentration profiles. The counterflow was generated by two opposed ducts, with methane being introduced from the bottom duct and air introduced from the top one. The results showed that the maximum value of the temperature occurred on the oxidizer side of the stagnation plane, T_{max}=1950 ^{o}K. The structure of the reaction zone was not affected substantially by the differences in the flame's location. The peak of the temperature profiles showed a gradual decrease with increasing strain rate (increasing the oxidizer jet velocity) until extinction. Extinction occurred at a strain rate of 213 sec^{-1}. The temperature then decreased rapidly with a small further increase in the strain rate.

Tsuji and Yamaoka (1982) studied the structure and extinction of premixed stagnation flow by using counterflow twin flames established in the forward stagnation region of a porous cylinder. Profiles of temperature and concentration of some stable species were determined along the stagnation stream line across the twin flames near the extinction limits. For low stagnation velocity gradients (low burner exit velocity), the two luminous flame zones were separated and the concentration of carbon monoxide and hydrogen were very low near the stagnation surface. Thus the intermediate reactants were almost completely consumed in the flame zone. As the stagnation velocity gradient increased, the two luminous flame zones became closer to each other and the concentrations of carbon monoxide and hydrogen increased markedly, and the reactions were not completed in the flame zone.

Their results also showed the dependence of the maximum flame temperature and the distance between the two luminous flame zones (from the centre of one luminous flame zone to the centre of the other one), ΔY^*, on the equivalence ratio of the mixture and the stagnation velocity gradient. At extinction of the lean flame, the two luminous flame zones were close to each other and the maximum flame temperature increased slightly at first as the stagnation velocity gradient was increased and then decreased as the flame approached the extinction limit. In the case of a rich flame, the two flame zones were considerably separated and

the maximum flame temperature was almost constant, independent on the stagnation velocity gradient except near the extinction limit.

Chen et al (1987) investigated the extinction characteristics of double premixed flames in the counterflow streams of two opposing cylindrical jets. They measured the axial, radial and circumferential velocity profiles for jets of equal angular velocities rotating in opposite directions. An exhaust system for the removal of the combustion products was incorporated in the lower burner to prevent the heating of the upper burner. However a downward bend of the flame peripheries was induced by it. They reported that, when the volumetric concentration of the fuel in both burners were kept identical, no thermal or concentration interactions between the flames occurred. They also reported that extinction of the double flames could be achieved by various mechanisms, for example, by: a reduction of the fuel concentration, a dilution of the mixture by inerts, or by high stretch rates (produced by increasing the jet velocity or the angular velocity or decreasing the separation distance between the burners).

Their results showed that, for lean methane-air flames, the volumetric fuel concentration at extinction for a given mixture velocity first decreased with increasing angular velocity (ω) up to a critical value, and subsequently increased with increasing (ω). The authors also

concluded that the expression for the stretch rate for counterflow systems, namely (V_o/H) where (V_o) is the jet exit velocity and (H) is the separation distance, cannot be used in the presence of rotation.

Lin and Sohrab (1987) followed the work of Chen et al (1987). They used the same burner arrangement to demonstrate the characteristics of diffusion flames in counterflow formed by two jets streams with angular velocities which were equal in magnitude but opposite in directions. They found that a recirculation zone first began to develop at the jet centreline near the stagnation plane, and as the angular velocity (ω) increased the recirculation zone grew in size both axially and radially. Their results showed that, for the case when air was introduced (lower jet) in opposition to fuel-nitrogen mixture (upper jet), the diffusion flame was located on the air side of the stagnation plane due to the difference in the mean densities of the jets.

Their results also showed that , for any flow velocity, the critical minimum fuel concentration at extinction depended on the angular velocity. They also found that the stagnation plane was no longer a well defined planar surface because the mixing of oxidizer and fuel occurred in a thick zone. The flow rotation in the case of the counterflow diffusion flame resulted in the formation of a soot layer on the fuel side and the thickness of the soot layer increased with the jet angular velocity.

Sato (1982) studied the combined effects of the velocity gradient and the Lewis number (Le) of the deficient reactant (oxygen in rich mixture and fuel in lean mixture) on the behavior and extinction of a laminar premixed flame in a stagnation flow. The stagnation velocity gradient was not measured experimentally and the flow velocity at the nozzle exit was used as a measure of the stagnation velocity gradient. Their results showed that, as the stagnation velocity gradient was increased, the twin flames approached each other and finally extinction occurred. The stagnation surface was situated at the centre of the twin flames and could be considered as an adiabatic surface. He reported that, in this kind of flow in both the isothermal and reacting cases, the strain rate is constant along the radial direction.

He found that, for the case of Le<1 (lean propane or butane-air and rich methane-air), as the velocity gradient was increased, the flame temperature decreased, and the flame was extinguished at some distance from the stagnation surface. For Le>1 (lean methane-air and rich propane or butane-air), the flame temperature increased with increasing velocity gradient and reached a maximum value followed by a decrease. The Lewis number is defined here as the ratio of the mass diffusivity to the thermal diffusivity.

Ishizuka and Law (1982) investigated the effect of downstream heat loss on the extinction of a stretched premixed flame. Two kinds of burner arrangements were used, one was symmetrical opposed burners (counterflow), for which conductive heat loss downstream of the flame could be considered to be negligible because of symmetry. The other was a single burner system with a water-cooled stagnation surface above it (stagnation flow) for which a small amount of downstream heat loss existed. Their results showed that downstream heat loss had almost no influence on the extinction limits. They also found that, for a given surface separation distance, the stagnation surface distance for the counterflow set up was only half of that for the stagnation flow arrangement. They concluded that extinction by stretch alone was possible only when the deficient reactant was the less mobile one.

Law et al (1986) investigated the propagation and extinction of stretched premixed flames by using the symmetrical counterflow flame configuration. Velocity profiles and flame speeds were mapped for the extinction conditions. They found that the flame speeds at extinction were finite and generally higher than the corresponding laminar flame speed. Results also showed that the laminar flame speed basically varried linearly with the stretch rate for rich methane-air mixtures, while this relation existed only for the lower values of the stretch rate for lean mixtures. By approaching the state Ω^*(fuel concentration at extinction) the flames were

steady and planar because at this state the flames were by definition nearly adiabatic, stretchless and completely reacted.

Puri and Seshadri (1986) investigated the extinction limits and temperature profiles of counterflow diffusion flames. The flames were stabilized between counterflowing streams of a fuel diluted with nitrogen (lower burner) and of air diluted with nitrogen (upper burner). The burners consisted of two ducts of 25.4 mm inner diameter through which gaseous reactants were introduced, while the distance between the ducts was maintained constant and was equal to 14.88 mm. Exhaust suction was used to pull the combustion product gases into a heat exchanger surrounding the lower duct. Measurements were made of the critical fuel molar concentration and the critical oxidizer molar concentration at extinction as a function of the stagnation velocity gradient (strain rate at extinction).

$$\text{Strain rate at extinction} = (-V_{o2}/H)\ (1+(V_{o1}/-V_{o2})(\rho_1/\rho_2)^{0.5})$$

where :

V_o = duct exit velocity

H = separation distance

ρ = flow density

1,2 represent the lower and upper ducts respectively

The results showed that the diffusion flame could not be stabilized at a molar concentration of methane below 0.151 and a molar concentration of propane below 0.08. The limiting molar concentration of oxygen for extinction of a diffusion flame with methane as the fuel was 0.15 and with propane as the fuel was 0.137. The results also showed that the overall reactivity for propane is larger than that for methane.

Rogg (1988) investigated numerically the effect of strain rate on the structure of counterflow premixed laminar flames. He concluded that, in the case of twin flames, where two identical reactant streams are directed toward each other, such a configuration can be developed in a flow with turbulent scales and intensities large enough to cause the two parcels of reactants to approach one another. In this case, extinction strain rates decrease with decreasing mixture strength.

Sohrab and Law (1984) analyzed the extinction of laminar counterflow premixed flames in the presence of volumetric radiative heat loss. They concluded that, in double symmetric situations, the radiation effect was more significant since it was the only possible mode of downstream heat loss. The influences of downstream versus upstream radiative losses on the extinction conditions were found to be different; the extinction condition was sensitive to downstream loss. Their results also showed that radiative heat loss was relatively unimportant in affecting

flame extinction as compared with flame stretch except for massively radiating flames.

Kostiuk et al (1988) estimated the effect of the total strain rate applied on a flame on the turbulent extinction limit. The flame was produced by the use of counterflowing streams of two opposed premixed jets. They reported that extinction appeared to be related to the total strain rates (a_T) applied on the flames, which is composed of: (1) the bulk strain rate (a_b) caused by the mean flow, and (2) the turbulent strain rate (a_t) caused by the random velocity fluctuations.

$$a_T = a_b + a_t$$

where: $$a_b = 2V_o/H$$

$$a_t = ((A\, u'^3)/(\upsilon\, L))^{0.5}$$

Their results showed that, as expected, extinction occurred at high flow velocities and small nozzle separations. They concluded that the velocity at extinction decreases as the nozzle separation decreases, due to bulk straining. An asympotic flow velocity was found at which extinction was essentially independent on nozzle separation and extinction being affected only by turbulent straining.

Kobayashi et al (1989) investigated the extinction limits and flame diameters at the limits for a stretched cylindrical premixed flame, radial-flow nozzle burner (RNB) and compared the results with those obtained for a counterflow premixed flame, produced by a counterflow nozzle burner (CNB). They used the characteristic velocity gradient as a measure of the flame stretch. The velocity gradient expressed as $(2V_o/H)$ for the case of counterflow flame and as $(2V_o/D_r)$ for the case of cylindrical flame.

They found that no significant effects of the nozzle outlet diameter and the burner setting direction on the extinction diameter (the smallest diameter of the luminous flame zone). They also found that the formation of an axisymmetric flame was limited to the range of Φ near the flammability limits, in the case of porous cylinder burner. Comparing the extinction diameter, RNB, with the extinction distance, CNB, it was found that the former did not seem to become smaller than the latter. This was because the distance easily becomes zero with the increase in the flame strength. They also reported that the extinction diameter was larger than the extinction distance over the whole flammable range of the equivalence ratio.

Although many investigators have studied the stagnation flow (flame) in both stagnation point flow and opposed flow, there are

still many gaps in the investigations through downstream influence between opposed flames approaching each other. No measurements have been effected for mixtures near the flammability limits, because of buoyancy effects.

1.3 Objective and Present Contribution

The present research is fundamental in nature. It reflects the need to develop combustion models which possess acceptable validity for the range of turbulent reacting flows from physically controlled turbulent reactions through to extinction. The research has been carried out to provide and extend the experimental information on turbulent counterflow flames. The experiment adopts the counterflow of two combustible gaseous streams to produce the two primary premixed flames which can interact with each other through downstream influences. The selection of this counterflow configuration is based on the considerations that it can be easily built in the laboratory.

The counterflow is generated by two identical, vertically-oriented, and axially-aligned burners through which two identical mixtures of fuel and air are introduced. The experimental programme has been arranged to provide an extensive and detailed mapping of temperature, species concentration, and ion-current profiles.

A wide range of nozzle Reynolds number and equivalence ratio are considered along with the effect of the burners separation distance.

1.4 Outline of The Thesis

The remainder of the thesis is contained in four chapters. The next chapter provides a detailed description of the test-rig used in the experiments and the flow arrangements. It starts with a general description of the test-rig, followed by a description of the burners including their alignment and the systems used for supplying air, gas, and co-flowing air to them. The safety precautions and the flame stabilisation techniques are also described in this chapter.

Chapter (3) describes the techniques used for temperature, concentration, and ion-current measurements. The temperature measurements were carried out using fine wire thermocouples, quartz-microprobes and gas chromatography were used for species concentration, and a water-cooled ionization probe was employed for the ion-current measurements. A detailed description for the errors associated with each technique is also reported.

Chapter (4) concerns the measurements carried out in a single flame in order to characterize the flames to be studied in the case of

counterflow. Total flame length and inner core length were determined for different running conditions. Axial temperature profiles were obtained for a wide range of Reynolds number and equivalence ratio. All of the measurements were supported by photographs. This chapter also reports the principal study programme on the turbulent counterflow flames. The measurements include those of the radial and axial profiles of temperature, species concentration and ion-current.

Chapter (5) summarizes the main conclusions of the present work and provides suggestions for future work.

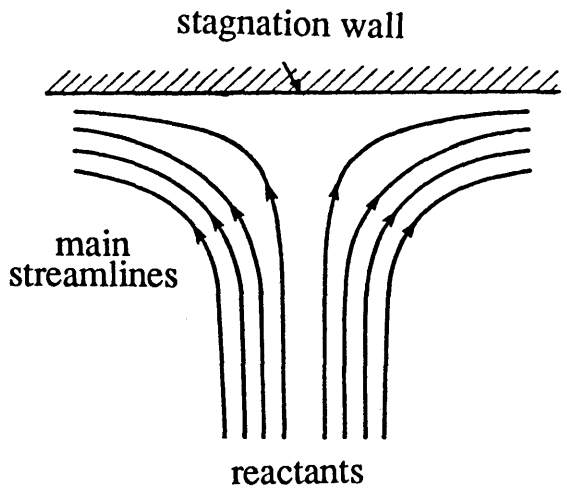

Fig. (1.1) Axisymmetric stagnation point flow.

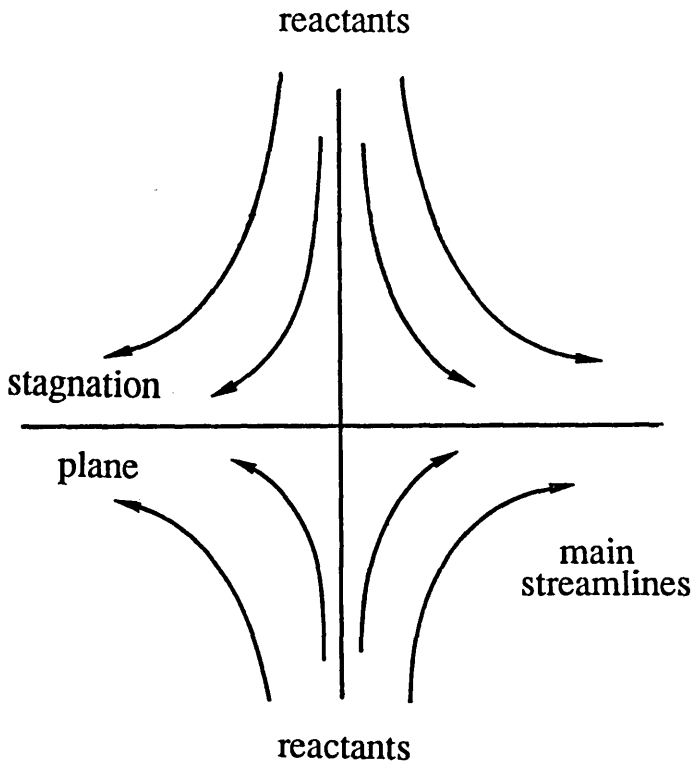

Fig. (1.2) Axisymmetric counterflow streams.

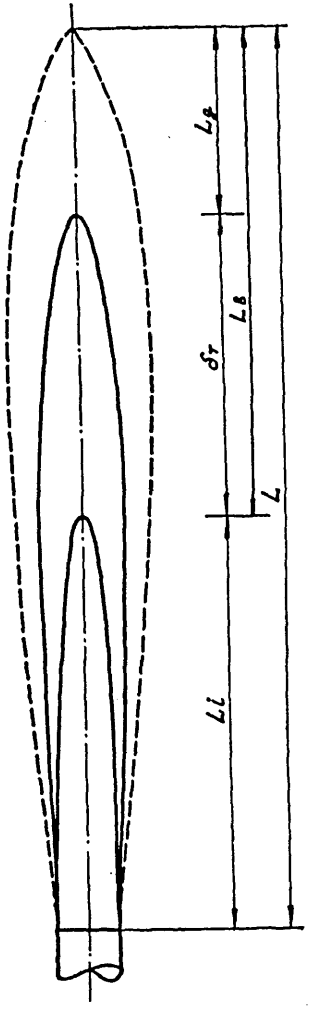

Fig. (1.3) Sketch of a free burning premixed jet.

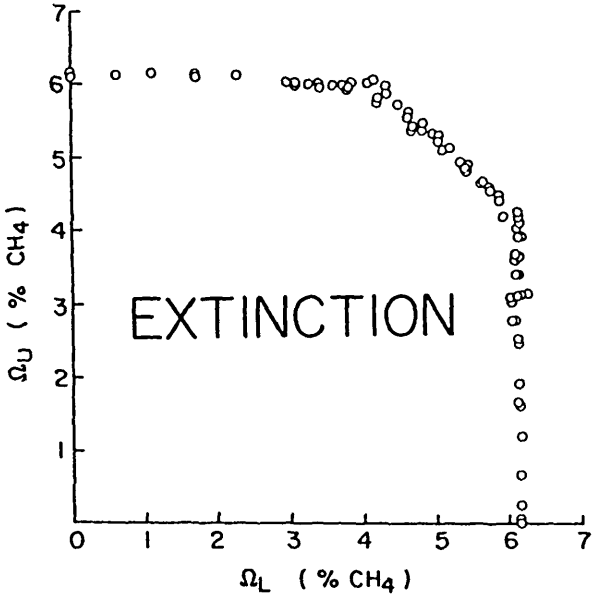

Fig.(1.4) The extinction poundary for two lean premixed methane-air flames, Sohrab et al (1984).

CHAPTER 2

TEST RIG AND FLOW ARRANGEMENT

2.1 The Test Rig

The test rig consisted of two opposed burners giving two opposed jets to produce the counterflow flame. These burners were vertically orientated and axially aligned. Partially premixed gas and air were introduced by the burners and hydrogen was used as a stabilizing gas. Co-flowing air was introduced around the two burners in order to minimise the buoyancy effects and to ensure symmetry of the counterflow flame. The upper burner was cooled with a water jacket in order to prevent any preheating for the mixture introduced by it. For safety reasons, flame traps were used to prevent flash back. The layout of the test rig and the flow arrangement are shown in Fig. (2.1). Photographs of the test rig and associated flowmeters appear in plate (2.1).

2.2 Burners Description

2.2.1 Burners and alignment

Two identical burners were used in the present experimental study. The mounting of the burners on the vertical

supporting mechanism is shown in Fig. (2.2). The burners were secured to a steel stand via two identical steel frames, separated by 0.6m. The steel frames were vertically aligned using a sensitive spirit level. The upper burner was vertically adjusted by means of horizontal steel frames. The lower burner was vertically aligned with the upper burner by using a three dimensional movement mechanism. The axes of the two burners were checked and aligned with the aid of four cylindrical plugs, Fig. (2.3a), having small holes drilled along their axes. These plugs were inserted in both ends of the burner tubes and alignment was achieved by passing a light through the four plugs. The centre of the measuring probes (quartz microprobe, thermocouple or ionization) was made coincident with the centre of the counterflow flame by using a tapped plug, Fig. (2.3b). This plug was located at the burner tip and the measuring probe was centred with the tip of the plug.

A design consideration influencing the burner pipe arrangement was the fact that prediction procedures require the initial profiles of mean velocity, species concentration and turbulence energy to be specified. Since fully developed turbulent pipe flows are well documented and profiles for this condition for all of the above quantities are available, it was decided to use a circular tube burner long enough to ensure fully developed exit conditions. The choice of the burner diameter was made after trials using tubes of various diameters. The final choice

was dictated by the need to:

(1) obtain a reasonable flame size for measurements,

(2) avoid the excess amount of heat produced by combustion.

The burner (used for the present experimental work) consisted of a thick walled (2 mm) stainless steel tube with 13.7 mm inner diamater. The exit end of the tube was machined to a thickness of 0.25 mm to minimize the effect of wall disturbance on the exit profiles, Fig. (2.4) shows the burner details. Schlichting (1968) reports that fully developed pipe flow is achieved in an axial length of about 40 diameters. It was agreed to use the present burner with140 cm (~ 100 D) in length to ensure fully developed flow at the burner exit.

2.2.2 Air supply system

Because of the high flow rate which was required for the experiment compressed air was used. An air filter and pressure regulator were incorporated in the air line before mixing with the fuel. The air flow rate was measured by a calibrated rotameter. A large vessel was incorporated in the air line in order to dampen the fluctuations

2.2.3 Gas supply system

In all the experiments carried out in the present work the fuel was natural gas. The gas properties and composition are cited in table (2.1). Because of the low pressure of the natural gas in the main, a compressor was necessary to achieve the required flow rate. The gas flow rate was measured by a calibrated rotameter.

2.2.4 Mixing system

The calibrated air and gas were mixed prior to their introduction into the burners in order to ensure identical composition in the two jets. The mixing procedure was achieved by introducing the air through a pipe of 25 mm inner diameter with the gas being injected into it at different locations, Fig. (2.5) shows the mixing pipe details. The distance between the fuel injection and the mixture exit was about 50 pipe diameters so that a good mixing between the air and gas was achieved. After mixing, the mixture was divided into two streams and a rotameter was incorporated in each stream to ensure that the same mixture flow rate was introduced to each burner. A pressure gauge and a needle valve were connected to each rotameter to ensure that the same mass flow rate is being supplied to each burner.

It was essential in the present experiment that the flow studied should be fully turbulent since flows of the industrial practice are so. The calculation of the Reynolds number (or the burner exit velocity) was based on the density and viscosity of the mixture at the burner exit. The effects of equivalence ratio on the density and viscosity of the mixture are presented and discussed in appendix I.

2.3 Flame Stabilisation

The flames were stabilised at the burner exits by annular pilot flames of hydrogen. The pilot tube was long enough to ensure a uniform inflow at the exit planes. Collets were arranged along the outer surface of the inner tube to provide a symmetrical pilot flame at the burner exit. The exit wall thicknesses of the stabilising gas tube were thin, 0.25 mm, to reduce the disturbances. Figure (2.4) shows the annular tube arrangements with the main burner tube. The hydrogen was supplied from a high pressure cylinder and its flow rate was measured by a calibrated rotameter. The maximum flow rate of hydrogen was always less than 0.5% of the minimum flow rate of the fuel used in the experiment. Therefore, the effects of hydrogen pilot on the species concentration measurements could be neglected.

2.4 Co-flowing Air

Visual observation of the counterflow flame and measurements with the thermocouple probe showed that the buoyancy affected the top part of the flame so that the temperature of air above the counterflow flame was always higher than that for the lower one. Therefore co-flowing air was introduced from two ducts of same dimensions located annularly about both burners. The diameter of these ducts was chosen to be suitable according to the radius of the counterflow flame. The co-flow air ducts were fabricated from stainless steel in a conical form having a contraction ratio of 8, see for example Law et al (1981), Masri and Bilger (1986) and Puri and Seshadri (1986). Figure (2.6) shows the duct dimensions. A number of fine wire screens were placed in the ducts near the end of the contractions to ensure flat velocity profiles at the exit of the ducts. The co-flowing air flow rate was measured by using standard orifice plates. The velocity of the co-flowing air was kept constant throughout the experimental programme, 1 m/sec. This velocity was chosen with the aid of thermocouple probe located above the counterflow flame such that the temperature of the air above the counterflow flame was always the same as that for the lower one.

2.5 Cooling System

Two cooling arrangements were used in the present experiment. The upper burner was cooled in order to eleminate preheating of the mixture, Fig. (2.7a). In addition, water cooled disks were located above and under the counterflow flame to prevent the convective heat to preheat the co-flowing air, Fig. (2.7b).

2.6 Safety Precautions

Because the present experiment deals with premixed gases (fuel+air), flash back can occur in the supplying pipes. Flash back occurs if the flow velocity at the burner exit is less than the burning velocity of the fuel used, Barnard and Bradley (1985). To eliminate the possibility of flash back flame traps can be used. Careful design of the flame trap was necessary so that the device would be safe for all the conditions which were likely to be encountered. The design of the flame trap depends on the quenching diameter and quenching distance of the fuel used. The quenching diameter, d_T, of a particular gas mixture is the minimum diameter of tube through which a flame can propagate. The quenching distance, d_Q, is a related quantity and refers to flame propagation between parallel plates. The two quantities are related by the expression, Potter (1960):

$$d_T = 1.54\ d_Q. \qquad (2.1)$$

Therefore the design of the flame trap depends on the quenching distance rather than the quenching diameter. The minimum quenching distance for natural gas is 2 mm, Rose and Cooper (1977). Figure (2.8a) shows the design of the flame trap used in the present study. It consisted of 4 mm balls contained in a steel pipe of 12.5mm in diameter restrained by wire meshs. The balls' size was chosen so that the distance between adjacent balls was less than the quenching distance, Fig. (2.8b). A flame trap was located at the upstream end of each burner.

Table (2.1) Physical Properties and Chemical Composition of Natural Gas

(a) Physical Properties

Properties		
Density	0.7283	Kg/m3
Moleculer weight	17.18	Kg/Kmol
Specific heat	36.34	Kj/Kmol.K
Calorific value	35.05	Mj/m3
Viscosity	1.087	gm/cm sec

(b) Volumetric composition

Gas	% Volume
Methane	93.63
Ethane	3.25
Nitrogen	1.78
Propane	0.69
Butane	0.27
Carbon dioxide	0.13
Pentanes	0.09
Helium	0.05
Hexanes	0.03
Benzene	0.02
Toluene	0.01
Octanes	0.01

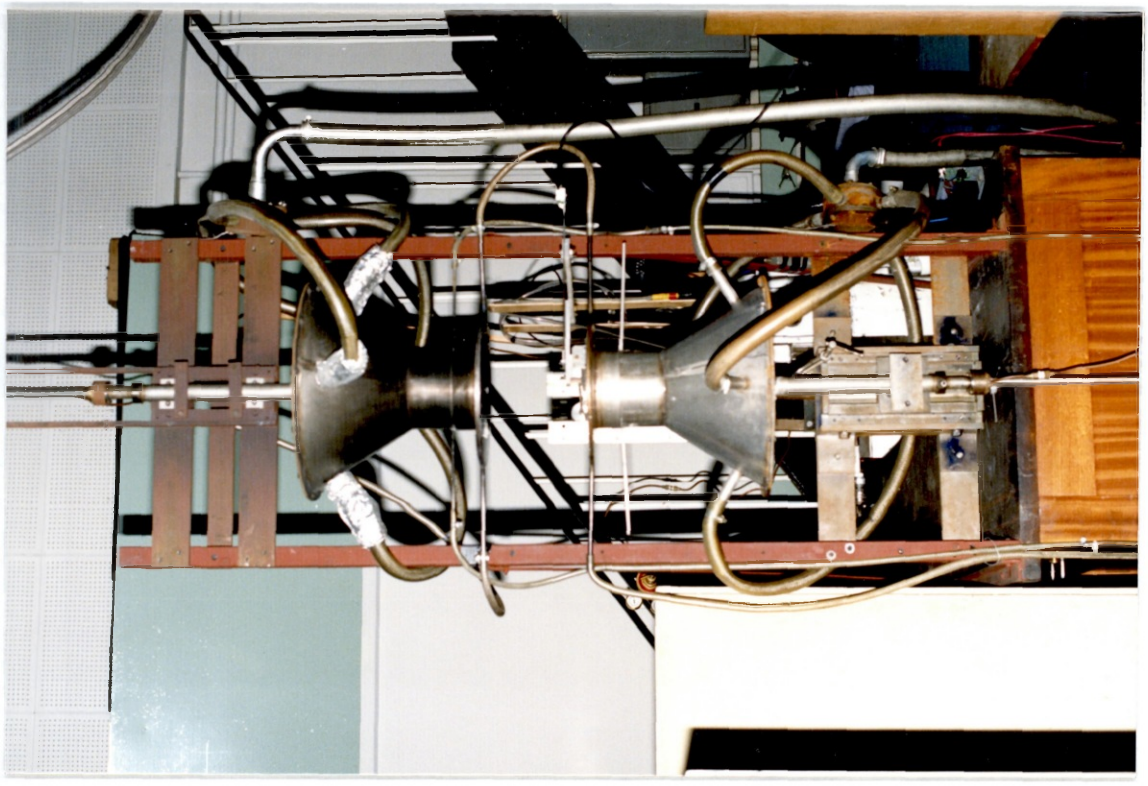

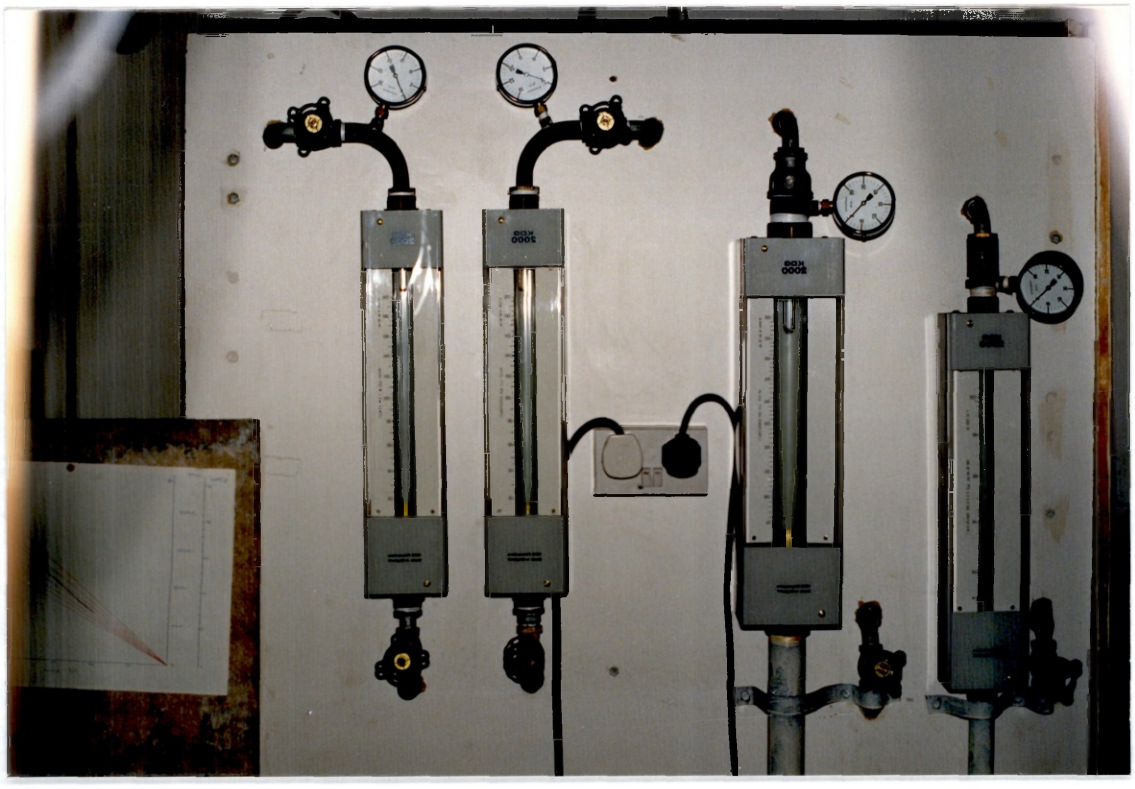

Plate (2.1) Test rig and flow arrangements.

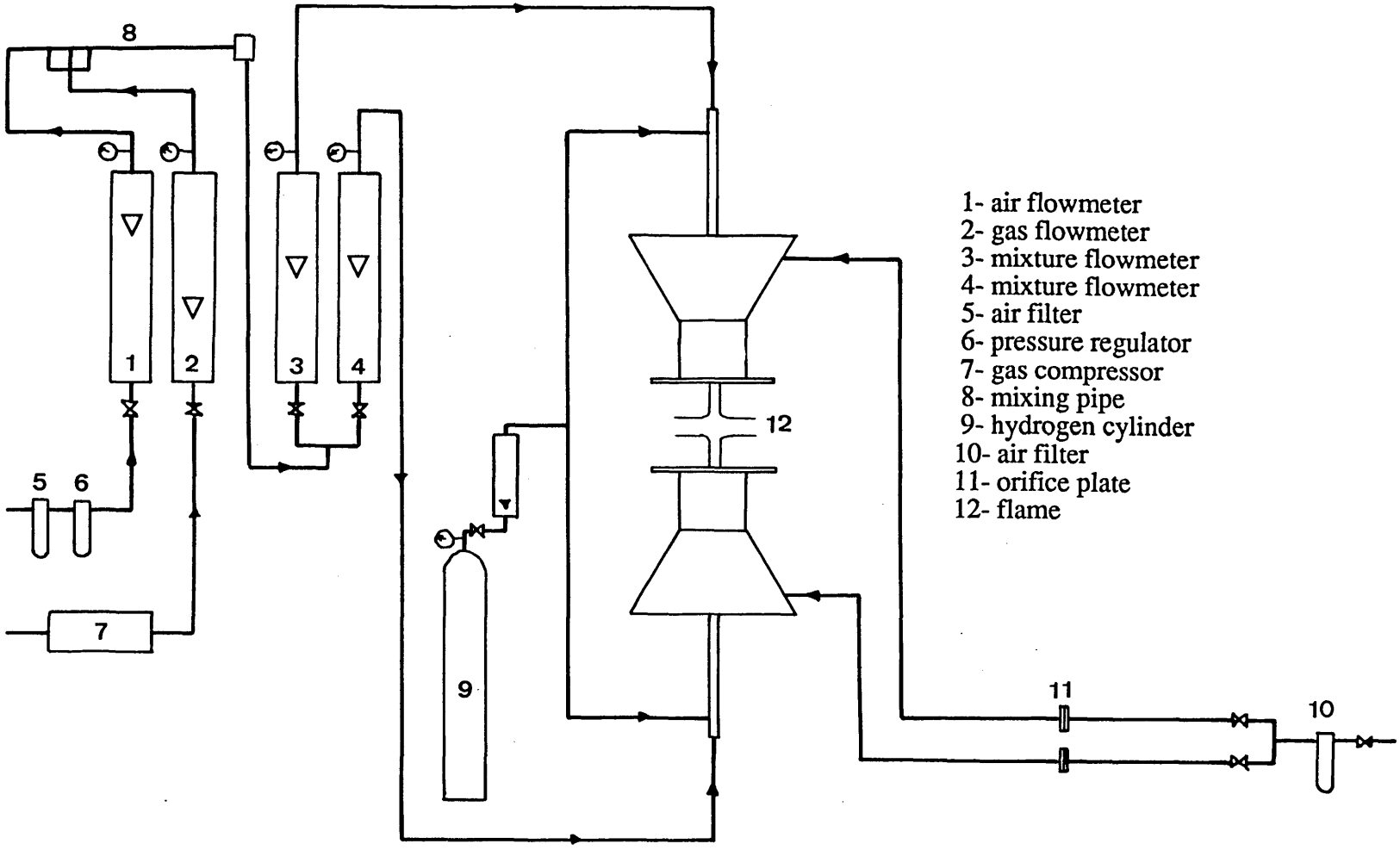

Fig. (2.1) Layout of the test rig and flow arrangements.

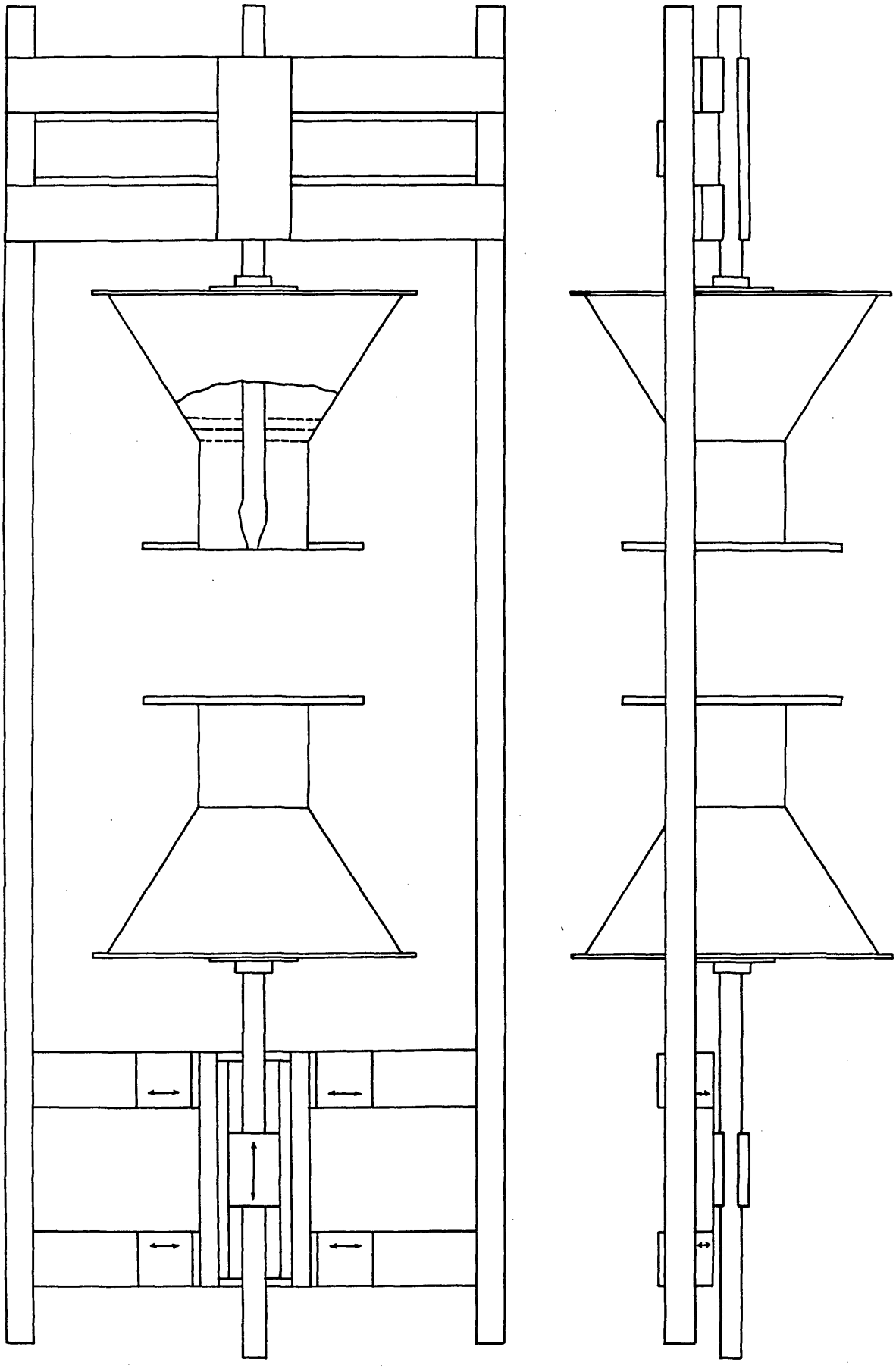

Fig. (2.2) Vertical stand for mounting of the burners.

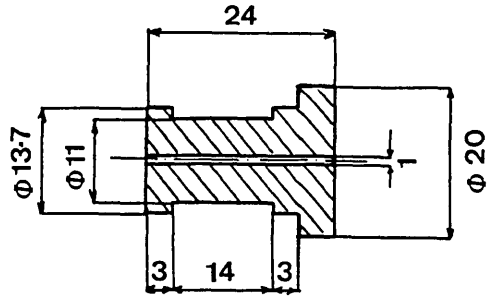

Fig. (2.3a) Cylindrical plug.

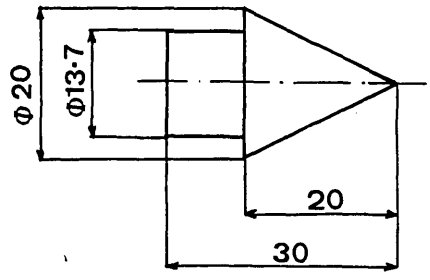

Fig. (2.3b) Taped plug.

dimensions in mm

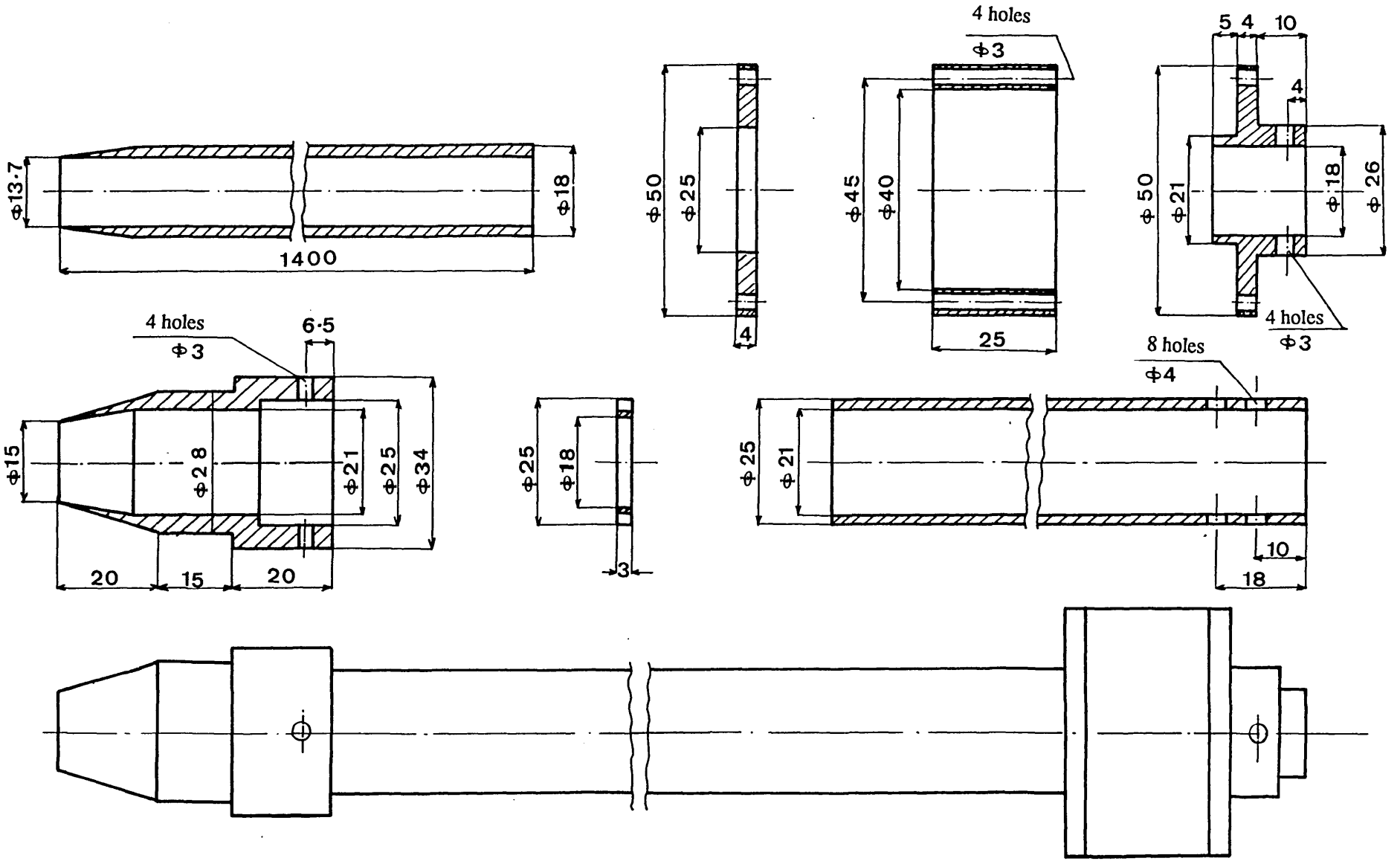

Fig. (2.4) Burner dimensions and annular pilot flame tube arrangement.

dimensions in mm

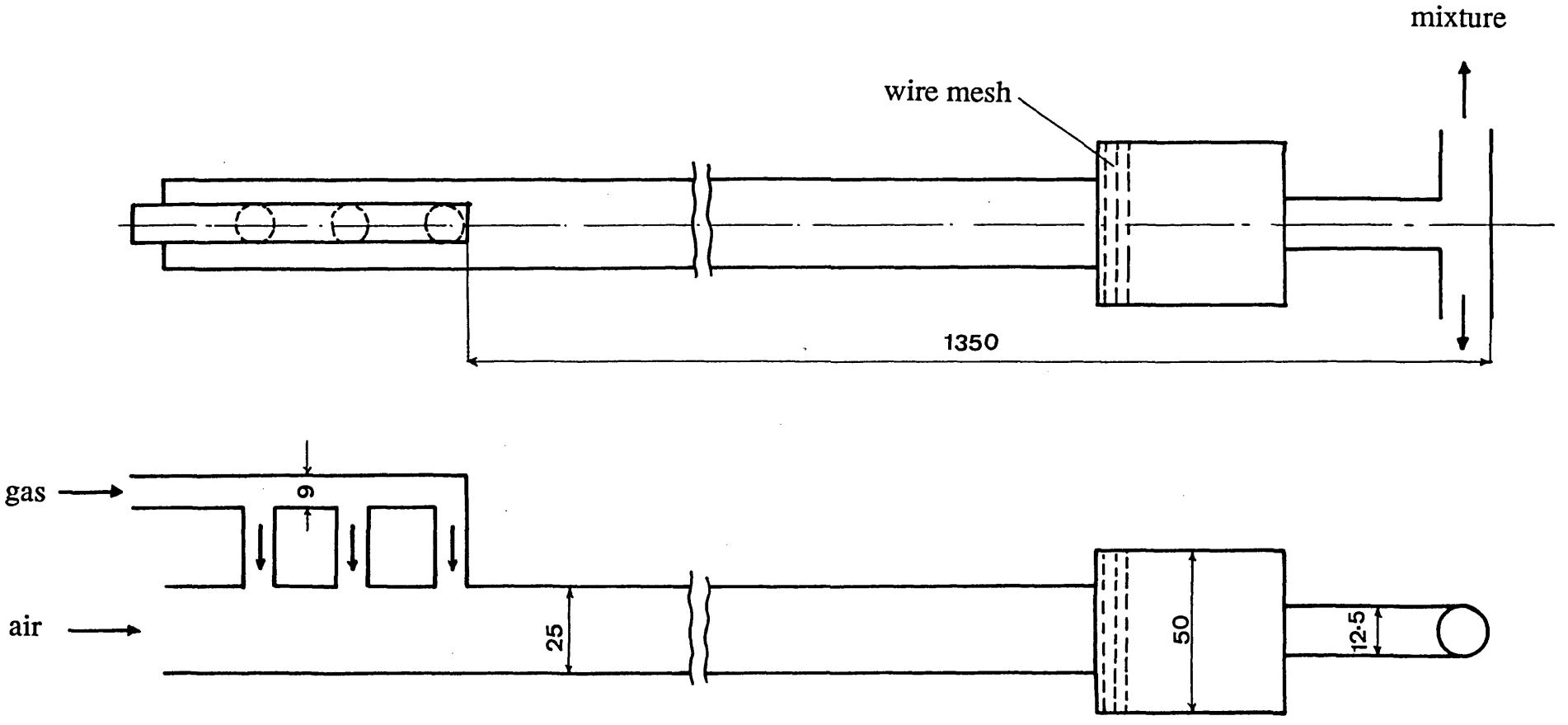

Fig. (2.5) Mixing pipe.

dimensions in mm

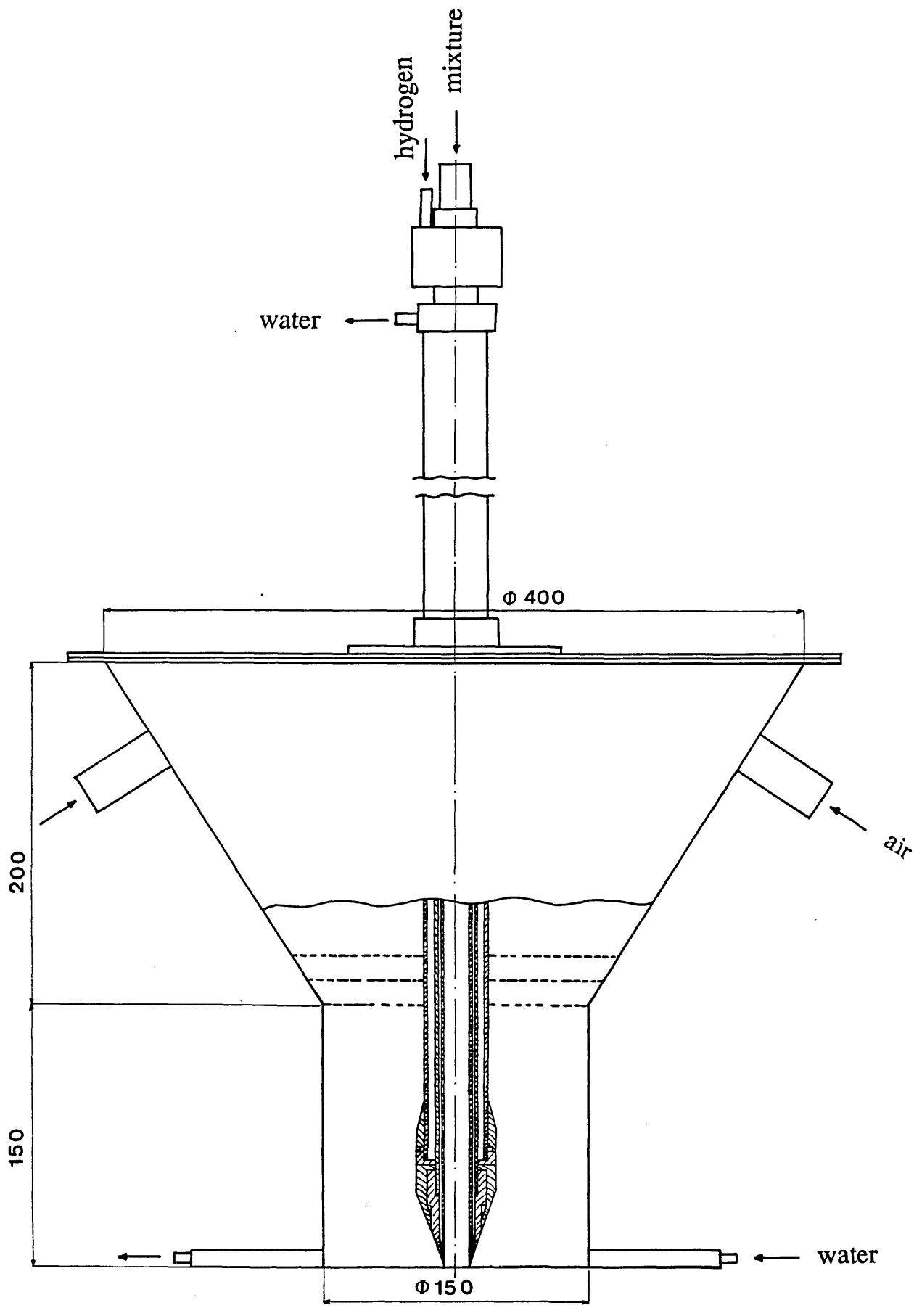

Fig. (2.6) Arrangement of the coflowing air.

dimensions in mm

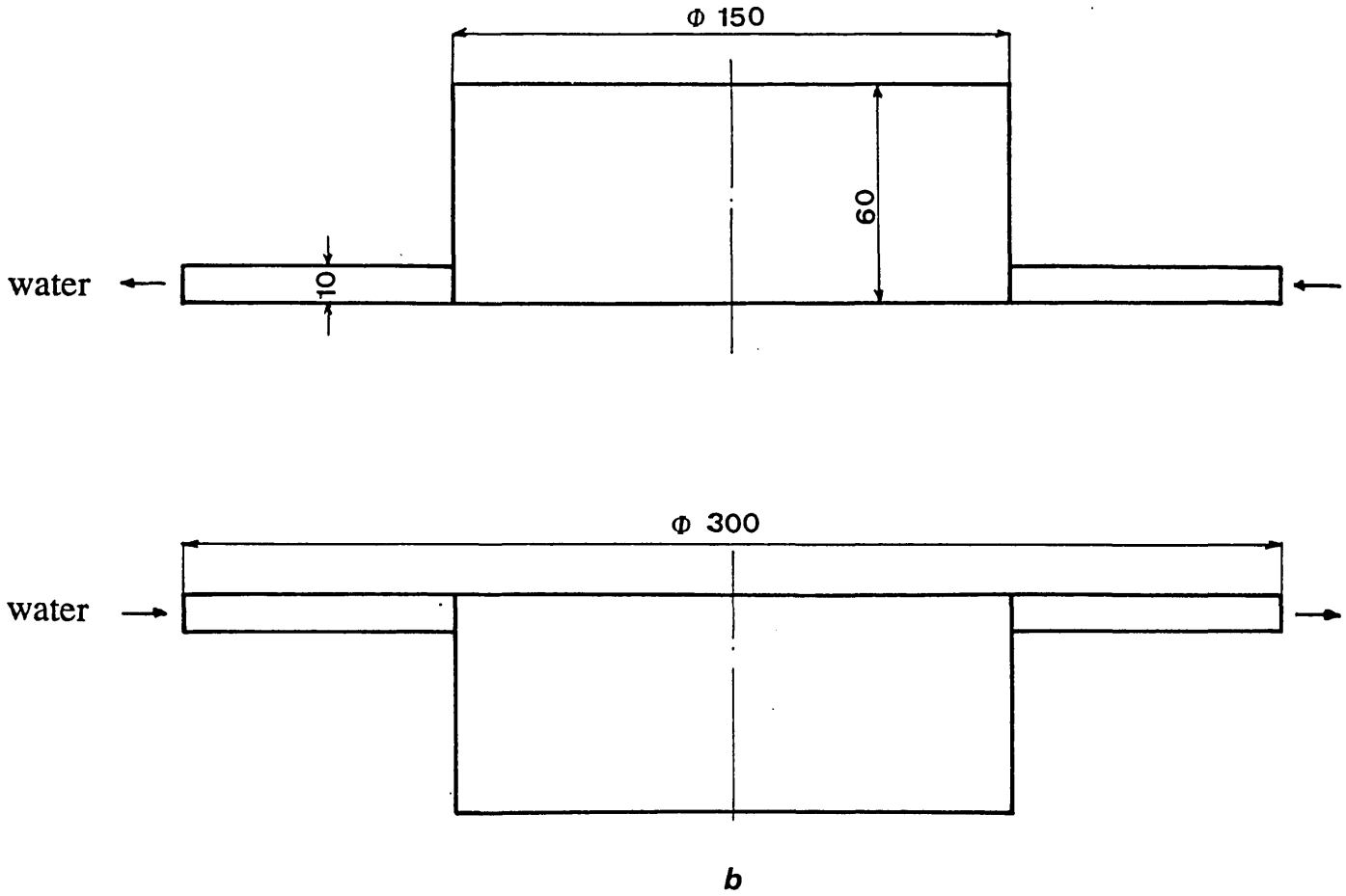

b

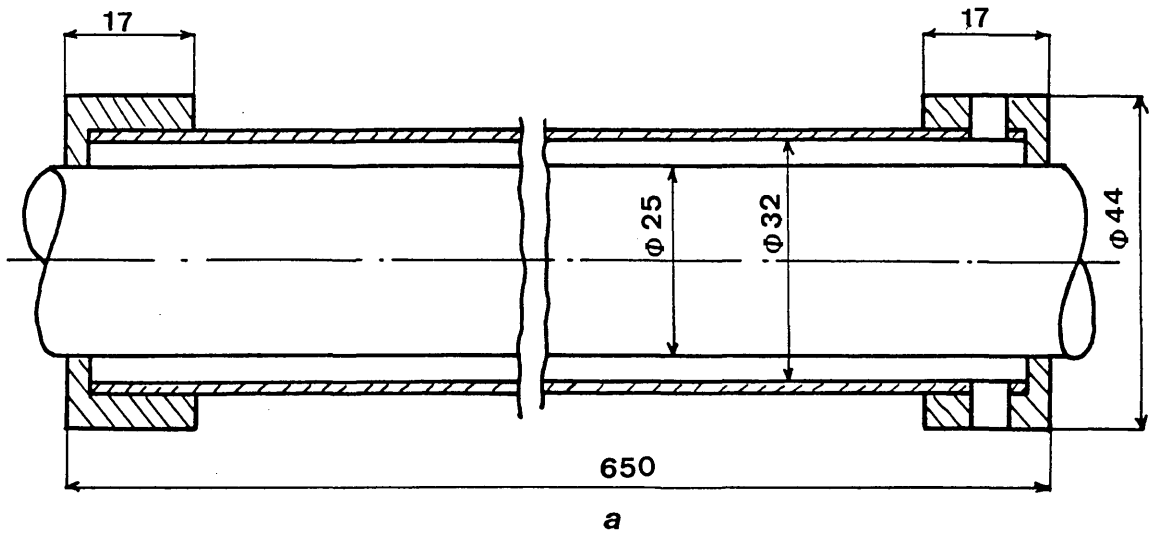

a

Fig. (2.7) Cooling water arrangements.

dimensions in mm

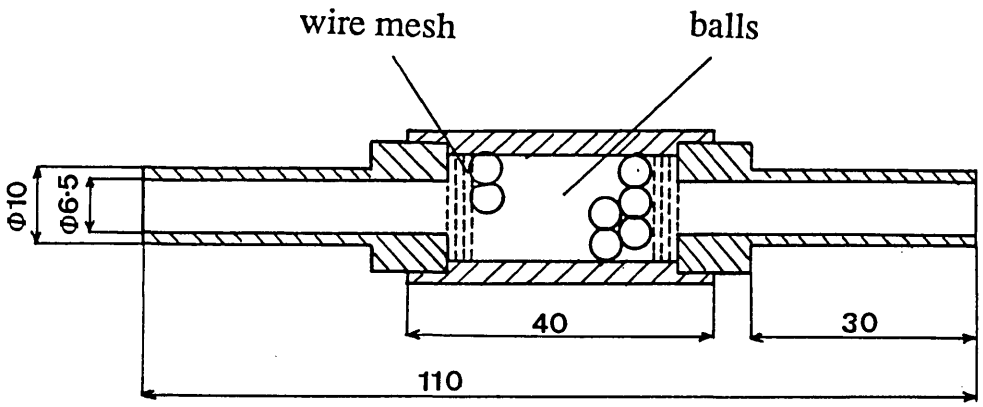

a

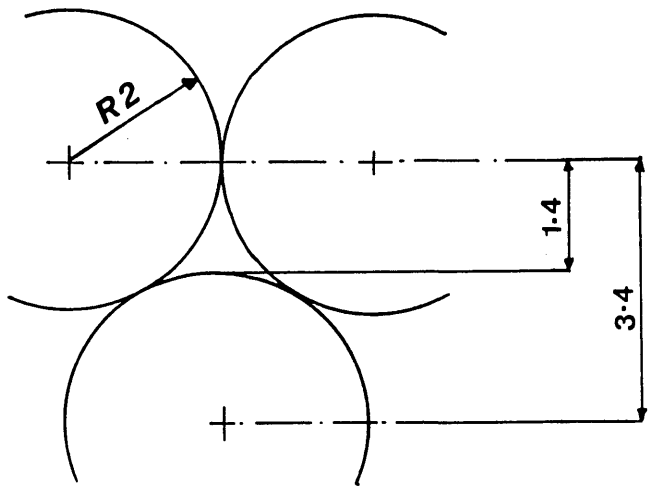

b

Fig. (2.8) Flame trap.

dimensions in mm

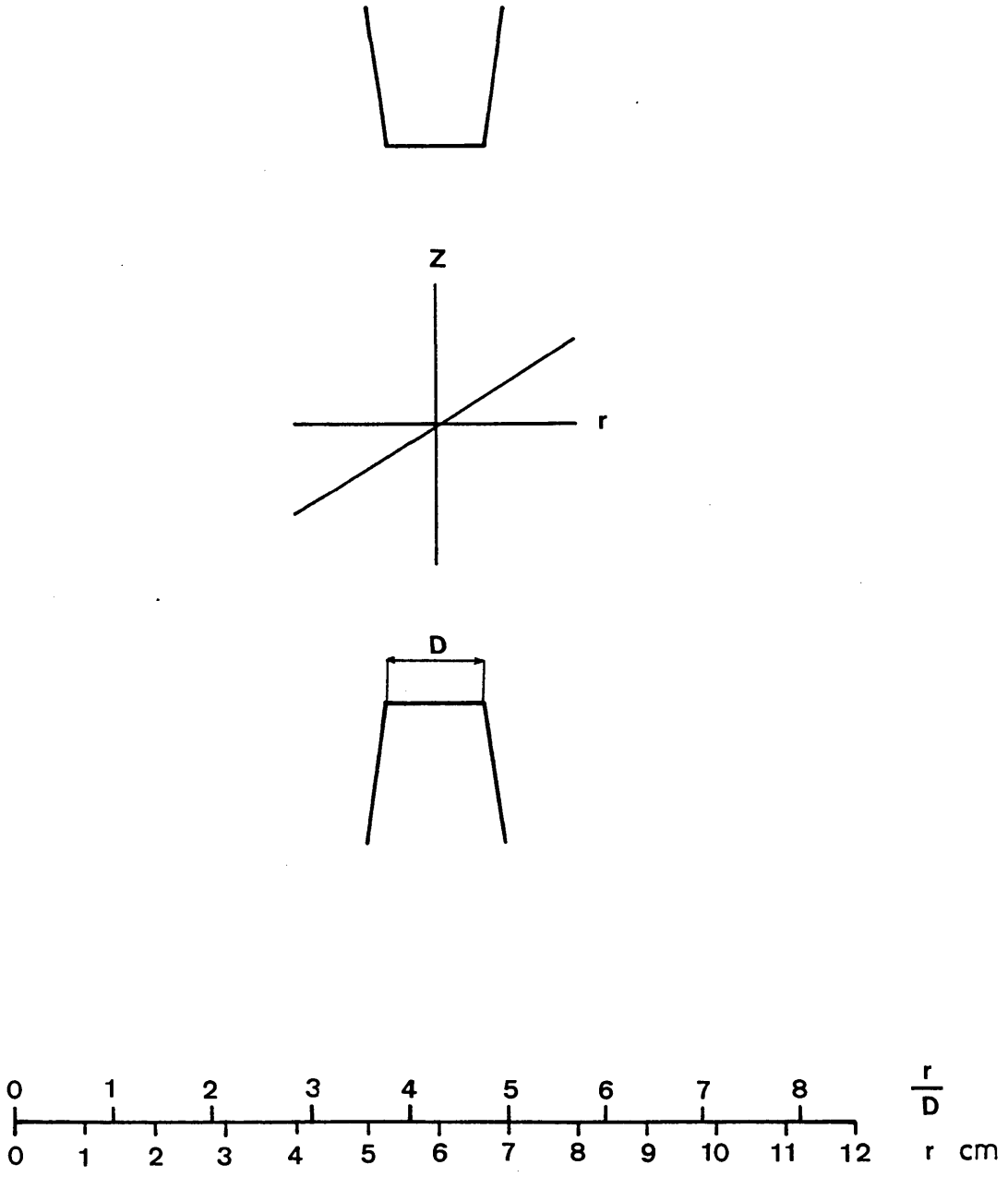

Fig. (2.9) Burner axes.

CHAPTER 3

MEASURING TECHNIQUES

3.1 Introduction

Since temperature, species concentration and ion current demonstrate, as chemistry properties of a flame, the combustion phenomenon, these quantities have been measured in the present experimental procedure. In this chapter the different techniques for each measuring quantity are summarized. Section (3.2) concerns some of the techniques that can be used for temperature measurement, for example, the water-cooled suction pyrometer, optical technique and the fine wire thermocouple. Techniques used for species concentration measurements are presented in section (3.3), for example, the CARS method, infrared analyzers and gas chromatography. Section (3.4) presents the mass spectrometer and the ionization probe both of which can be used for measurement of ion current. The laser sheet technique is used for photographing the counterflow flame, section (3.5). Some concluding remarks are presented in section (3.6)

3.2 Mean Temperature Measurements

3.2.1 Temperature measurement techniques

Since temperature is a characteristic parameter of the system at equilibrium, many techniques have been developed for its measurement for example:

1- the water-cooled suction pyrometer,

2- the optical techniques, and

3- the fine wire thermocouple.

1- The Water-cooled suction pyrometer technique

The mean temperature of a flow can be measured by using a water-cooled suction pyrometer, see Khalil et al (1976), El-banhawy (1979) and Attya and Whitelaw (1981) for example. In the suction pyrometer probe, the thermocouple element is shielded and gases are sucked past it. Shielding the thermocouple significantly reduces the radiant heat transfer by increasing the temperature of the surroundings to a representative gas value. The extent to which the true temperature is measured by a suction pyrometer depends on the geometrical details and operating conditions, see Chedaille and Braud (1972) and Attya (1983). These can be summarized as: the number of shields and their geometry, the suction velocity and the bead position inside the shields. The suction

pyrometer is extremely bulky due to the shields and the presence of the cooling passage. This and the influence of suction, increase the aerodynamic and thermal disturbance in the flow field. For these reasons this technique has not been used in the present study.

2-The optical technique

The temperature in combustion systems can also be obtained by using optical techniques. Examples of these diagnostic techniques include Raman scattering, Rayleigh scattering, coherent anti-stokes Raman spectroscopy (CARS). The optical technique in general consists of a high power laser, spectrometer, optical components and fast on-line minicomputer. Some example applications of optical techniques to flame studies include the work of Lapp and Hartley (1976), Biarski et al (1979), Hall (1979), Kowalik and Kruger (1979), Sochet et al (1979), Greenhalgh (1983) and Laurendeau (1988). Optical techniques would appear to hold-out the prospect of obtaining, with fairly good spatial resolution, comprehensive time-resolved temperature in combustion systems and because of this great effort is presently being devoted towards their development. Because sophisticated and expensive equipment is required, the optical techniques were not of interest as a diagnostic tool for the present study.

3- The fine wire thermocouple technique

Thermocouples are widely recognized by scientific institutions and by industry as a very useful direct means of measuring temperature in reacting, non-reacting, laminar or turbulent flows. Although the fine wire thermocouple is a direct technique for temperature measurements, the thermocouple temperature generally differs from the actual gas temperature. This error arises from three principal sources:

1- Conduction in the wires.

2- Thermal radiation exchange with the surrounding.

3- Thermal inertia of the probe.

The last source of error is because of the finite mass of the thermocouple has a finite response time.

3.2.2 The fine wire thermocouple

The local mean temperature in the present study was obtained by using the fine wire thermocouple, Fig. (3.1). This technique was chosen for the following reasons:

1-its economy and the lack of need of very elaborate instrumentation,

2- its minimal aerodynamic and thermal disturbance on the flow field,

3- calibration of individual thermocouples is not required,

4- it has a high spatial resolution because the measurement volume is confined to the thermocouple bead.

Numerous publications have appeared describing the use of different wire materials, size and configurations of the thermocouple probe, see Bradley and Mathews (1968), Lockwood and Odidi (1975), Ballantyne et al (1976), Lenz and Gunther (1980), Lockwood and Moneib (1982), Heitor et al (1985), Harris et al (1986), Katsuki et al (1987) and Bicen et al (1988). The choice of a thermocouple for flame measurements is dictated by the maximum temperature levels and the melting point of the thermocouple wires. Considerations of the mechanical strength of the wire and its applicability of use in particular situations, such as oxidizing surroundings, have been discussed by Bradley and Mathews (1968) and Billing (1964). The thermocouple employed in the present temperature measurements was platinum- platinum/13% radium.

Regarding to section (3.2.1), thermocouple temperature generally differs from the actual gas temperaturte. Figure (3.2) is a sketch of the geometry of the simply supported thermocouple on which the principal modes of heat exchange and the resultant temperature distribution along the wire are indicated.

The error due to heat conduction from the thermocouple junction along the wire is given by Scotsmann (1970) as:

$$\Delta T_c = (T_g - T_t) (1/\cosh(a L) \qquad (3.1)$$

where:

$$a^2 = 4h/kd$$

If the ratio of the wire lengh(distance between the supporting wires) to its diameter (L/d) is large, the conduction heat transfer to the supporting wires can be neglected and so there is no effect on the temperature of the junction due to conduction losses, see Moneib (1980). Bradley and Mathews (1968) and Abdalla et al (1982) recommended this value to be in excess of 200. They also found that the conduction losses for thermocouple wire of platinum-platinum/13% radium and 40 μm in diameter to be less than 0.2%. The same conclusion have been reported by Attya (1983). Therefore the choice of 40 μm wire diameter and an (L/d) equal to 250 (L = 10 mm), in the present study, are acceptable.

The second error associated with the thermocouple is the heat exchange by radiation . The radiation error(ΔT_r) is defined as:

$$\Delta T_r = \sigma A_j \varepsilon (T_t^4 - T_s^4) / h \qquad (3.2)$$

Where (h) is the convective heat transfer coefficient, which may be

expressed as:

$$h = {}^{k}/_{d_b} \left(2 + 0.31 ({}^{u\ d_b}/_{\upsilon})^{0.62} \right) \qquad (3.3)$$

see Becker and Yamazaki (1978).

The values of d_b, ε and k in the present study are 44 μm, 0.21 and 0.111 W/m.°K respectively. u=0 and T_s=300 °K were taken in order to estimate the maximum radiation error. The maximum radiation error was found to be 38 °K at T_t=2000 °K(about 2%). The same value has been reported by Moneib (1981). Attya and Whitelaw (1981), Hassan (1983), Masri and Bilger (1984) and Koda and Fujiwara (1986) reported that, the radiation heat loss is less than 3% for a themocouple wire diameter up to 40 μm. Because of the small value of the radiation loss it has been neglected in the present temperature measurements.

The rate of heat accumulation to an element of the wire, neglecting the radiation and conduction, is equal to the rate of convective heat transfer to the element, expressed by:

$$v\ \rho_w\ c_w\ (dT_t/dt) = h\ A\ (T_g - T_t) \qquad (3.4)$$

$$T_g - T_t = (v\ \rho_w\ c_w / h\ A)\ (dT_t/dt) \qquad (3.5)$$

$$T_g = T_t + \tau\ (dT_t/dt) \qquad (3.6)$$

where:

$$\tau = (v\ \rho_w\ c_w / h\ A) \qquad (3.7)$$

The value of (τ) is called the thermocouple time constant. Hassan (1983), concluded that the use of 40 μm fine wire thermocouple will allow measurement of the true averaged gas temperature with an expected uncertainty of not more than $\pm$ 2.8 %.

Holderness et al (1969), Odidi (1974), Starner and Bilger (1985), Liu et al (1986) and Katsuki et al (1987) have estimated the catalytic effects of the bare wire thermocouples. Their results suggest that the differences between measurements obtained with coated and uncoated thermocouples are mainly due to variation in radiation losses associated with the difference in emissivity of coated and uncoated wires. Schoenung and Hanson (1981) show that the temperature measured by coated and uncoated thermocouples corrected for radiation are the same in the temperature range from 1500 °K to 1900 °K and an equivalence ratio range 0.7 to 1.4, these values encompass those of the present work. The catalytic effect of the bare-wire thermocouples is therefore considered unimportant and no coating was used here.

The thermocouples of the present study were made of platinum and platinum-13% radium wires of 40 μm diameter. The thermocouple wires had a hot-junction diameter of approximately 1.1 times the wire diameter with the measuring element 10 mm being long. The hot-junction was unshielded and was installed and supported on wires

of the same materials as those of the junction. These wires were supported in a twin-bore ceramic tube with an external diameter of 2.5 mm. The ceramic tube was placed inside a stainless steel tube of 3.5 mm external diameter. The fine wire thermocouples were designed so that the length between the junction and the supporting wire ensured a negligible temperature gradient along the wire and consequently minimal conduction loss. Because of the smallness of the wires the thermal and aerodynamic disturbances at the measurement location are small.

3.3 Concentration Measurements

Gas concentration measurements are probably the most valuable of the various sources of information for the study of the combustion field. Gas samples are readily extracted from flames by sampling probes and analyzed, but uncertainties exist arising from difficulties of ensuring representative sample of the flame at the measuring location, interference of the probe with the flow pattern upstream of the sampling nozzle and from the need to provide rapid analysis of very complex gaseous mixtures. These difficulties have been considered by many research workers, for example, Westenberg et al (1957), Yanagi (1972), Kent et al (1973), Beck et al (1975), Clark and Meller (1980), Colket et al (1982), Kramlich et al (1987) and Arai and Hiroyasu (1988) in their efforts to minimize the errors in the

concentration measurements. A description of the concentration technique used in the present study is given in the following sections.

3.3.1 Sampling system

A typical sampling system in flames study generally consists of sampling probe, sampling line and vapour traps. The major requirements of a combustion gases sampling system are the:

1- conservation of the initial characterisitics of the sample (that is the prevention of any further chemical reactions in the sample),

2- extraction of a sample representative of the conditions at the measuring point in a flow,

3- separation of gaseous, liquid and solid phases, and

4- precise and, if possible, rapid analysis of the gaseous mixure to be analysed.

The first two conditions concern the design and selection of the sampling probe. The third condition is related to the design of the sampling line. The fourth condition concerns the selection of the analyzing technique.

3.3.1.1 Sampling probe

Tine (1961) has discussed in some detail three methods that can be used to quench the chemical reaction in samples extracted from a

flame. These methods are:

1- quenching by diluting the sample with suitable cold fluid as, for example, in direct water-quench probes,

2- quenching the sample by convective heat transefer from the sample to a coolant as in water-cooled probes, and

3- quenching by rapid expansion of the sample as in quartz microprobes. The last method is also known as aerodynamic quenching.

Hassan et al (1983) concluded that water-cooled probes do not freeze the reaction as rapidly as direct water-quench probes. The same conclusion has been reported by Lewis and Smoot (1981). The disadvantage of using a direct water-quench probe is that some gaseous species, for example, carbon dioxide(CO_2) and unburned hydrocarbon (UHC) dissolve in water, Hirji (1986). Godoy (1982), mentioned that quenching rate cannot be assured with the water-cooled probes. An additional consideration is that direct water-quench probes and water-cooled probes are big in size and can disturb the flow, particulary in a small scale laboratory flow, such as in the present one.

The present experiments rely on aerodynamic quenching to suppress chemical reactions in the gas sampling system effected by the use of quartz microprobes. The advantages of this kind of probe are:

1- the size of the microprobe is small, minimizing the flow disturbance,

2- quartz has the ability to withstand high temperatures and has minimal catalytic effect on the flame gases, as indicated by Fristrom and Westenberg (1965),

3- since the probe is uncooled the question of it being a heat sink (which can reduce temperature and enthalpy in the region being sampled) does not arise.

Aerodynamic quenching is also of a particular interest due to the exceptionally high quenching rates that may be achieved, see Fristrom et al (1957).

An aerodynamic quench in a gas sampling probe is defined as a rapid reduction in static temperature and static pressure achieved by quickly accelerating the flow to supersonic speed. Fristrom and Westinberg (1965), reported that, since a supersonic flow may be maintained in a large scale area-ratio nozzles, it may also be maintained in a small scale, large area-ratio passages such as those found in the tip region of microprobes, Fig. (3.3). They also concluded that a microprobe having a large area ratio tip will provide aerodynamic quenching of the combustion gas samples, provided that the pressure ratio across the probe is large enough. Lazzara and Biordi (1973) used a quartz microprobe in lean methane, oxygen-argon flames. Their results showed that the reaction could be frozen in the quartz microprobe. Lockwood and Syed (1975) also used a quartz microprobe to obtain quenched gas samples for

oxygen concentration measurements. These authors also made trials with the addition of water cooling, but found no difference in the recorded results between the cooled and uncooled probe. It was concluded that the sudden expansion provided sufficient quenching.

Probe measurements in combustion flows are usually associated with uncertainties in the measured quantities due to expected thermal and aerodynamic interference between the probe and the surrounding gases. Probe effects are mainly related to the probe size, geometry and probe operating conditions, such as, suction pressure and suction velocity. In turbulent combusting flows, probe-gas interference effects are difficult to quantify due to the fluctuating nature of the measured quantities and the large variations in flow conditions from point to point within a turbulent flame, Hassan (1983).

In the present study two different quartz microprobes have been tested in order to see the effect of the probe size on the measurement of carbon monoxide (CO), carbon dioxide (CO_2), oxygen (O_2) and methane (CH_4) concentration. Figure (3.4) shows the two probes, probe (A) is 2mm and 3mm, while probe (B) is 4mm and 5mm internal and external diameter respectively. Fristrom and Westinberg (1965) recommended a tapered shape of the probe tip that gives the least

disturbance to the flow to be sampled. Herein the tip of the probes reduced to an orifice of 200 μm and 400 μm for probe (A) and probe (B) respectively, giving an expansion ratio of about 100. Results of the test performed, Fig. (3.5) show that the difference in the measurements between the two probes are within the repeatability limits. Probe (A) was selected for the species concentration measurements in order to minimize interference effects of the probe body on the flow, in particular near the burner axis. A similar probe has been used by Syed (1977).

Attempts to use probe with isokinetic sampling,(suction velocity equals to local gas velocity) in turbulent combustion have been described by Varnos et al (1969), Kent and Bilger (1973) and Bowman (1977). The errors associated with departures from isokinetic conditions were not quantified in detail. Tine (1961) indicated that it is difficult to guarantee isokinetic sampling in turbulent combustion. In the present experiment a study has been done in order to estimate the effect of the suction velocity on the concentration measurements. Results of the test performed are shown in Fig. (3.6). A small change of both the CO and CO_2 concentrations of around 0.65 %, and a change of the O_2 and CH_4 concentrations of around 1.0 % result from a variation of the suction velocity from 30 m/sec to 90 m/sec. The results for higher suction velocities indicated that the probe was extracting samples from points

remote from the tip. Hassan (1983), has also studied the effect of the suction velocity on the measurements of species concentration. He decreased the suction rate from the probe to the minimum flow required by the analyzers. He reported that a deviation from the maximum suction velocity reduces quenching efficiency. Herein the working suction velocities were of the range 30 m/sec to 90 m/sec, it was concluded that the isokinetic sampling has no meaning with this kind of probes.

3.3.1.2 Sampling line

The sampling line used in the present study is shown in Fig. (3.7) and Fig. (3.8). Water vapour was separated from the gas sample with a water condenser near the probe. The sample then passed through a dryer containing calcium chloride for the removal of the remaining moisture. An ice bath containing glass wool was incorporated after the dryer in order to separate any further condensed vapour. Because the sampling line was under negative pressure, one of the major sources of operational difficulties was the leakage of air into the line. In order to test for leakage the probe was operated normally, nitrogen free of oxygen was introduced at atmospheric pressure to the probe tip and was supplied to the oxygen analyzer. Obviously, if the system is free of any leakage a zero oxygen concentration would be measured.

3.3.2 Concentration measurement techniques

Different techniques have been developed for species concentration measurements. These techniques are:

1- Coherent Anti-Stokes Raman Spectroscopy (CARS),

2- Infrared analyzers,

3- Gas chromatography.

1- CARS technique

The CARS technique in general is a wave mixing process wherein incident laser beams at frequencies W1 and W2, with a frequency difference appropriate to the molecular species being probed, interact to generate a coherent signal at frequency W3=2W1-W2. By analyzing the spectral distribution of the CARS signal, species concentrations can be determined. CARS spectra have been recorded in a variety of flames from N_2, O_2, CO, CO_2, H_2, H_2O, CH_4. The greatest advantage of this technique is its high immunity to interference, see for example, Zinn (1977), Eckbreth (1980) and Greenhalgh (1983). Because sophisticated and expensive equipment is required, the CARS technique has not been used in the present study.

2- Infrared analyzers technique

The infrared analysis technique is the most common for the measurement of carbon monoxide(CO) and carbon dioxide(CO_2) species concentration. Its main advantage is that the values of the species concentrations can be read instantaniously. The disadvantage of the technique is that the measurement of any other species concentration such as oxygen and unburned hydrocarbon (UHC) needs separate analyzers. A high flow rate of the sample to be analyzed will be required and demanding a bigger probe.

3- Gas chromatography technique

Gas chromatography may be used to analyze species concentration of combustion gases such as, carbon monoxide(CO), carbon dioxide(CO_2), oxygen(O_2), nitrogen(N_2) and unburned hydrocarbons (UHC). The concentrations of the analyzed gases are traced on a chart recorder as a series of sequential triangular peaks. The chart is called a chromatogram and the area under these peaks is directly proportional to the concentration of species in the sample. A typical chromatogram is shown in Fig. (3.9). Known samples can be used in order to calculate the proportionality factor for each species. The main disadvantage of this

technique is that longer analyses times are required than for the other methods. The advantages are :

1- only a very small sample is required and therefore a relatively small probe can be used, and

2- all the sample species can be analyzed by the same analyzer.

3.3.3 Gas chromatography

The species concentration measurements in the present study have been performed using a gas chromatograph, Pye Unican (serial no. 212763), Fig. (3.10) shows its main components. Chromatography is based on the distribution of components between two phases, one is stationary with a large surface area and the other is a carrier gas that moves in contact with the stationary phase. A carbon molecular sieve was used as the stationary phase, Drummond (1987). Kaiser(1970) has described its use for light gas analysis. Hydrogen and helium can be used as a carrier gas to give high sensitivity and allow more rapid analysis, Cowper and Derose (1983). Helium is much preferred on safety grounds and also because it is not a component of combustion gas mixtures. The helium flow rate was controlled through both the reference phase and the stationary phase by the use of pressure regulator and flow controller.

The sample injector, Fig. (3.11a) has two positions, the:

a- Fill position, which allows the gases to be analyzed to flow through a sample loop, Fig. (3.11b).

b- Injection position, through which a small volume of the sample flow into the carrier gas, Fig. (3.11c).

The carrier gas takes the sample into the column which is constructed of glass and is 2.8 m long and 2 mm in diameter. It is welded to metal sealed exit termination which enables the column to be operated at temperatures up to 400 °C. A thermal fuse is incorporated to prevent thermal runaway. In the column, separation of gases takes place at different temperatures, for example, separation of oxygen and nitrogen takes place at room temperature, Godoy(1982). At the end of the column components of the sample being separated enter the detectors.

3.3.3.1 Thermal conductivity detector (TCD)

The chromatograph has two thermal conductivity detectors, one for the sample flow and the other for the reference flow. TCD is used for measurements of species such as, oxygen, nitrogen, carbon monoxide and carbon dioxide. Figure (3.12) shows the TCD circuit diagram, a given electrical current passes through the filaments(thermistor)and the carrier gas flows through both. The thermistors alter their temperature until they reach an equilibrium temperature, where the rate of heat loss is

balanced by the rate of energy input. This is a function of the thermal conductivity of the surrounding carrier gas, helium. When a different gas enters the detector it has a lower thermal conductivity than the helium and the thermistors assume a new equilibrium temperature. The two filaments are incorporated as two elements of a wheatstone bridge circuit and the difference in resistance is amplified and recorded to produce the chromatogram.

3.3.3.2 Flame ionization detector (FID)

The FID, Fig. (3.13), was used for unburned hydrocarbon (UHC) concentration measurements. In general FID operates by measuring the thermal conductivity of a gas which is directly proportional to the concentration of charged (ionized) particles within the gas, ionization being provided by a flame, Godoy(1982). The sample is mixed with hydrogen-helium and air and burnt in a small jet flame where ions are formed. The electrical resistance of the flame is monitored continuously, the resistance decreases when an organic vapour is present to supply a source of ions. This change is amplified and recorded to produce a chromatogram. Because TCD and FID produce two chromatograms a two channel chart-recorder is used.

The chromatographer is calibrated with a known sample, a bottle of standard gases are used. Samples of carbon monoxide, carbon dioxide, methane and ethane in nitrogen are analyzed as reference components. Calibration checks are carried out at start and end of each set of data in order to maintain a consistent level of accuracy.

3.4 Ionization Measurements

3.4.1 Nature of the measurements

The ionization phenomenon produces mainly positive ions and free electrons, although some electron capture may occur giving negative ions. This phenomenon exists for most of the chemical reaction processes. The combustion phenomenon involves some degree of ionization and the degree of ionization is strongly related to the combustion reaction, Ahlheim and Gunther(1979). Because in the reaction zone radical concentrations frequently exceed the equilibrium values, so ion concentrations greater than those corresponding to equilibrium are also produced, Barnard and Bradley (1985). Hirano et al (1981) have reported that the levels of ionization are greatest in the reaction zone and fall off on both the unburnt and burnt gas sides . Ahlheim and Gunther(1979) also reported that ionization measurements give a good survey of the reaction fields in non sooting or blue flames. The existence of ions in flames has long been known. There have been

many studies devoted to ion concentrations in flames, for example, Lockwood and Odidi (1975), Clement and Smy (1979) and Suzuki and Hirano (1982), mostly in premixed flames that are especially related to kinetics of combustion.

Ionization measurements to determine the position and structure of the flame front in turbulent flames have been performed by many investigators, for example, Karlovitz et al (1951), Richmond et al (1956), Tsuji and Hirano (1970), Basu and Bhaduri (1972), Lockwood and Odidi (1975), Ahlheim and Gunther (1979), Fox and Bertrand (1981), Ventura et al (1982), Brophy and Wilbur (1986) and Calcote and Keil (1988). Ionization measurements combined with measurements of species concentration and temperature may be expected to provide a good picture of the reaction field. The most common approach to ionization measurements is to introduce a pair of electrodes into the gas and measure the current flowing when a potential difference is applied across them.

3.4.2 Ionization measurement techniques

Two common techniques have been developed for ionization measurements, they are:

1- the mass spectrometer, and

2- the ionization probe.

3.4.2.1 The mass spectrometer

The mass spectrometer consists in general of three principle parts, the (1) sampling cone (probe), (2) vacuum chamber, and (3) the ion detector . The ions are extracted from the flame through a sampling cone and brought into a high vacuum system where, after separation from the burnt gases, they can be accelerated and measured. It is also possible to collect the ions as soon as they enter the extraction apparatus and, knowing the amount of gases and collected ions, to calculate the ion concentration in the sample, Deckers and Tiggelen (1957). For more details see Calcote (1963), Olson and Calcote (1981) and Michaud et al (1981).

Although the mass spectrometer is one of the common techniques used for ionization measurements, there are some problems related to its arrangement.

1- Since a flame cannot be run at the very low working pressure (10^{-5} mm mercury) of a mass spectrometer, a sample of the flame has to be expanded through a hole and behind this hole the burnt gases have to be pumped away while the ions are kept in a straight beam by means of an electrostatic field maintained by a system of electrodes. If the hole is too narrow most of the ions will lose their charge by collision with the walls, but if the hole is too large no pumping installation would be sufficient to

obtain a satisfactory vacuum, Deckers and Tiggelen (1957).

2- If the passage through the intermediate region (between the sampling cone and the ion detector) is not short enough a randomized redistribution of the initially nearly homogeneous ion velocities cannot be avoided.

3- The surface area of the protecting tube is quite large compared with that of the wire exposed to a flame, as in the case of ionization probe (see section 3.4.2.2), Calcote (1963), which can disturb the flow.

The mass spectrometer is not of interest in the present ionization measurements because it cannot be located in the flame.

3.4.2.2 The ionization probe

The other technique which can be used for ionization measurements is the ionization probe. The ionization probe has been described by many authors. In general the ionization probe consists of the (1) probe wire (sensor), (2) insulator, and (3) the probe body, Fig. (3.14). If a potential difference is applied across the probe, the flame ions are attracted to it when passed through a flame.

Karlovitz et al (1953) introduced the use of the ionization probe for measuring positive ion concentrations in turbulent flames. They tested many probes, consisting of a negatively-biased wire (500 μm

to 800 μm diameter). This wire carried in insulating ceramic tube, with part of the wire (from a few mm to 30 mm) exposed to the flame. However, their measurements were of limited accuracy because the probe, not being streamlined, disturbed the flame, Denniston et al (1957). This factor caused their data, at any given radial position, to be dependent on whether or not the probe had traversed the flame axis.

Ahlheim and Gunther (1979) employed an ionization probe with exposed part of 2 mm for measurements of ionization currents in free-jet diffusion flame. The probe wire was insulated with an alumina tubing , cooled with a water jacket. They reported that the temperature of the alumina should not exceed 1000°C, since its electrical conductivity increases strongly at higher temperatures. They also concluded that, whereas ionization peaks are numerous in the main reaction zones, they are rare in the other zones of the flame.

Suzuki and Hirano (1982), measured the ion-current correlations in a turbulent premixed flame by using two ionization probes. The sensor of each probe was a platinum wire of 100 μm in diameter with 1.5 mm being exposed, which was kept at -10v (potential difference). The probe was covered by a water-cooled copper pipe, leaving an exposed probe tip of 15 mm. The ion-current correlations were measured by changing the location of one probe with respect to the

other, and the distributions of the maximum ion-current correlations at the side and top of the turbulent flame zone were obtained.

The same probe configuration has been used by Ventura et al (1981) in the investigation of the flame structure by measuring the mean ionization current. They found that the peak value of the mean ion-current profiles at different axial locations increases with Reynolds number(Re). This work was followed by further work of Ventura et al (1982), where, using the same probe, they performed ionization measurements in the transitional region of partially premixed flames. They concluded that flames with higher equivalence ratios, requiring more additional air for complete combustion, have a more irregular flame structure.

Suzuki et al (1979) and Hirano et al (1981), studied the effects of the probe potential, size and velocity of an ionization probe on the ion current recorded when the probe traverses a premixed, two-dimensional flame. The effect of the probe velocity was examined by fixing the probe on a rotating circular disk so that the probe axis would be parallel to the flame and pass it at 6 mm from the burner port. They concluded that the insulation temperature should be always less than 300 °C in order to maintain its insulation properties. This was achieved by keeping the probe velocity always higher than 1 m/sec. They also

concluded that the use of 100 μm platinum wire with 2 mm exposed part and -10v as a potential difference across the probe gave the optimum performance.

The present ionization probe consisted of 100 μm platinum wire (sensor) with an exposed portion of 2 mm. The wire was carried in an insulating ceramic tube with internal and external diameters of 0.2 mm and 0.8 mm respectively. The ceramic tube was placed inside a stainless steel tube of 0.9 mm and 1.6 mm internal and external diameters. A water jacket with 5 mm external diameter was used, Fig. (3.14). Efforts were made in order to reduce the probe diameter near the tip. The probe was first used with a 15 mm of the stainless steel tube covering the ceramic without cooling, Fig. (3.15a). This resulted in the insulation becoming an electric conductor at high temperature locations in the flames. Subsequently the probe was cooled up to the tip but by reducing the water jacket to 3 mm (external diameter) and 20 mm long (from the probe tip), Fig. (3.15b). This design did not achieve sufficient cooling for the tip.

In a final redesign the stainless steel tube covering the insulator was cooled up to the probe tip 5 mm (external diameter) water jacket. The water inlet passage was designed in order to ensure efficient cooling for the probe tip. The tip of the probe was machined in order to reduce the flow disturbance at the measuring location. The body of the

probe was the positive electrode while the sensor was connected to a negative voltage of -10v. The ionization signal sensed by this device was passed through a 1 MΩ resistance to convert the current into a voltage signal.

3.5 Flow Visualization

It is recommended that all new flow configurations should be visualized before quantitative measurements are attempted. Visualization methods usually provide qualitative information. Some of these methods are Schlieren, shadowgraph and laser sheet. They can provide useful information by themselves and are very helpful in guiding the use of more quantitative methods.

Flow visualization using smoke has been used to elucidate flow patterns. This technique does not appear to have been used in turbulent flames, no doubt due to the difficulties of using a refractory smoke and distinguishing between scattered and luminious radiation. Such flames have traditionally been visualized by Schlieren and shadowgraph techniques and by direct photography. These visualizations suffer from the disadvantage that the information is integrated across the flame. The visualization technique used in the present study concerned a

slice of laser light (laser sheet) passed through a seeded flame and the light scattered from the seed was photographed, presenting a cross section of the flame.

3.5.1 Laser sheet technique

Figure (3.16) illustrates the experimental set-up of the laser sheet-lighting technique for observing the flame. The technique is simple and easy to implement. The only major equipment items required were a laser, seeder and camera. The laser sheet was simply generated by passing a laser beam through a cylindrical lens as shown in the figure. The present experiment has been performed using titanium dioxide as seeding particles.

3.5.2 Seeding system

It is important, with this kind of technique, to ensure that the flow under investigation to be uniformly seeded. Trials were made to use a fluidized bed as a seeder, Fig. (3.17), but preliminary observations showed that this kind of seeder did not give a uniform seeding. Therefore a cyclone aerosol generator, Fig. (3.18), was used in order to ensure a uniform seeding. The powder at the base of the column was entrained by the flow and carried out by the central vortex. Because two opposed

burners were used in the present study, two identical seeders were incorporated.

3.6 Concluding Remarks

* The fine wire thermocouple was used for mean temperature measurements. Although there are some errors associated with this technique, these errors were found to be small (arround 6%) for 40 μm pt./pt.-13%rd. wires.
* The quartz microprobe was chosen for the present concentration measurements because of its size (small compared with other sampling probes) and because it provides good quenching.
* A water-cooled ionization probe was used for the measurements of mean ion current. The probe was cooled up to the tip in order to maitain the ceramic as an insulator even in high temperature locations in the flame.
* The counterflow flame has been visualized by using the laser sheet technique with titanium dioxide powder being used as the seeding particles.

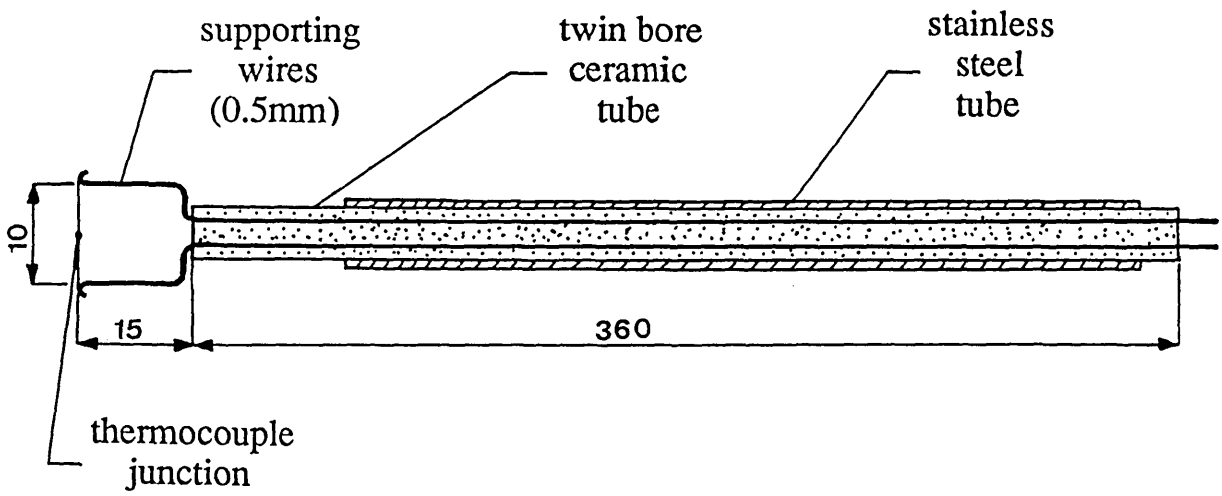

Fig. (3.1) Thermocouple probe.

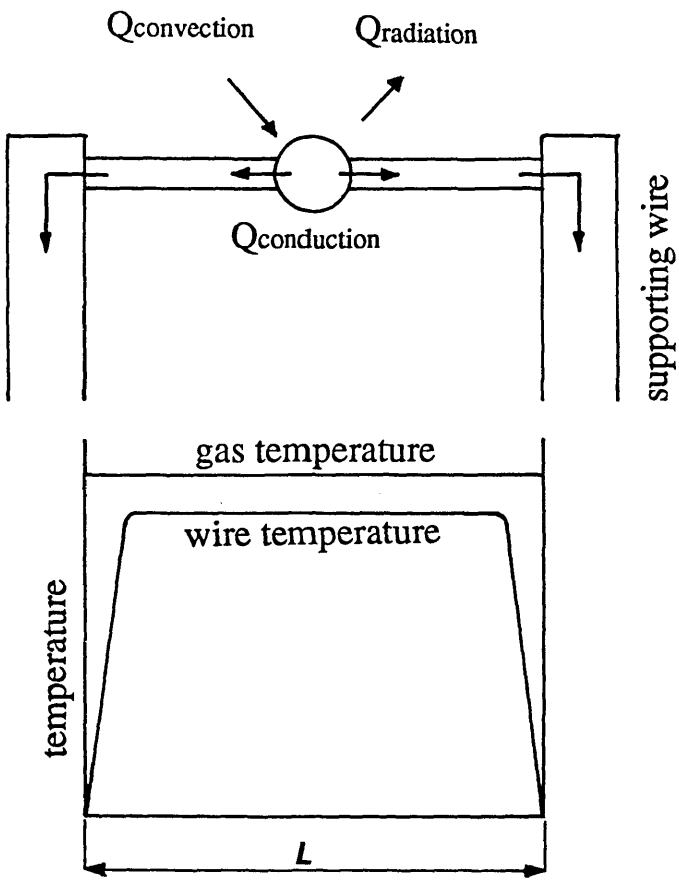

Fig. (3.2) Sketch of simply supported thermocouple.

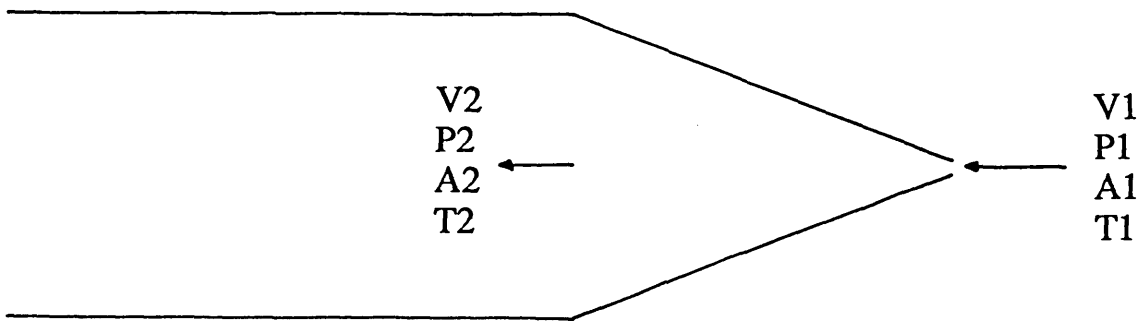

Fig. (3.3) Microprobe tip.

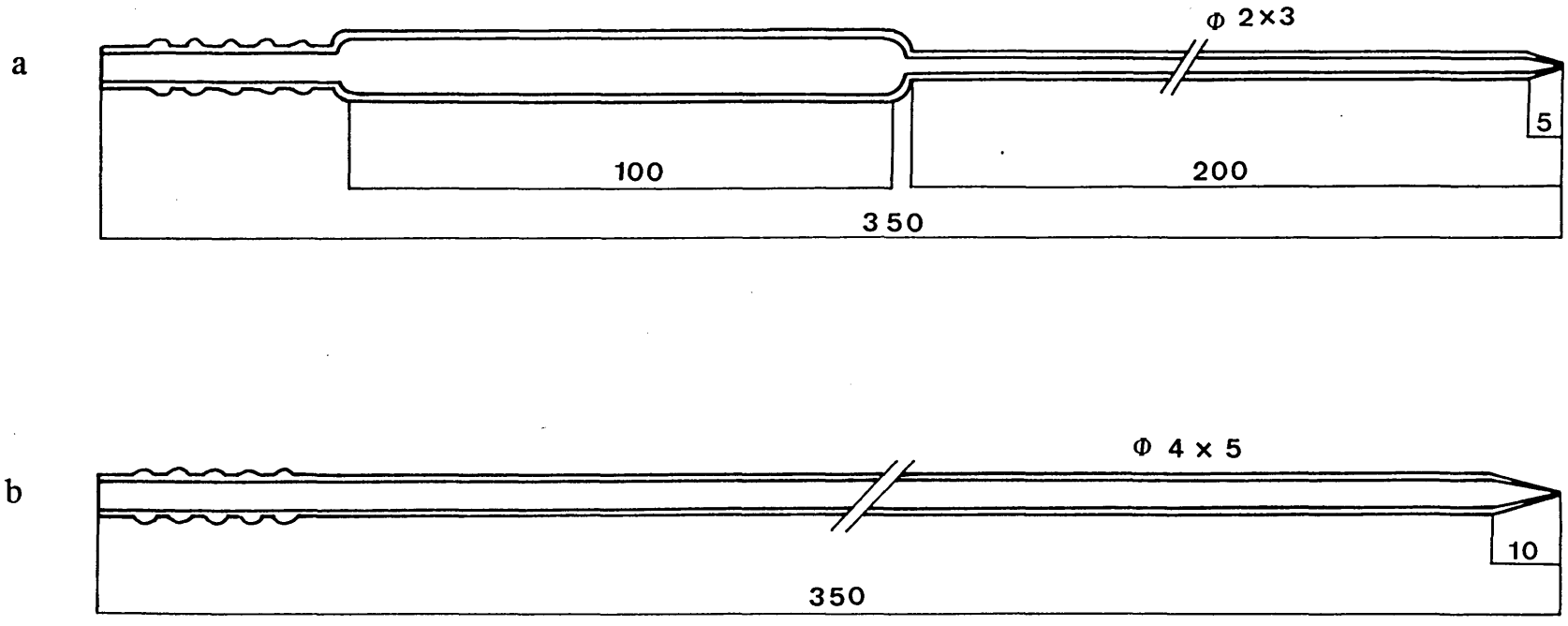

Fig. (3.4) Quartz microprobe.
(a) 200 μm orifice diameter
(b) 400 μm orifice diameter

dimensions in mm

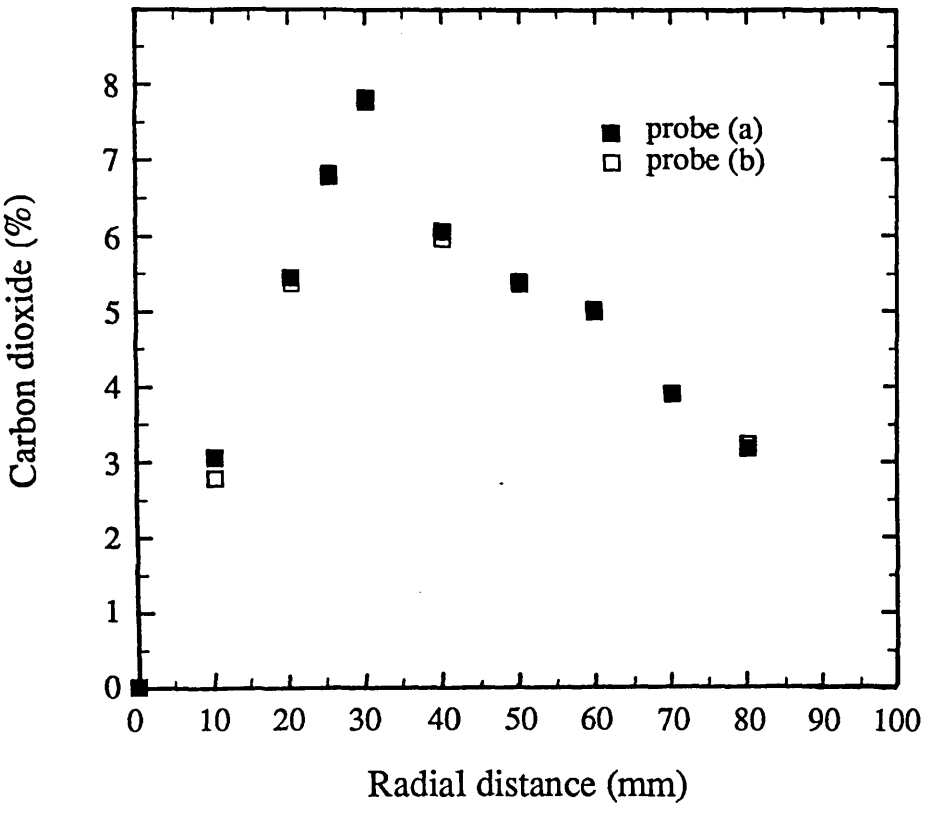

b

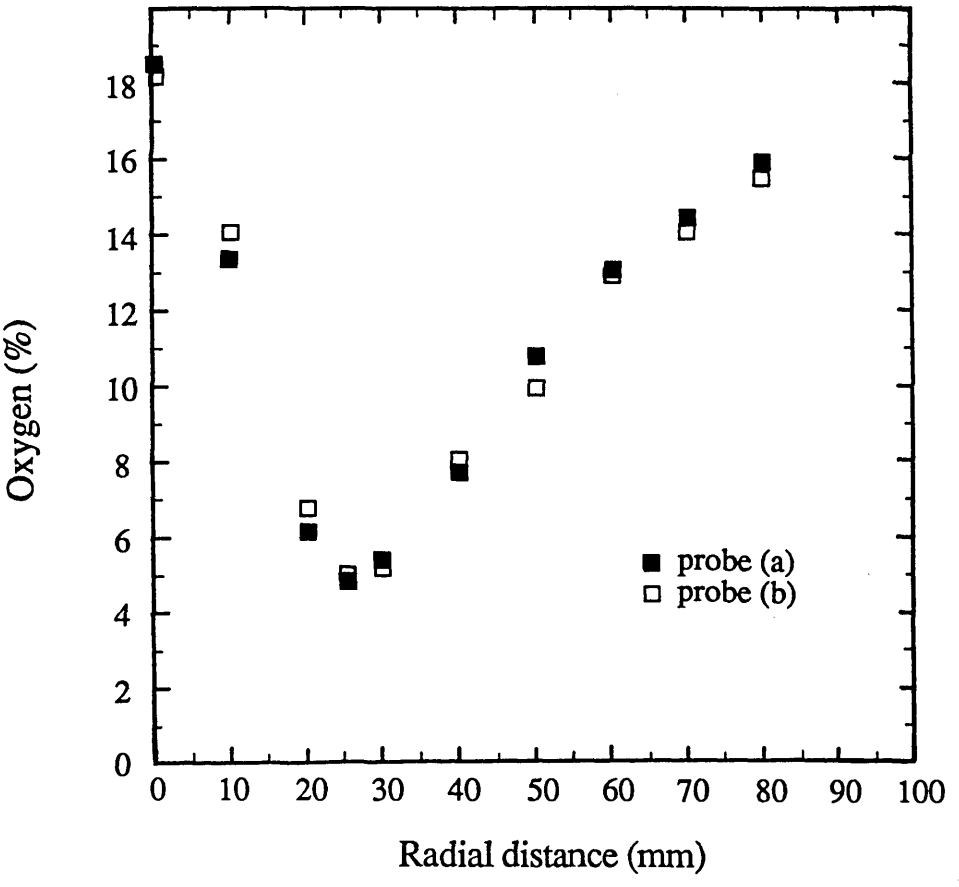

a

Fig. (3.5) Effect of different probes on the concentration measurements.

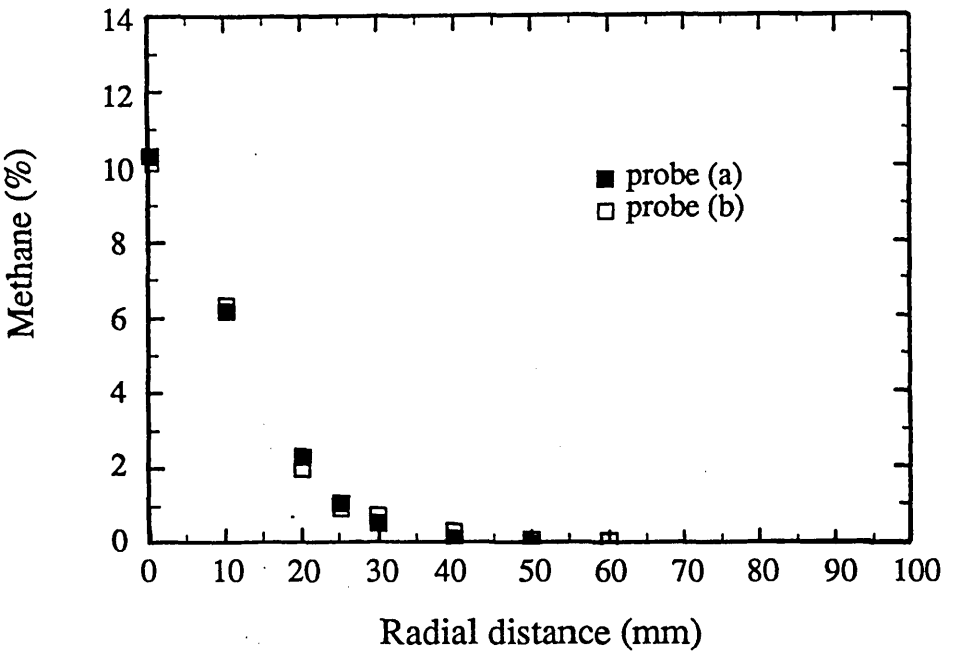
Methane (%)
14
12
10
8
6
4
2
0
0 10 20 30 40 50 60 70 80 90 100
Radial distance (mm)
probe (a)
probe (b)

d

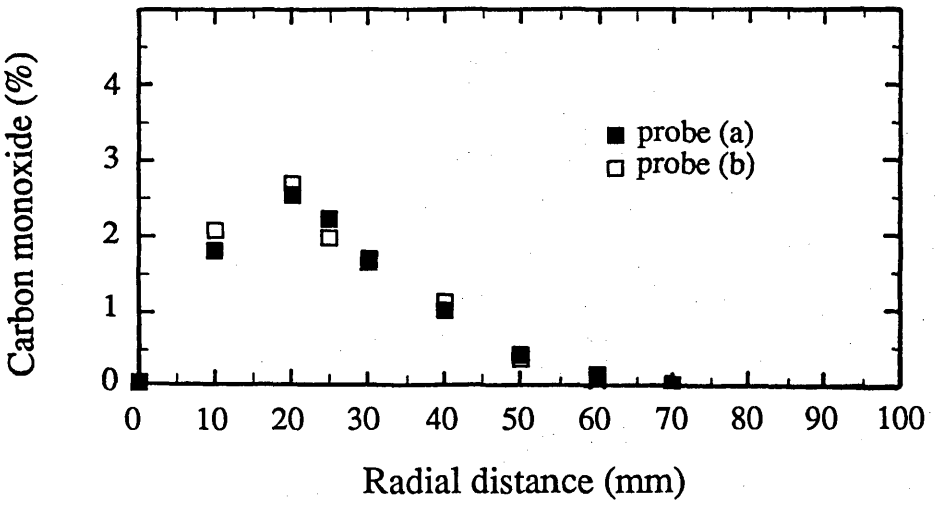
Carbon monoxide (%)
4
3
2
1
0
0 10 20 30 40 50 60 70 80 90 100
Radial distance (mm)
probe (a)
probe (b)

c

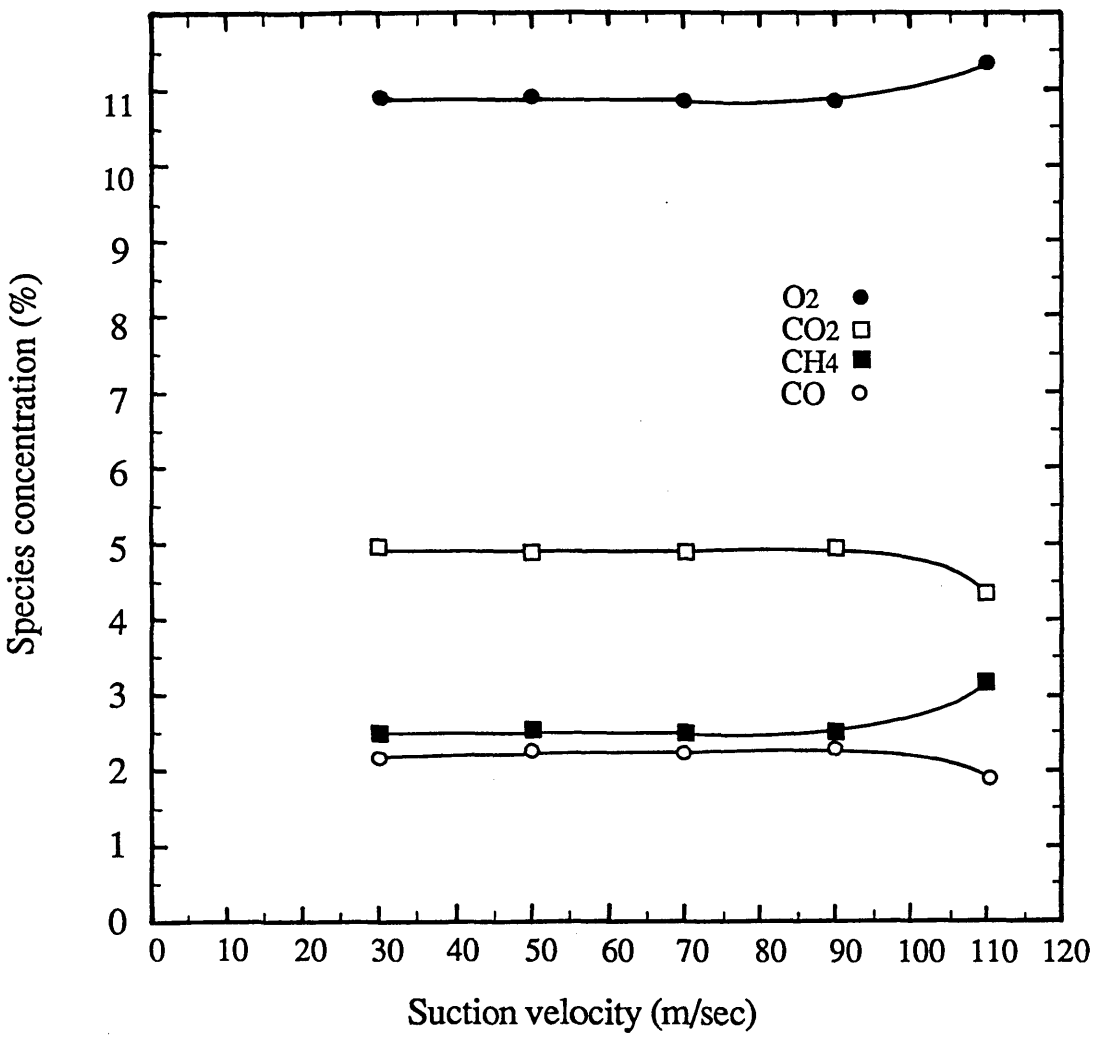

Fig. (3.6) Effect of suction velocity on the concentration measurements.

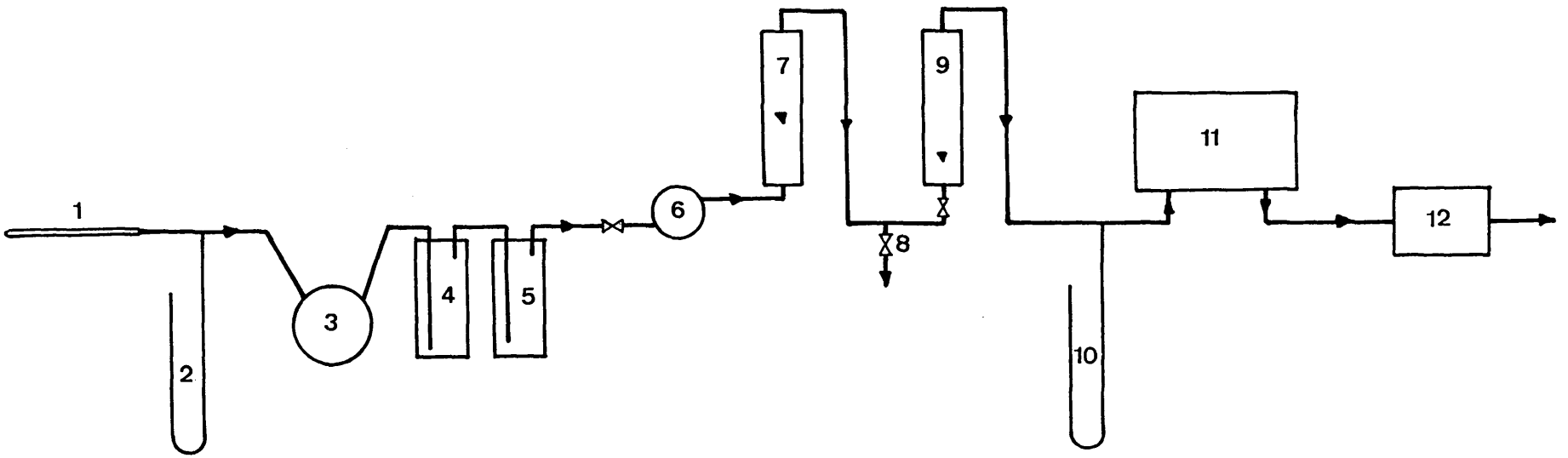

1- sampling probe
2- mercury manometer
3- condenser
4- dryer
5- ice path
6- suction pump
7- flowmeter
8- by-pass valve
9- G.C. flowmeter
10- water manometer
11- gas chromatographer
12- oxygen analyzer

Fig. (3.7) Layout of the sampling line.

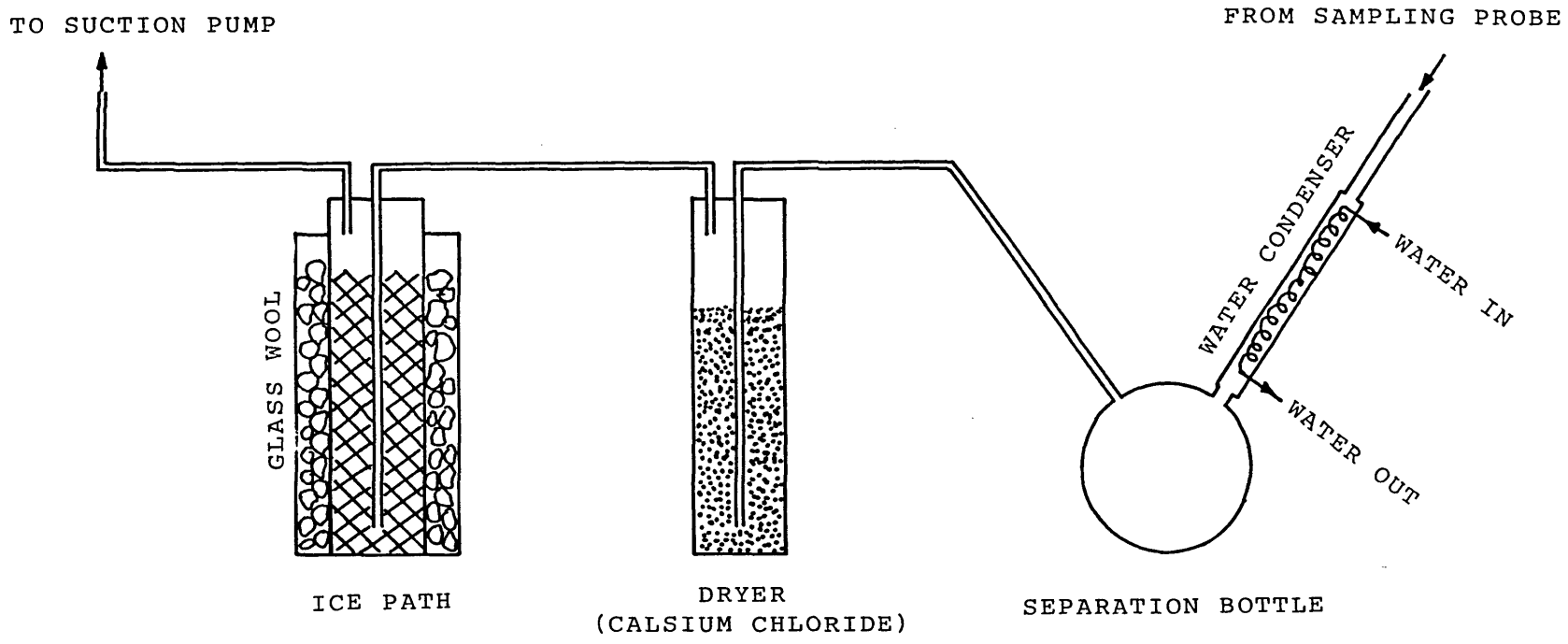

Fig. (3.8) Drying line.

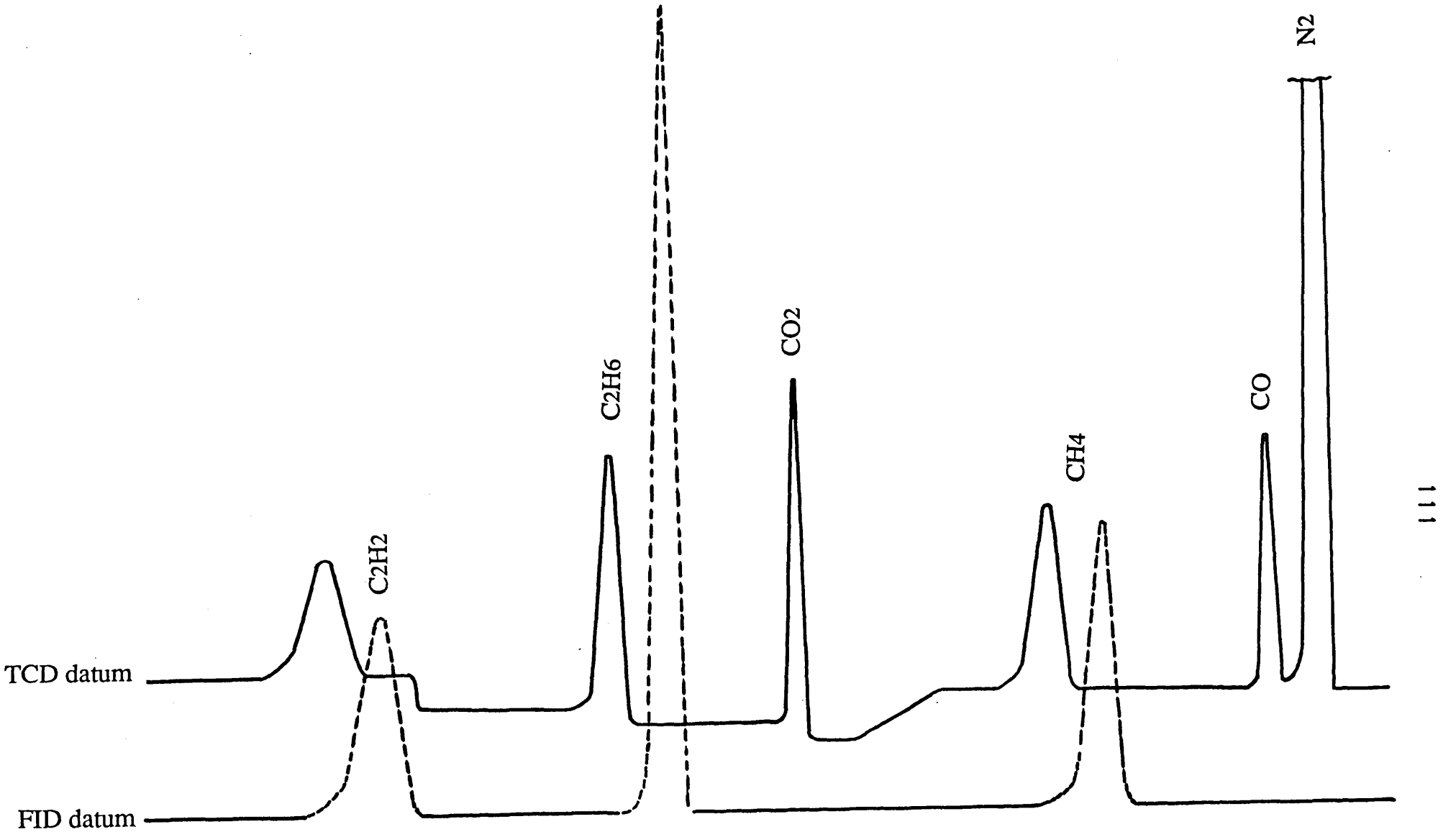

Fig. (3.9) Typical chromatogram.

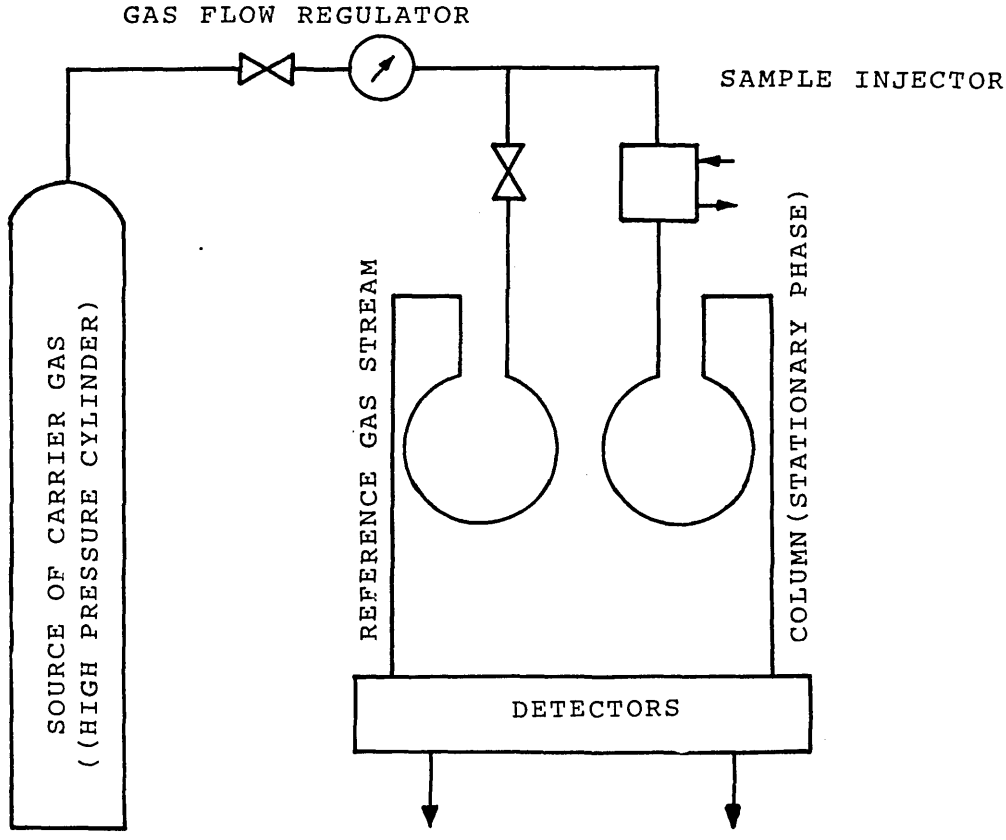

Fig. (3.10) Gas chromatographer.

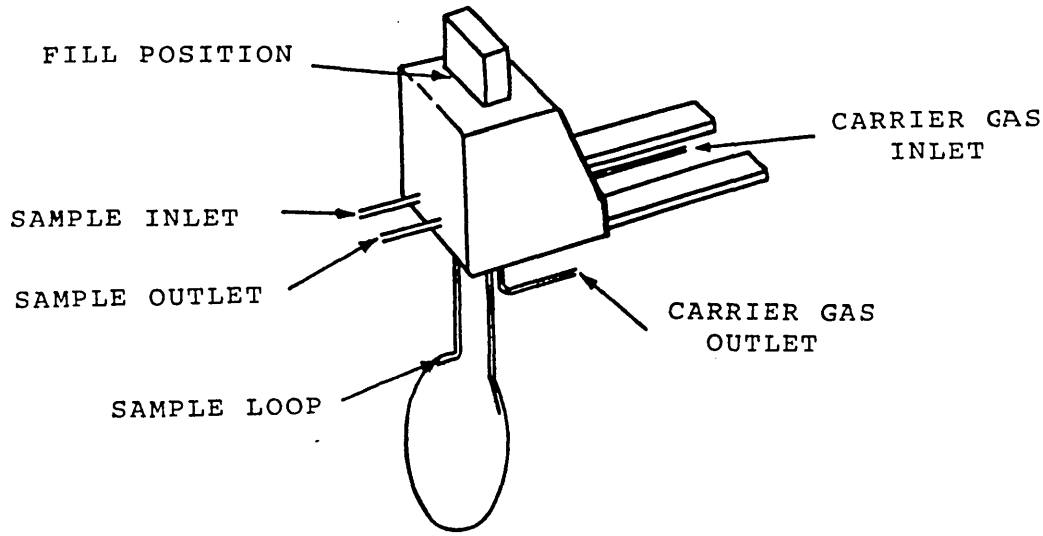

(a) SAMPLE INJECTOR

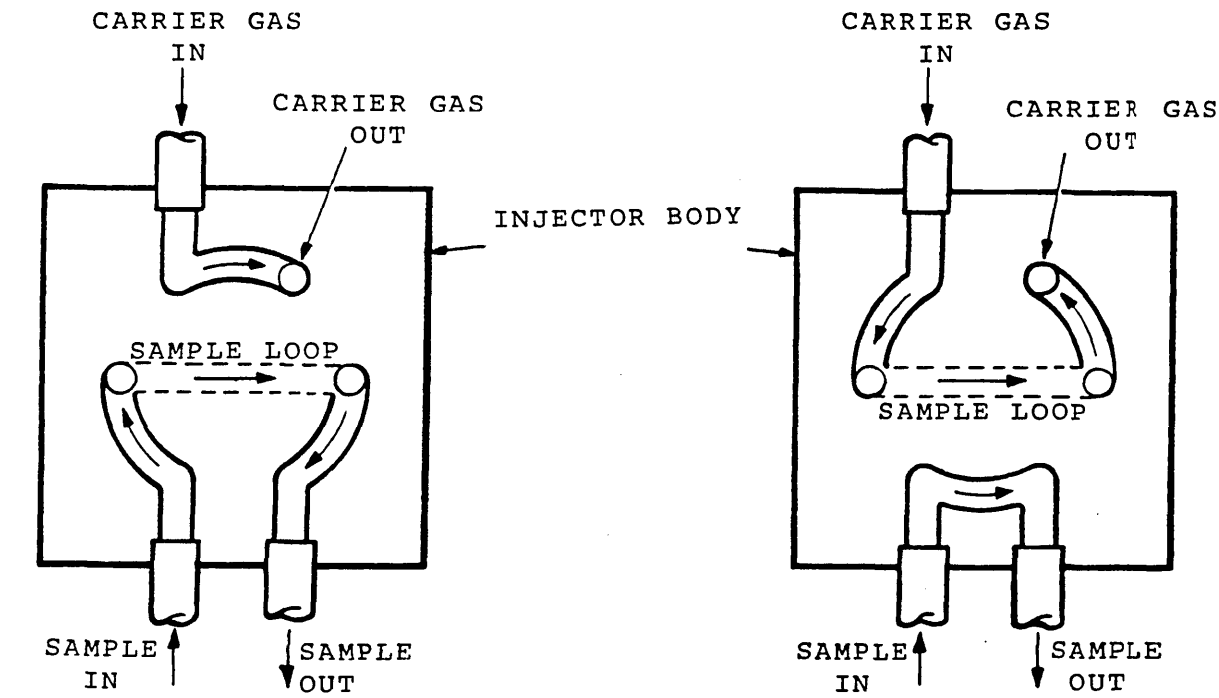

(b) FILL POSITION

(c) INJECTION POSITION

Fig. (3.11) Sampling injector.

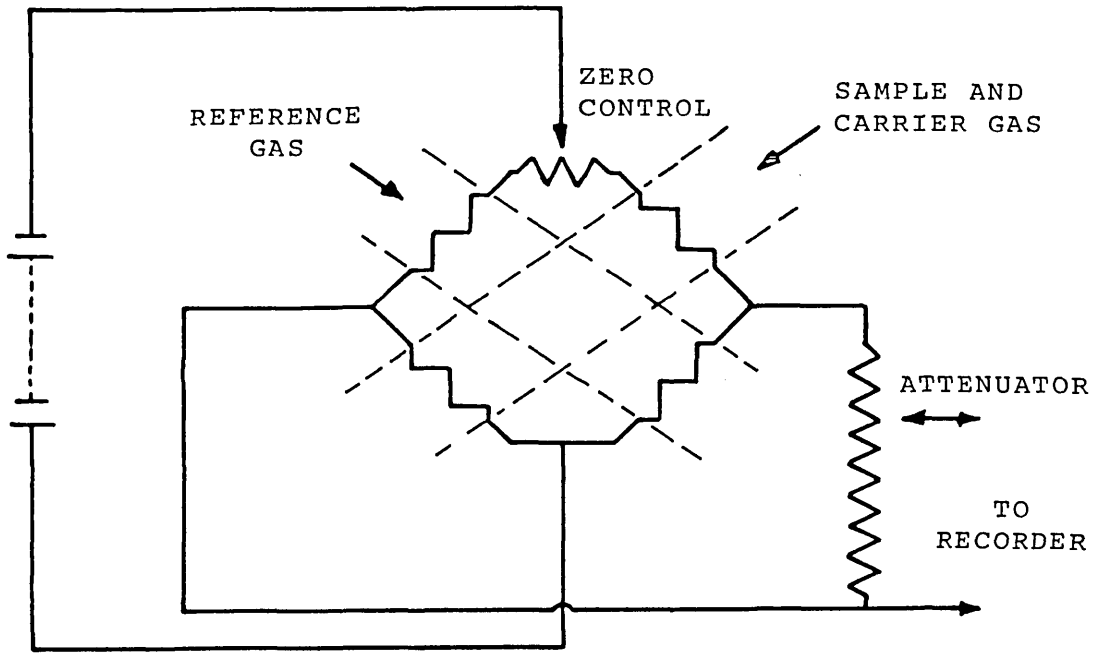

Fig. (3.12) Thermal conductivity detector.

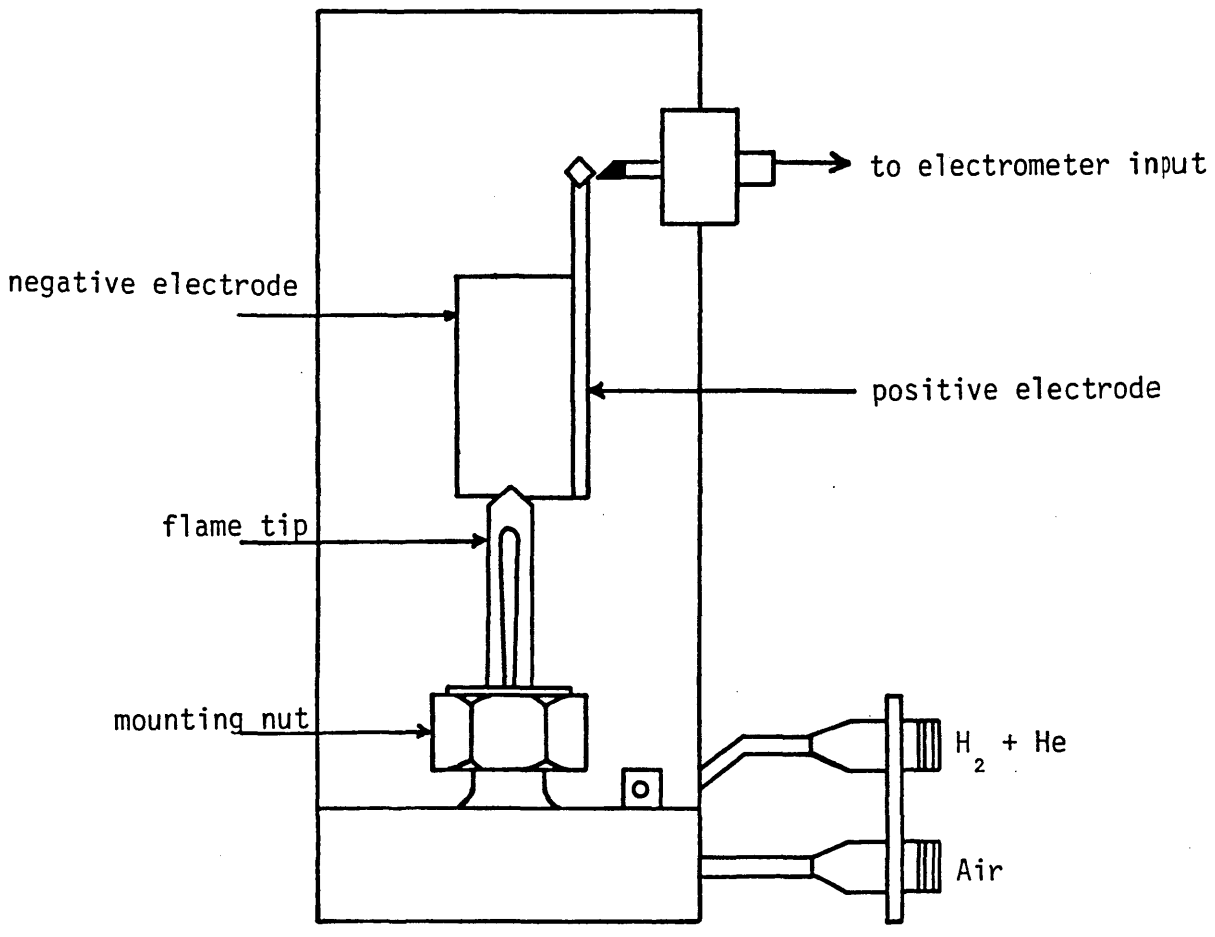

Fig. (3.13) Flame ionization detector.

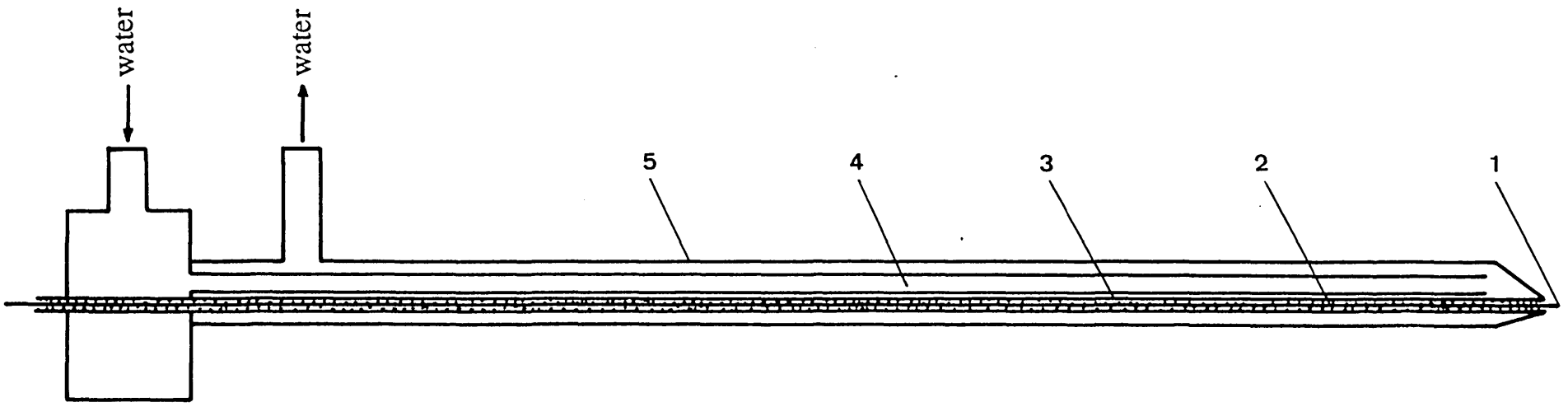

(1) platinum wire (sensor) 0.1mm
(2) ceramic tube (insulator) 0.2mmx0.8mm
(3) stainless steel tube 0.9mmx1.6mm
(4) stainless steel tube 1.3mmx2.0mm
(5) probe body (stainless steel) 4.0mmx5.0mm

Fig. (3.14) Ionization probe.

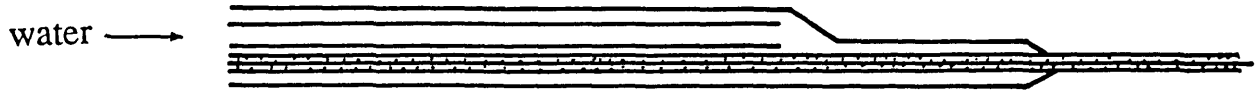

a

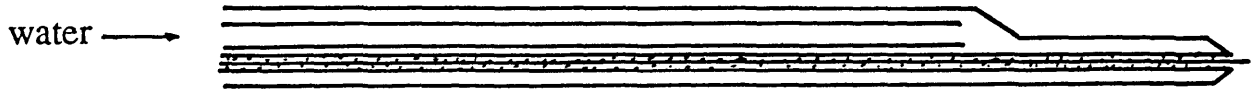

b

Fig. (3.15) Ionization probe (preliminary design)

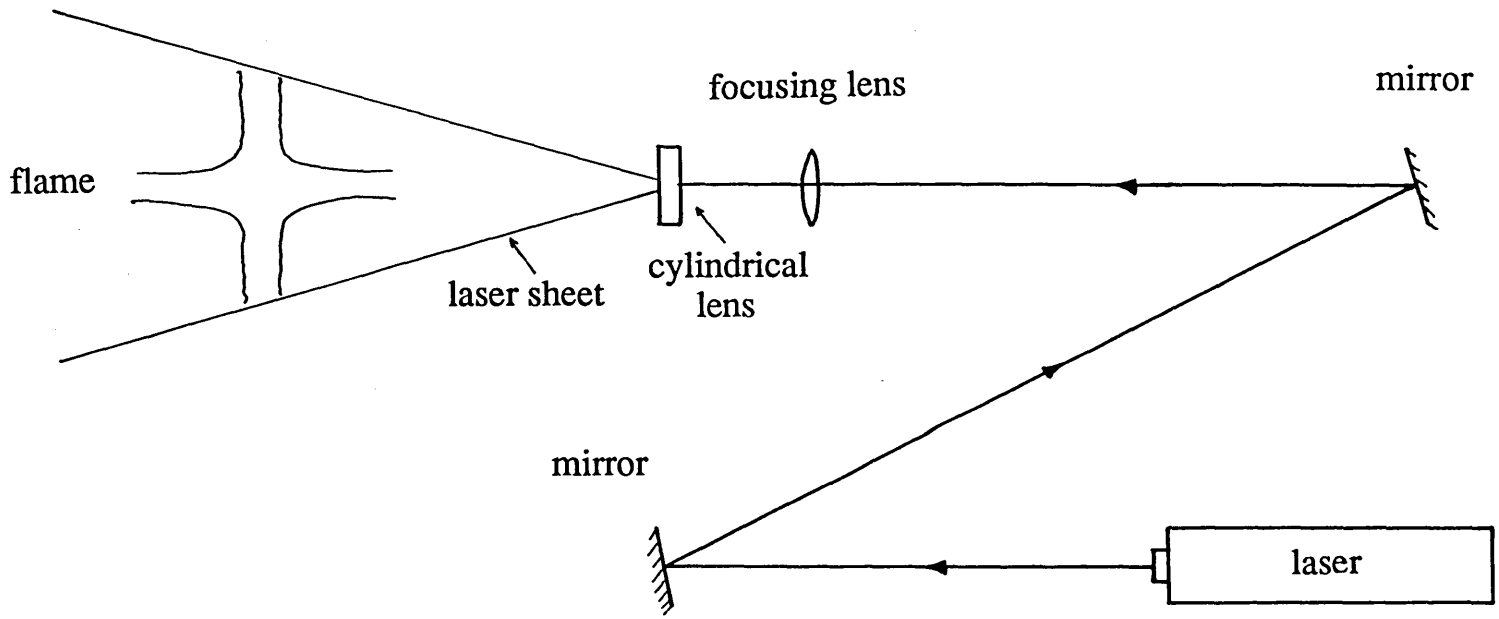

Fig. (3.16) Laser sheet technique.

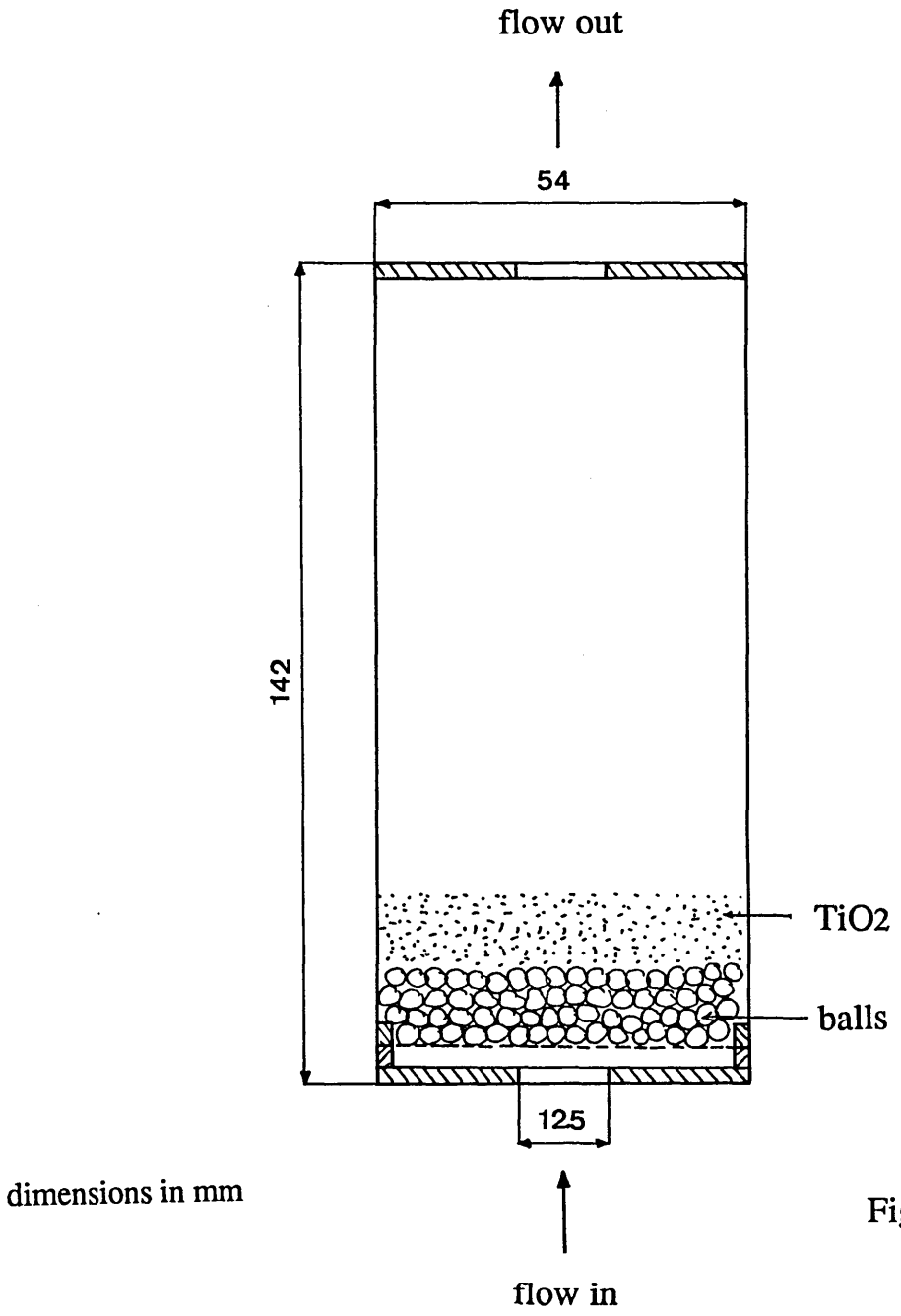

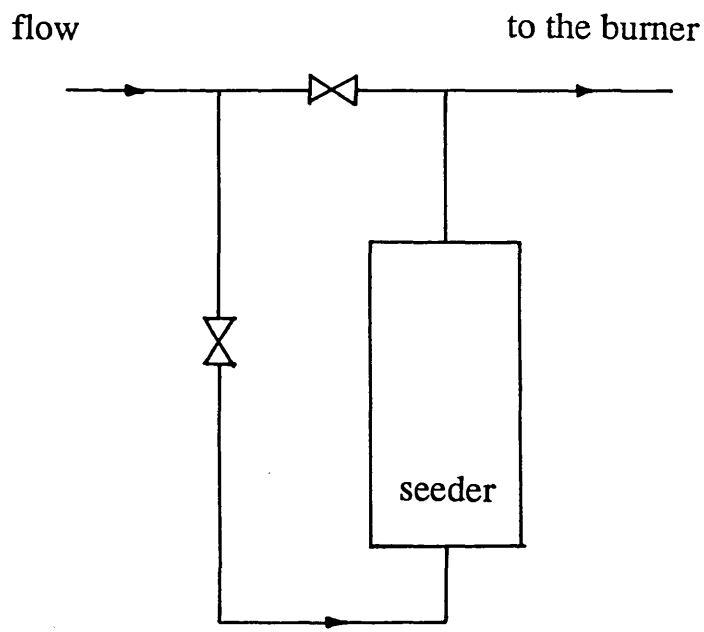

Fig. (3.17) Fluidized bed.

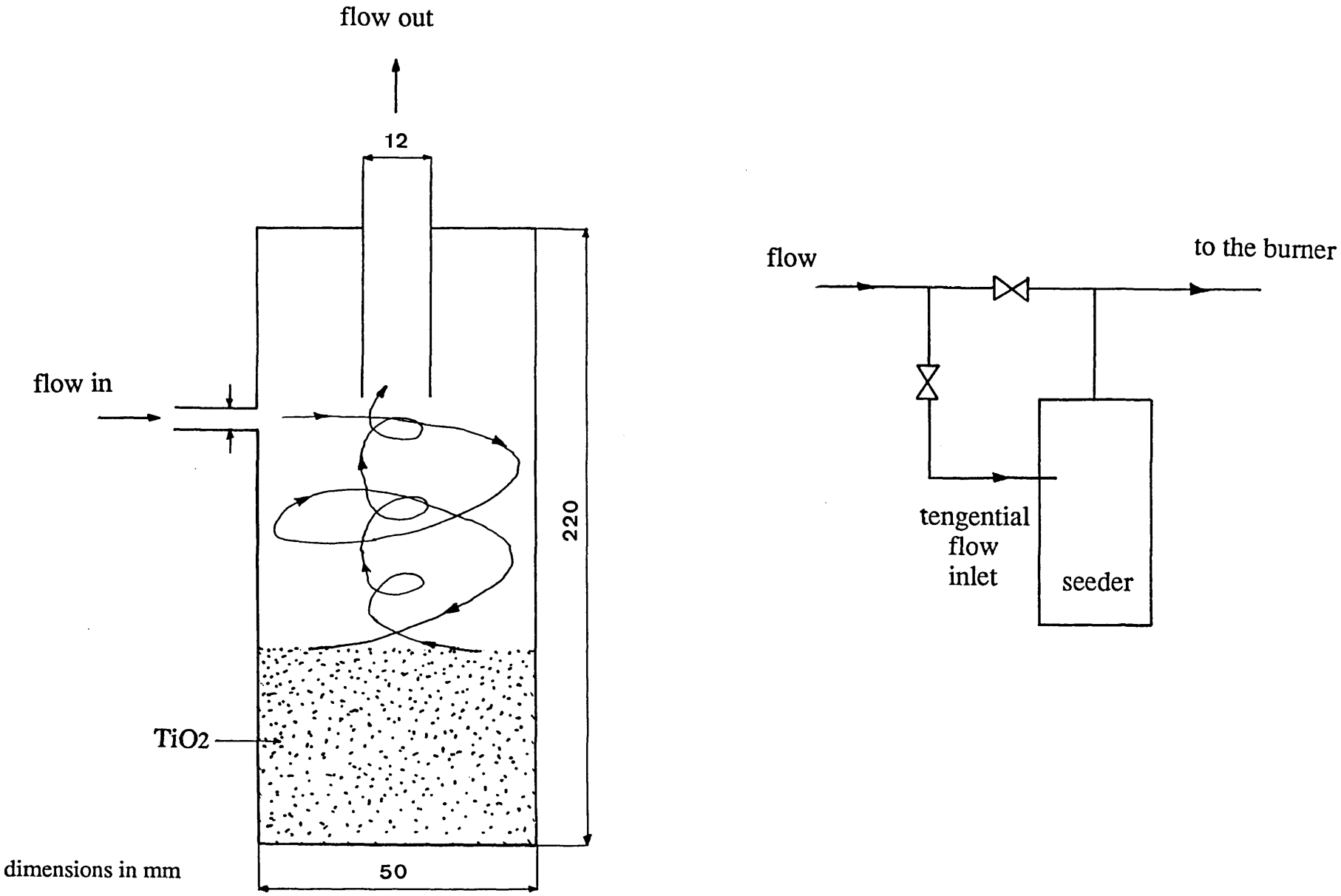

Fig. (3.18) Cyclone aerosol generator.

CHAPTER 4

PRESENTATION AND DISCUSSION OF EXPERIMENTAL RESULTS

4.1 Introduction

This chapter presents and discusses the experimental results obtained in the present study of counterflow and single flames. In the case of the counterflow flame, results include measurements of mean axial and radial temperature profiles as well as of axial and radial ion-current profiles. Measurements of mean species concentration are carried out in the radial direction only. The results also include, in the case of single flame, measurements of mean axial temperature profiles in order to help in delineating the run conditions for the case of counterflow flame. Photographs have been taken for the single flame case for a wide range of Reynolds numbers and equivalence ratios.

The remaider of this chapter is contained in seven sections. Section (4.2) concerns the single flame study. Characterization of the flame studied is provided in section (4.3). Section (4.4) provides and discusses the detailed results performed in the counterflow flames in order to check the repeatability of the measurements and the flame symmetry. The general behaviour of the counterflow flame is presented in section (4.5). Section

(4.6) discusses the effect of burner separation on the counterflow measurements. Section (4.7) deals with the effect of Reynolds number and equivalence ratio. Extinction limits for the counterflow flame are presented in section (4.8), for differing operating conditions.

4.2 Single Flame Study

This section presents and discusses those experimental results carried out in a free jet single flame in order to delineate the run conditions for the case of the counterflow flame. The results include axial mean temperature profiles as well as photographs of the flame. The effects of Reynolds number and equivalence ratio on the structure of a single flame are presented and discussed as they play the main roles in the combustion system as independent parameters.

The single flame run conditions are specified in table (4.1). Natural gas is used in the present study and its physical properties and chemical compositions are given in table (2.1). Before commencing the tests (measurements), the flame studied was run until steady state conditions were reached. The lower burner was used because of the buoyancy effects.

Although a jet flow becomes turbulent in the conventional sense if its Reynolds number is higher than (3000), modellers and

experimentalists use flow with Reynolds number higher than this value in order to ensure that the flow is fully turbulent since this is the basis for several of the assumptions of common turbulence models. In practice the maximum value of Reynolds number is limited by gas and air supply systems. The maximum Reynolds number used in the present study is (20000). Rich mixtures are used in the present experiment ($\Phi>1$), where Φ is the equivalence ratio. This ratio is equal to the fuel-air ratio of the mixture to the stoichiometric fuel-air ratio.

4.2.1 Characterization of the single flame

Structure studies of premixed flames show that temperature increase smoothly across them, together with the product concentration, whilst the concentration of fuel molecules decreases in a corresponding manner, Fig. (4.1a) illustrates typical profiles, see Barnard and Bradley (1985). Fig. (4.1b) shows the mean axial temperature profile in the present study of a single flame for Re=16000 and Φ=1.46. The figure indicates three zones of: (1) the cold and preheating zone, (2) the reaction zone and (3) the products zone.

An element of the flow can receive heat in two ways: either from the chemical reactions occuring within it or by conduction from neighbouring gas, Barnard and Bradley (1985). Referring to Fig. (4.1a),

two distinct regions can be recognized, separated by the point of inflexion of the temperature profile. Commencing at low temperature it can be seen that, for any given cross-section, the heat flow into the region due to conduction is greater than the corresponding heat loss because the gradient is greater on the high temperature side. Beyond the point of inflexion the converse is true, that is, the heat loss exeeds the heat gain. However, at this temperature the reaction rate has increased sufficiently for heat to be produced by chemical reaction. The temperature therefore continues to increase through the flame although at a progressively slower rate, and eventually reaches a constant value when all the fuel has been consumed and reaction ceases. As a result, the end of the cold and preheating zones can be identified at the point on the temperature profile where the maximum temperature gradient occurs, Li, Fig. (4.1a).

Plates (4.1) , a to e, show the structure of single flames for a wide range of Reynolds number and equivalence ratios and the cold inner core can be seen clearly from the photographs. Figures (4.2) to (4.5) show the axial mean temperature profiles for different Reynolds numbers and equivalence ratios. The results show that Li increases with increasing Reynolds number (at a fixed value of equivalence ratio) because increasing the nozzle exit velocity (or Re) decreases the residence time, therefore combustion starts further downstream in the axial direction. The results also show that Li increases with increasing the equivalence ratio (at a fixed

value of Reynolds number) by moving the point at which the combustion starts downstream in the axial direction through which the entrained air assists the combustion. The effect of the equivalence ratio on Li is more pronounced than the effect of Reynolds number.The results of this experiment are summarized in figures (4.6) and (4.7). Photographs also show that the total height of the single flames is increased by increasing either the Reynolds number or the equivalence ratio.

4.2.2 Burner separation distance

A turbulent free jet flow initiates with a region of flow establishment, the so-called 'potential core' (constant axial velocity equal to the discharge velocity from the nozzle), Fig. (4.8). This region extends to about 6.5 nozzle diameter (D) see, for example, Davies (1972). The velocity gradients in this region are high, near the peripheries of the jet.

Trials were made for two flames impinging on each other for varying separation distances, see Fig. (4.9), in order to find the optimum positions for which steady and symmetric counterflow flames exist. It was found that, if the separation distance, H, is less than 13 D (H/2 <6.5D) the counterflow flame was found to oscillate around the physical stagnation plane. The separation distance in the present study is 20 cm (H/2=7.3D). From the results of the characterization of the single flame

and the burner separation distance studies, the run conditions for the counterflow flame can be determined.

4.3 Characterization of The flame Studied

Interaction between jets occurs if the jets impinge on each other. Figure (4.10) shows two opposing premixed jets with the same equivalence ratio and burner exit velocities. The figure shows that, for constant equivalence ratio and burner separation distance, four different flames can exist depending on the burner exit velocity. These flames are:

(1) two separated flames in which no interaction takes place between them with neither of them being affected by the removal of the other,

(2) two interacting flames, with the interaction occuring either in the reaction zone or the products zone of each flame. In this kind of interaction combustion is initiated prior to the plane of interaction,

(3) two interacting jets of unburned combustible gases. Combustion takes place downstream in the radial direction, and

(4) two flames separated by an extinction zone where no thermal or concentration interaction between the flames occurs.

For condition (4), removing one of the jets affects the other one, see Fig.(4.11).

The present study of the counterflow flame mainly concerns the third case, in which two combustible gases impinge on each other and combustion occurs downstream in the radial direction, plate (4.2). This flame is chosen in order to study the effect of a uniform strain field on two opposed premixed jets. All the radial profile measurements are performed in the stagnation plane of the counterflow flame. The axial profile measurements are performed at different radial distances, commencing at 2 cm from the burner axis, since closer to the burner axis the probe (thermocouple, quartz microprobe or ionization probe) acts as a flame holder.

4.4 Repeatability and Flame Symmetry

This section reports on the repeatability of the measurements carried out in the counterflow flame as well as on the measurements along and across the flame (radially and axially) which were performed in order to check its symmetry. The measurements to ensure symmetry of the counterflow flame have been effected in two perpendicular radial directions in the stagnation plane in order to check radial symmetry, and across the stagnation plane at different radial positions to check for axial symmetry.

Temperature

Figure (4.12) shows the repeatability of the mean radial temperature measurements. Results indicate a maximum temperature difference of about (3%) at a distance of 12mm (0.9D) from the burner axis, where the maximum temperature occurs. Also a difference of about (3%) is found downstream of the flame, where the effect of entrained air is pronounced.

Figure (4.13) presents the radial symmetry of the counterflow flame with the mean temperature measurements. Results show that the radial temperature profiles are symmetric in the radial directions of the counterflow flame. Figures (4.14) and (4.15) reveal good axial symmetry of the counterflow flame. The results show that the temperature profiles are symmetrically distributed in the present counterflow flame in both the radial direction and across the stagnation plane.

Species concentration

The results of the repeatability trials for the radial concentration profiles of O_2, CO_2, CH_4 and CO are shown in Fig. (4.16). A maximum O_2 concentration difference is found upstream of the counterflow flame, in the unburnt gas side, of about (4.5%) at 10mm

(0.75D) from the burner axis and downstream of the counterflow flame, in the burnt gas side, of about (5%) at 60mm (4.4D) from the burner axis, Fig. (4.16a). Repeatability of the CO_2 concentration measurements, Fig. (4.16b), shows a maximum difference of about (4.9%) at the location of maximum CO_2. Figure (4.16c) presents the repeatability of the CH_4 concentration and shows a maximum difference of about (5%) at a distance of 10mm (0.75D) from the burner axis, in the unburnt gas side. The CO repeatability, Fig. (4.16d), shows a maximum difference of about (8%) at the location of maximum CO.

Ion current

Figure (4.17) shows the repeatability of the ion-current measurements carried out in the counterflow flame. Again, the maximum disparity in the ion-current repeatability takes place in the unburnt gas side, through where the maximum ion-currents occur. The maximum difference was found to be about (4.7%) at a distance of 10 mm from the burner axis.

The radial symmetry of the ion-current in the counterflow flame has been checked for two different run conditions as shown in Fig. (4.18). The results show that the radial ion-current profiles are symmetric in the radial direction, excepting a slight difference at the location where the maximum ion-current occurs. Figures (4.19) and (4.20) present the axial

profiles of the ion-current carried out above and below the stagnation plane at different radial positions and for two different running conditions. As expected the axial ion-current profiles are found to be symmetric across the stagnation plane.

4.5 Counterflow Flame General Behaviour

Figure (4.21) shows the radial profiles of mean temperature, main species concentration, and mean ion current in the counterflow flame. The radial temperature profile shows a certain distance over which no temperature change occurs (no combustion). This is followed by a rapid increase in temperature due to combustion which is further followed by a round off maximum, round off minimum and then a temperature increase again producing another maximum and then a slight decline before reducing downstream in the burnt gas side.The temperature drop separating the two maxima can be explained from plate (4.3). The plate shows two impinging air jets (photograph by using the laser sheet technique). It is found that as the two jets impinge each other a minimum thickness, δ_{min}, in the radial direction exists and the effect of the entrained air can be pronounced within this position. Therefore the temperature drop exists because of the entrainment of air, then after mixing with the unburned gases the temperature increases again.

Figure (4.21) also shows the radial profiles of O_2, CO, CH_4 and CO_2 concentration. The results show that O2 decreases in the unburnt gas side to a minimum value and increases in the burnt gas side. It also shows that the maximum value of CO_2 concentration occurs at the same radial distance, where the minimum value of O_2 occurs. The CO profile shows an increase in the unburnt gas side with a maximum value, decreasing towards zero in the burnt gas side. One may also see that the CO maximum occurs before maximum CO_2, which can be explained by the fact that CO exists before the existance of CO_2. The CH_4 profile shows a decay towards zero.

The ion-current profile shows a certain distance over which no ions exist, a rapid increase in ion current on the unburnt gas side where combustion takes place, and a decrease on the burnt gas side. Figure (4.21) reveals that the measurements of mean temperature, species concentration and ion current follow similar trends and give a good picture for the reaction field of counterflow flames. Because the two jets impinge each other within the cold zone, it is found that combustion takes place at a radial distance of about D/2.

4.6 Burner Separation Distance

In the present experimental study for the counterflow case,the burner separation distance was set normally at 20 cm (H/2 =7.3D), a value which was found to maintain the counterflow flame symmetrically positioned on the physical stagnation plane. In addition, measurements of, temperature, species concentration and ion current were carried out for another two separation distances, 10 cm (H/2 =3.7D) and 30 cm (H/2 =11D) and these will be compared with those results performed in the case of H= 20 cm when studying the effect of burner separation distance on the measurements. The Reynolds number and equivalence ratio were kept constant and equal to 20000 and 1.78 respectively, values which ensured that, at these separation distances, the two jets impinge each other within the cold zone.

Figure (4.22) shows the mean radial temperature profiles for the different separation distances. The results show that the behaviour of the radial temperature profiles is the same for the three cases. A round off minimum occurring at the same radial distance, r_m, where the minimum thickness, δ_{min}, exists. The temperature drop at this distance increases with decreasing separation distance. This is because the total strain rate applied on the flame increases, Kotsiuk et al (1988):

$$a_T = 2V_o/H + \text{const. } V_o^{1.5}. \qquad (4.1)$$

The two jets impinging each other with higher velocity, allows the air and fuel in the mixture to move downstream in the radial direction and reduces the amount of fuel to be burned within this distance, r_m. This procedure also causes the maximum temperature to occur further downstream in the radial direction with decreasing separation distance as shown in the figure The results also show that the maximum temperature is slightly increased by decreasing the separation distance which can be attributed to good mixing takes place between the entrained air and the gases in the counterflow flame where combustion is completing downstream as explained above.

Species concentration measurements of O_2, CO_2, CO and CH_4 for the three separation distances are shown in figures (4.23) to (4.26) repectively. In order to ensure measurements of the mean of the species concentration, the sampling probe (quartz microprobe) was kept for a period of more than 20 min at the measuring location in the counterflow flame. The results for the O_2 concentrations show that, by decreasing the separation distance, the reaction zone moved downstream in the radial direction.The minimum value of O_2 is found to be unaffected by the separation distance. Although the equivalence ratios for the three separation

distances are the same, the effect of entrained air on the O_2 distribution for the separation distance of 10 cm (r<30mm) is shown upstream of the flame, in the unburnt gas side, which matches with the temperature drop between the two temperature peaks.

The rate of reduction in the O_2 concentration is found to be decreased by decreasing the separation distance because the strain rate increases. Downstream of the flame, in the burnt gas side, the O_2 concentration is increased by increasing the separation distance because combustion initiates earlier. The location where the minimum value of the O_2 concentration occurs is shifted downstream in the radial direction by decreasing the separation distance.

The results for the CO_2 and CO concentrations, figures (4.24) and (4.25), show that the maximum values of CO2 and CO do not change with the burner separation distance. The maximum values of CO_2 are found to be at the same radial locations as those for the minimum values of O_2. The maximum CO always occurs at smaller radial distances than the corresponding ones for CO_2. The CH_4 profiles for the different separation distances are shown in Fig. (4.26). The results show that the rate of decay of

CH_4 decreases by decreasing the separation distance, a trend which matches that of O_2 and CO_2 profiles. Although the results show that CH_4 is consumed before CO, mesurements were carried out until the CO disappeared on the chromatogram (G.C).

Figure (4.27) shows the radial ion-current profiles for the three separation distances. The results of these measurements show that the rate of increase of ions in the unburnt gas side is almost the same, independent on the separation distance. The maximum ion current remains flatter for a certain radial distance and then reduces again in the burnt gas side. This behaviour indicates that the combustion intensity remains constant for a certain radial distance where the main product is CO. It is also revealed that the maximum value of ion current remains flatter for a longer radial distance when the separation distance is reduced. This is because the flame moves downstream in the radial direction when the separation distance is reduced .

4.7 Effect of Reynolds Number and Equivalence Ratio

4.7.1 Reynolds number

4.7.1.1 Radial measurements

The effect of Reynolds number on the counterflow flame length (radial direction) is shown in figures (4.28) to (4.33). Three

different Reynolds numbers are considered, 12000, 16000 and 20000, corresponding to burner exit velocities of 12.67, 16.9 and 21.12 m/sec respectively.The equivalence ratio is kept constant of 1.46. The calculations of the Reynolds number and the burner exit velocity are based on the mixture values of density and viscosity. Equation (4.1) shows that increasing Reynolds number or burner exit velocity increases the total strain rate applied to the counterflow flame.

Figure (4.28) shows the effect of the Reynolds number on the radial temperature profiles. The results show that increasing the Reynolds number causes the maximum temperature to move downstream in the radial direction as a consequence of the reduction in the residence time.The results also show that the maximum temperature value is unaffected when increasing Reynolds number.

The effect of Reynolds number on the radial profiles of O_2, CO_2, CO and CH_4 is shown in figures (4.29) to (4.32) respectively. From profiles of the O_2 measurements, Fig. (4.29), it can be seen that increasing the Reynolds number moves the flame downstream in the radial direction. The minimum value of O_2 is found to be unaffected by Reynolds number. The rate of decrease in the O_2 concentration upstream of the flame (in the unburnt gas side) is reduced by increasing the Reynolds number because of

the increase of the strain rate. Downstream of the flame (in the burnt gas side) the O_2 concentration increases with decreasing Reynolds number because of the effect of entrained air and because combustion is initiated earlier.

The results for the CO_2 concentration, Fig. (4.30), show that the maximum value of CO_2 is not changed by increasing Reynolds number (as well as the minimum value of the O2 concentration). The maximum values of CO_2 are found to be at the same radial locations as those for the minimum values of O_2. Maximum CO values, Fig. (4.31), are always found to be at smaller radial distances than the corresponding CO_2 and O_2. Radial profiles of CH_4 for different Reynolds numbers are shown in Fig. (4.32). The results show that the rate of consumption of CH_4 decreases with increasing Reynolds number, which matches the behaviour shown by O_2, CO2 and CO profiles.

Figure (4.33) shows the radial ion-current profiles for an equivalence ratio of 1.46. These results show that the rate of increase of ions on the unburnt gas side increases with increasing Reynolds number because increasing the Reynolds number increases the velocity in the radial

direction and increases the strain rate, improving the mixing rate and as a consequence improving the combustion effiency. For the same reason, the maximum value of the ion current is found to increase with increasing Reynolds number, and the reaction zone length (radially) increases with increasing Reynolds number as shown in the figure as a result of the reduced residence time.

4.7.1.2 Axial measurements

Axial profile measurements are carried out commencing at 2 cm from the burner axis at 1 cm intervals up to 9 cm. Figures (4.34) and (4.35) show the axial profiles of mean temperature and mean ion current for Reynolds number of 12000, 16000 and 20000 respectively and for a constant equivalence ratio of 1.78. These results show that the thickness of the counterflow flame is unaffected when the Reynolds number is increased up to a radial distance of 30 mm (r/D = 2.2). Further downstream of this distance the thickness of the flame increases with increasing Reynolds number. This is because increasing the Reynolds number causes the flame to move downstream in the radial direction. Downstream of the flame the ion current decreases because of the increase in the flame thickness.

4.7.2 Equivalence ratio

4.7.2.1 Radial measurements

The effect of equivalence ratio on the counterflow flame is shown in figures (4.36) to (4.43). Three different equivalence ratios are considered, 1.24, 1.46 and 1.78. The Reynolds number is held constant at 20000. The method of calculation of the equivalence ratio is presented in Appendix 1. Radial temperature profiles for the three equivalence ratios are shown in Fig. (4.36). The results show that the temperature drop found between the two maxima decreases with decreasing equivalence ratio. This is because improved combustion is achieved by increasing the air in the mixture (or reducing the equivalence ratio) and most of the fuel in the mixture burns within the distance where the temperature drop occurs.The results also show that combustion initiates at smaller radial distances as the equivalence ratio is decreased because more air is supplied in the mixture. Downstream of the flame the temperature increases with increasing equivalence ratio because more fuel will be burnt for the mixture with higher equivalence ratios due to the entrained air.

Species concentration measurements of O_2, CO_2, CO and CH_4 for the different equivalence ratios are shown in figures (4.37) to (4.40) respectively. The O_2 concentration measurements, Fig. (4.37), show that

the rate of consumption of the O_2, upstream of the flame (on the unburnt gas side), increases with decreasing equivalence ratio because more fuel will be burnt within this region. On the burnt gas side, downstream of the flame, the O_2 concentration increases with decreasing equivalence ratio because most of the fuel in the mixture has been burnt and because of the entrained air effect. The results show also that the minimum value of O_2 is unaffected by the equivalence ratio. This behaviour is due to the fact that entrained air subistitutes the consumed oxygen for the greater equivalence ratio and thus alters the measured minimum value. The mechanism of the entrained air is governed by the shape of the flame, that is, more air is entrained into the flame with higher equivalence ratio. This is because flames of higher equivalence ratios have a more irregular flame structure, Suzuki and Hirano (1982).

Measurements of CO2 concentration, Fig. (4.38), show that the maximum value of CO2 does not change with the equivalence ratio in correspondence with the behaviour shown by the measurements of O_2 concentration. It can also be seen from the CO_2 profiles that with increasing equivalence ratio the location at which the maximum value of the CO_2 occurs is shifted downstream in the radial direction. In the burnt gas side, downstream of the flame, the CO_2 concentration increases with increasing

equivalence ratio, again following a mirror image of the O_2 profiles.

Figure (4.39) shows the CO concentration profiles for the three equivalence ratios.The results show that with increasing equivalence ratio (increasing fuel in the mixture) the maximum CO concentration is attained at greater radial distances. The CH_4 concentration profiles are shown in Fig. (4.40). It can be seen that with decreasing equivalence ratio CH_4 is, as expected, consumed earlier which matches the behaviour shown by the O_2 and CO_2 profiles upstream of the flame on the unburnt gas side.

The effect of equivalence ratio on the ion-current profiles is shown in Fig. (4.41). It can be observed that the maximum value of the ion current increases with decreasing equivalence ratio because more air is being supplied in the mixture, which alters the combustion efficiency. The results also show that upstream of the flame, on the unburnt gas side, the rate of increase of ion current increases with decreasing equivalence ratio because of the improvement in combustion. It is also seen that increasing the equivalence ratio shifts the flame further downstream in the radial direction, a behaviour which matches that of the temperature and species concentration.

4.7.2.2 Axial measurements

Figures (4.42) and (4.43) show the axial profiles of mean temperature and of mean ion current for equivalence ratios of 1.24, 1.46 and 1.78 respectively and for a constant Reynolds number of 20000. The results show that the thickness of the counterflow flame increases with increasing equivalence ratio. This is because increasing the equivalence ratio increases the amount of fuel to be burnt. Although high temperatures are observed downstream in the burnt gas side, no ions exist because most of the gases are product gases.

4.8 Extinction Limits

Because the degree of ionization is strongly related to intensity of the combustion reaction, Ahlheim and Gunther (1979), an ionization probe is used to identify extinction in the present study. Fig. (4.44) shows the radial ion-current profiles in the stagnation plane for a Reynolds number of 20000 (V_o=21.12 m/sec) and a burner separation distance of 20 cm. For different equivalence ratios, 0.54, 0.65 and 0.7. The results show that no ions exist in the stagnation plane for an equivalence ratio of 0.54 which means that the two opposed flames are at extinction. The results also show that with increasing equivalence ratio ions starts to exist in the stagnation plane and the maximum value increases with

increasing equivalence ratio.

The effect of burner separation on the burner exit velocity required to achieve extinction is shown in Fig. (4.45). The results show that this velocity increases with increasing separation distance due to the bulk straining and then remains constant independent of the separation distance due to the turbulent straining, see Kostiuk et al (1988). Figure (4.46) shows the effect of equivalence ratio on the burner exit velocity required for extinction. The results show that the burner exit velocity increases with increasing equivalence ratio. This is because increasing the equivalence ratio allows some of the fuel in the mixture to be burnt within the stagnation plane.

Figure (4.47) shows the results obtained when nitrogen is added to the fuel. Two conditions are shown: (1) fuel and nitrogen are introduced from both burners, and (2) air is introduced from the upper burner while fuel and nitrogen are introduced from the lower one. As expected, for the same fuel-nitrogen ratio, the velocity required to achieve extinction increases with increasing fuel in the mixture. The results also show that this velocity is always higher for the case of introducing fuel and nitrogen from the upper burner than that for the case of introducing air. This is because introducing fuel and nitrogen from the upper burner increases the amount of fuel to be burnt and as a consequence increases the velocity required to achieve extinction.

Table (4.1) Run conditions

Run	Mass flow rate (kg/hr)			Re	Φ	V (m/sec)
	Air	Gas	H2			
R1A1	14.597	1.1058	0.0058	12000	1.24	12.67
R1A2	14.279	1.2749	0.0058	12000	1.46	12.67
R1A3	13.836	1.5039	0.0058	12000	1.78	12.67
R2A1	17.028	1.29	0.0058	14000	1.24	14.79
R2A2	16.654	1.487	0.0058	14000	1.46	14.79
R2A3	16.146	1.755	0.0058	14000	1.78	14.79
R3A1	19.457	1.474	0.0058	16000	1.24	16.9
R3A2	19.04	1.7	0.0058	16000	1.46	16.9
R3A3	18.446	2.005	0.0058	16000	1.78	16.9
R4A1	21.899	1.659	0.0058	18000	1.24	19
R4A2	21.414	1.912	0.0058	18000	1.46	19
R4A3	20.755	2.256	0.0058	18000	1.78	19
R5A1	24.328	1.843	0.0058	20000	1.24	21.12
R5A2	23.8	2.215	0.0058	20000	1.46	21.12
R5A3	23.064	2.507	0.0058	20000	1.78	21.12

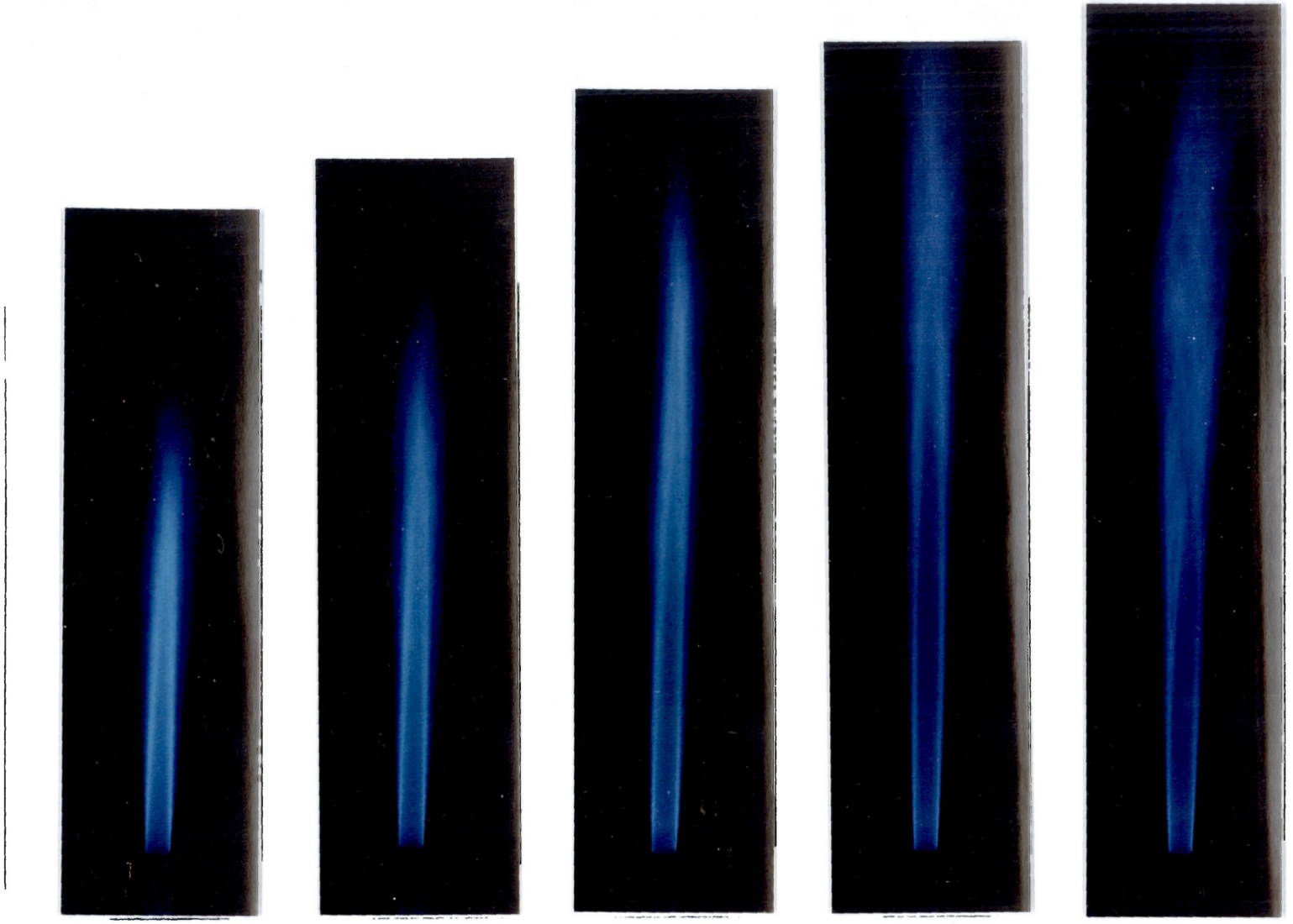

Φ=1.24 Φ=1.34 Φ=1.46 Φ=1.60 Φ=1.78

Plate (4.1) Photographs of single premixed flames.
(a) Re=20000

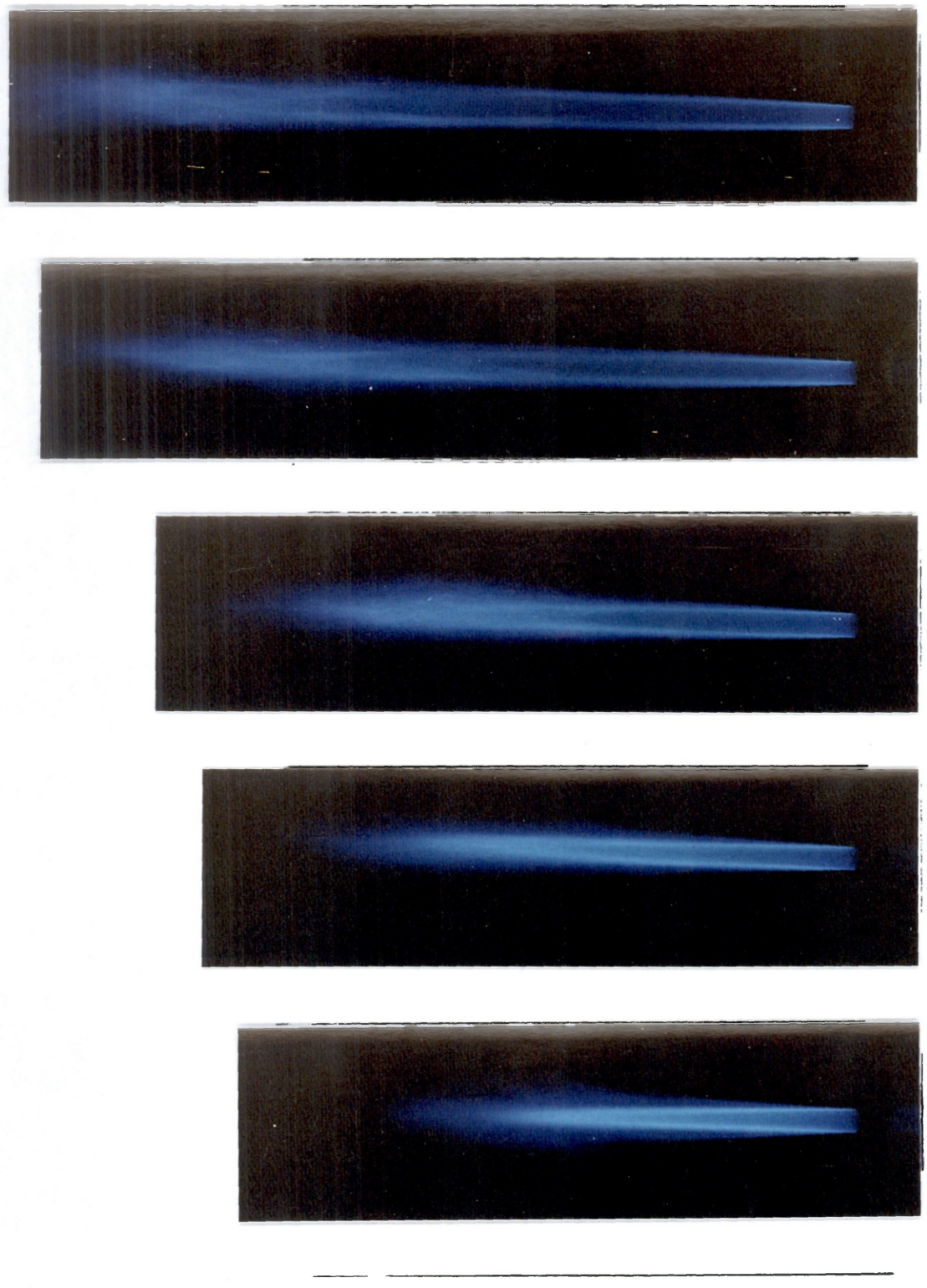

(b) Re=18000

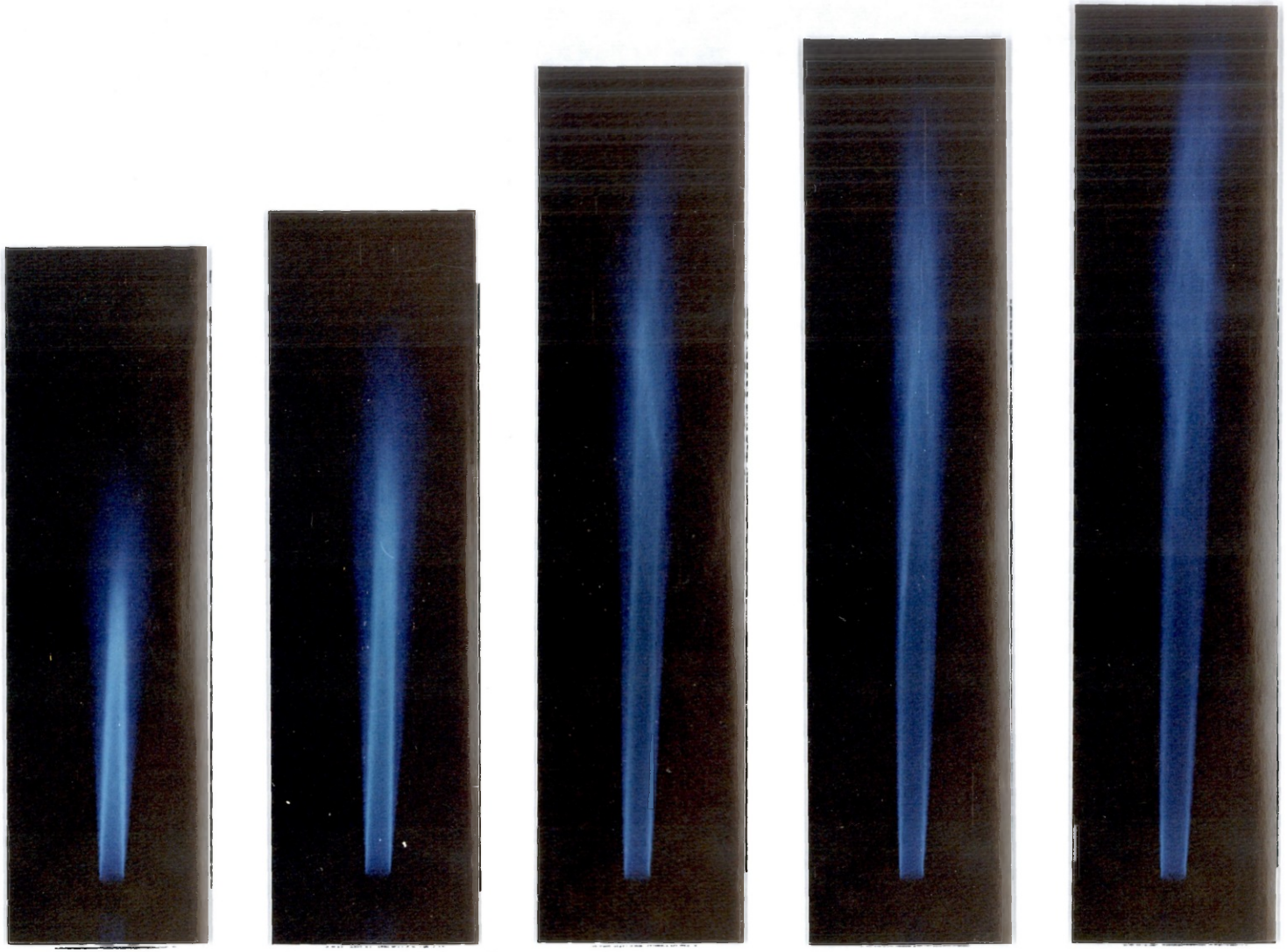

Φ=1.24 Φ=1.34 Φ=1.46 Φ=1.60 Φ=1.78

(c) Re=16000

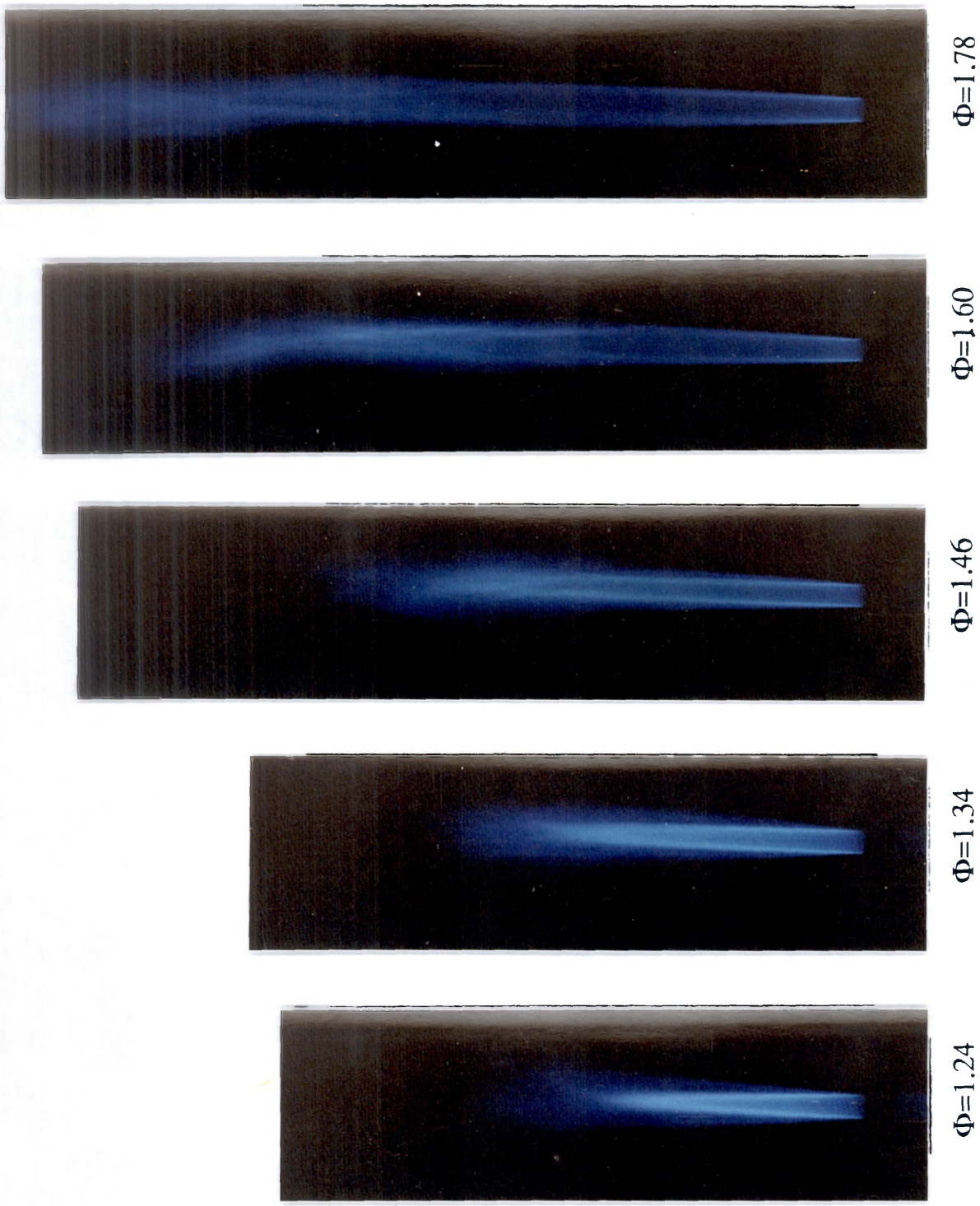

(d) Re=14000

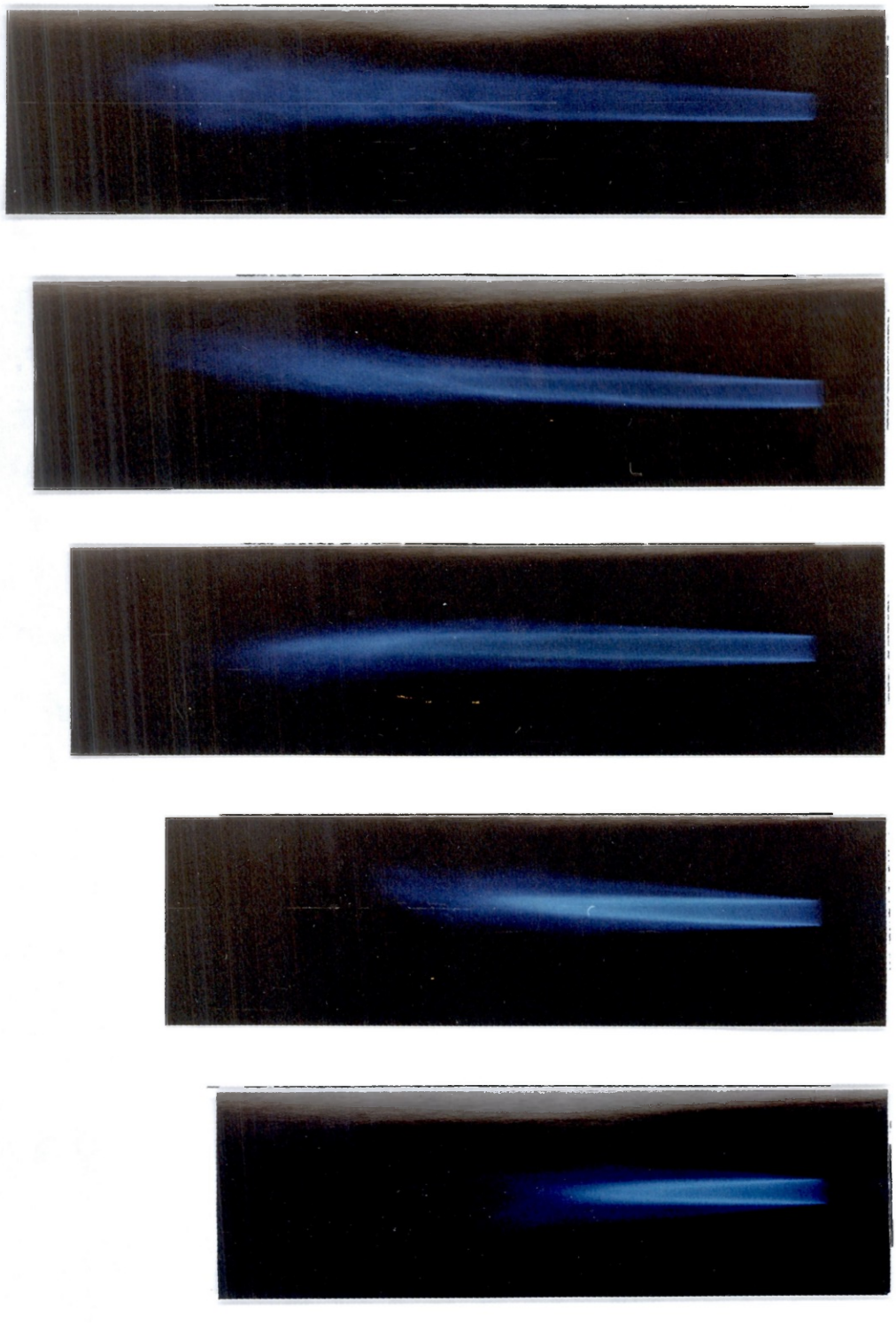

(e) Re=12000

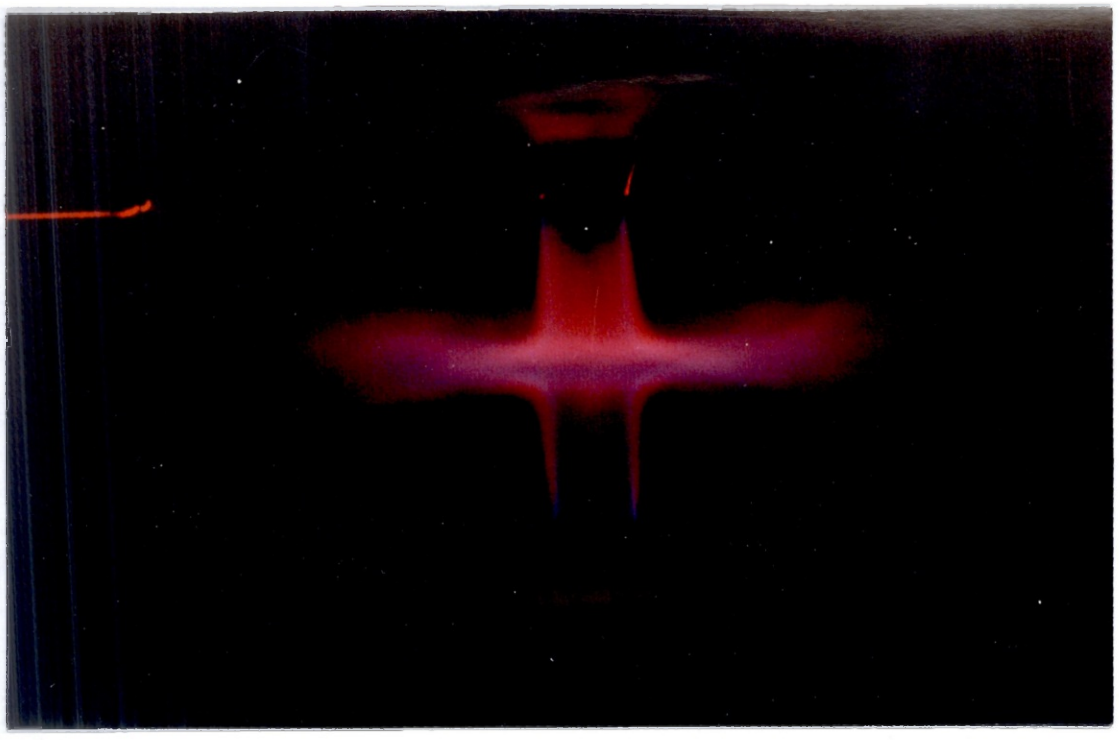

a

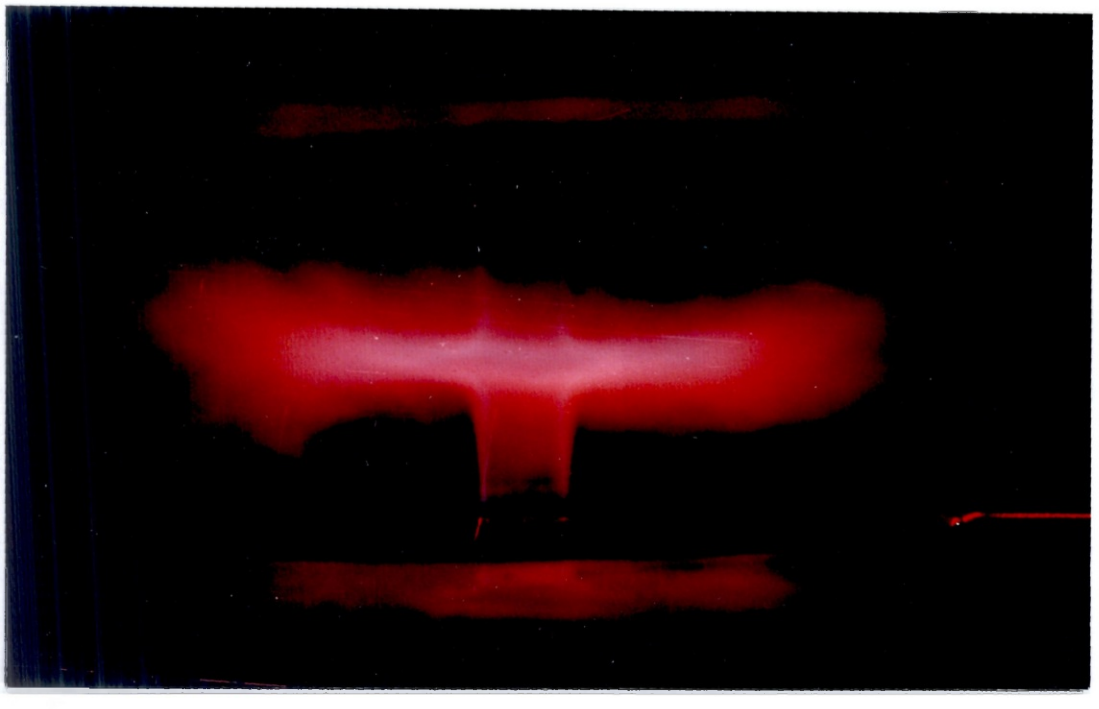

b

Plate (4.2) Two impinging jets of combustible gases.

(a) Re=16000 and Φ=0.71

(b) Re=16000 and Φ=1.03

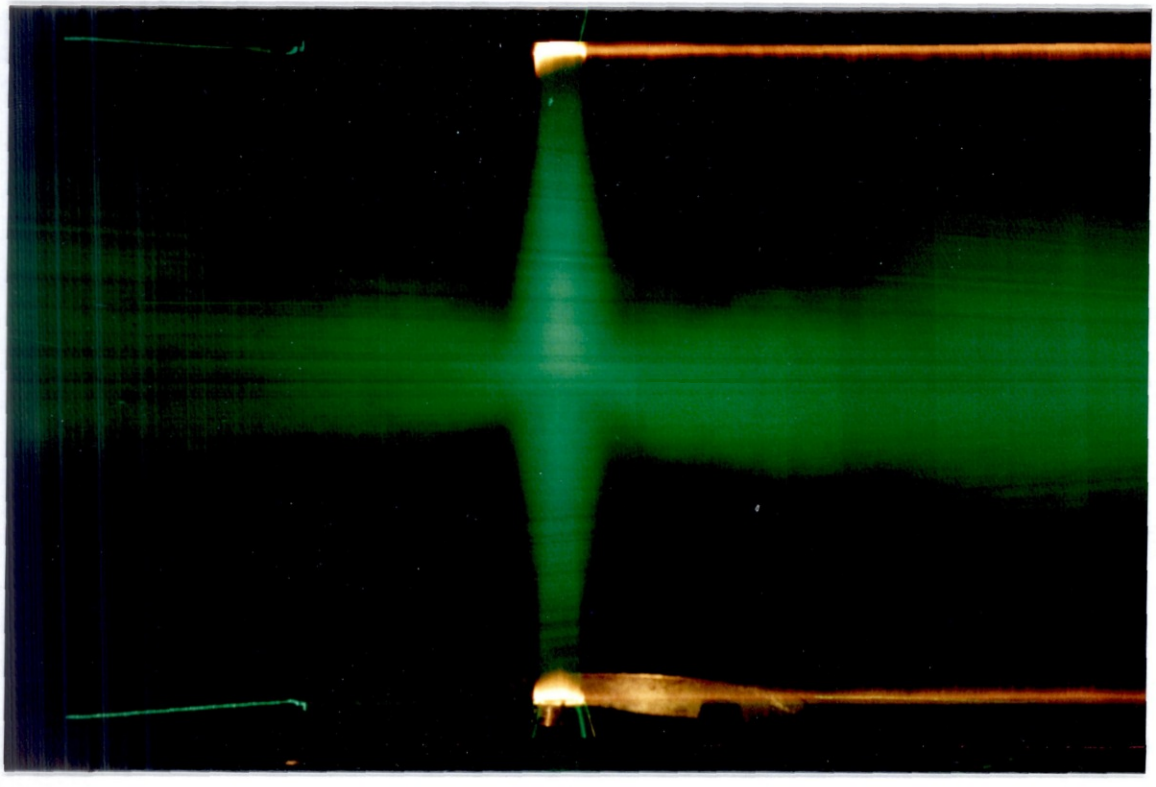

Plate (4.3) Two impinging air jets.

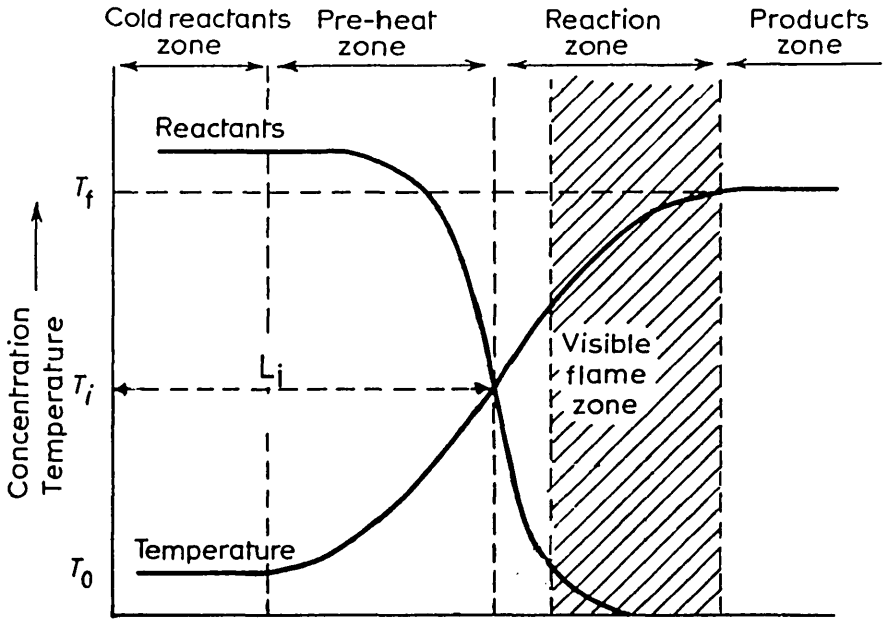

Fig. (4.1a) Concentration and temperature profiles through the premixed flame, after Barnard and Bradley (1985).

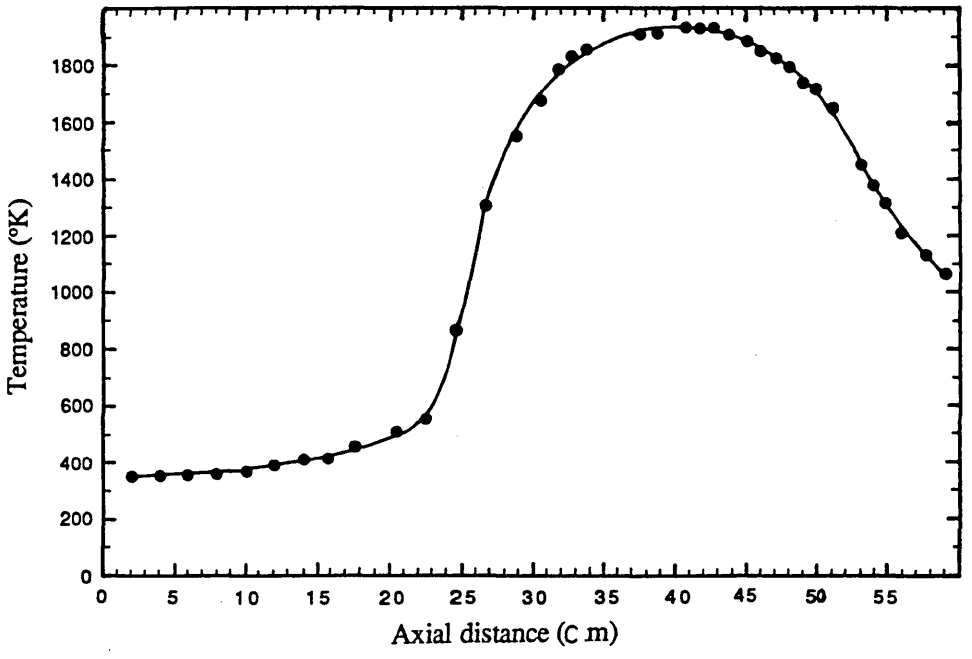

Fig. (4.1b) Axial mean temperature profile through the premixed flame for Re=16000 and Φ =1.46.

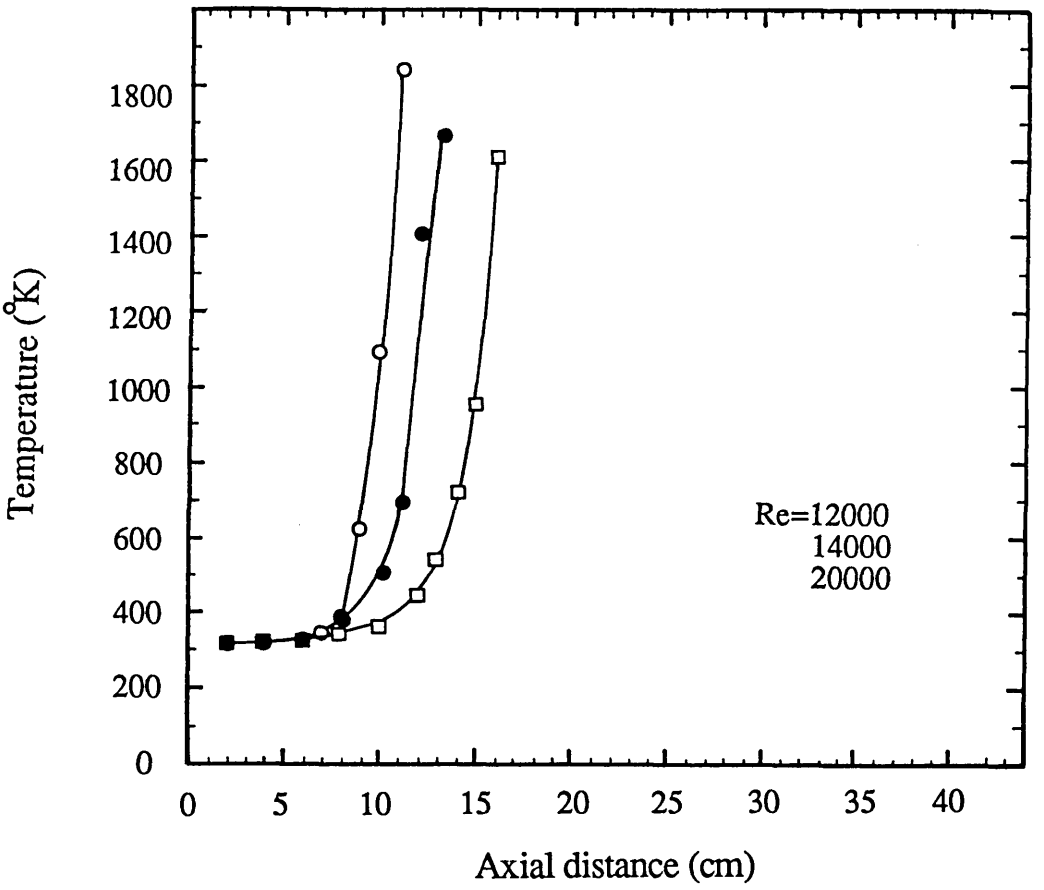

Fig. (4.2) Axial temperature profiles in the single flames for Φ=1.24.

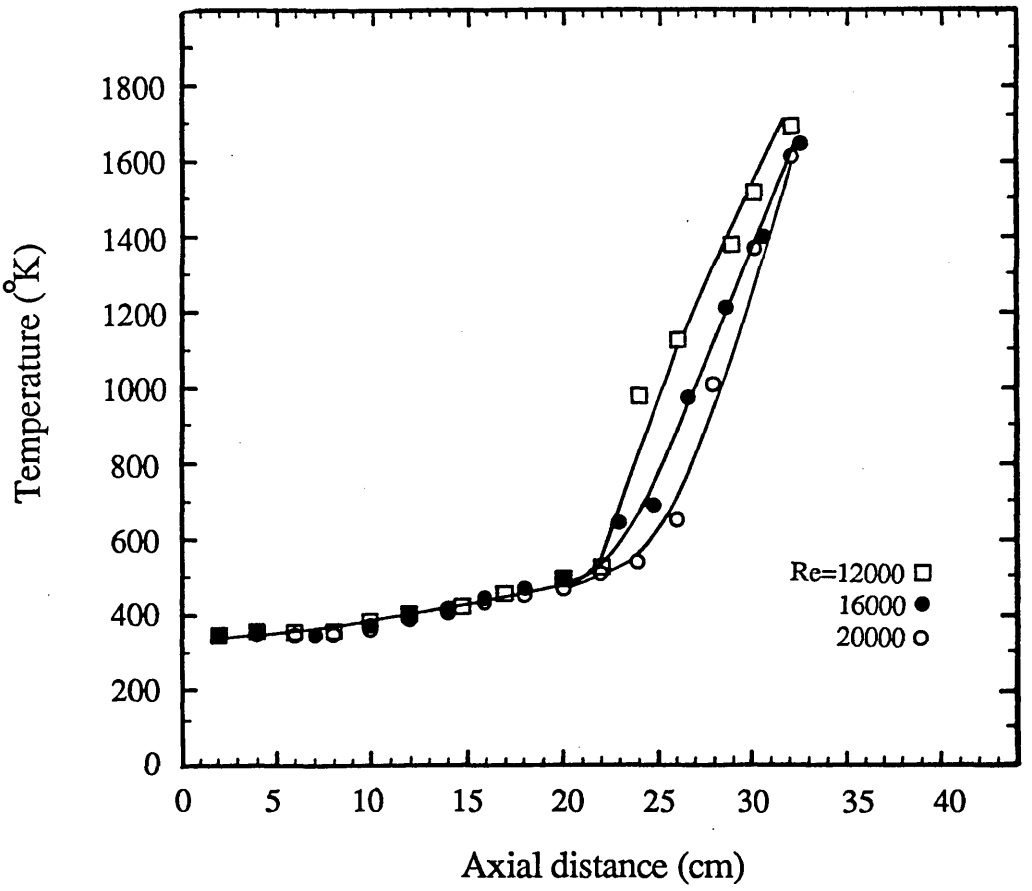

Fig. (4.3) Axial temperature profiles in the single flames for Φ=1.78.

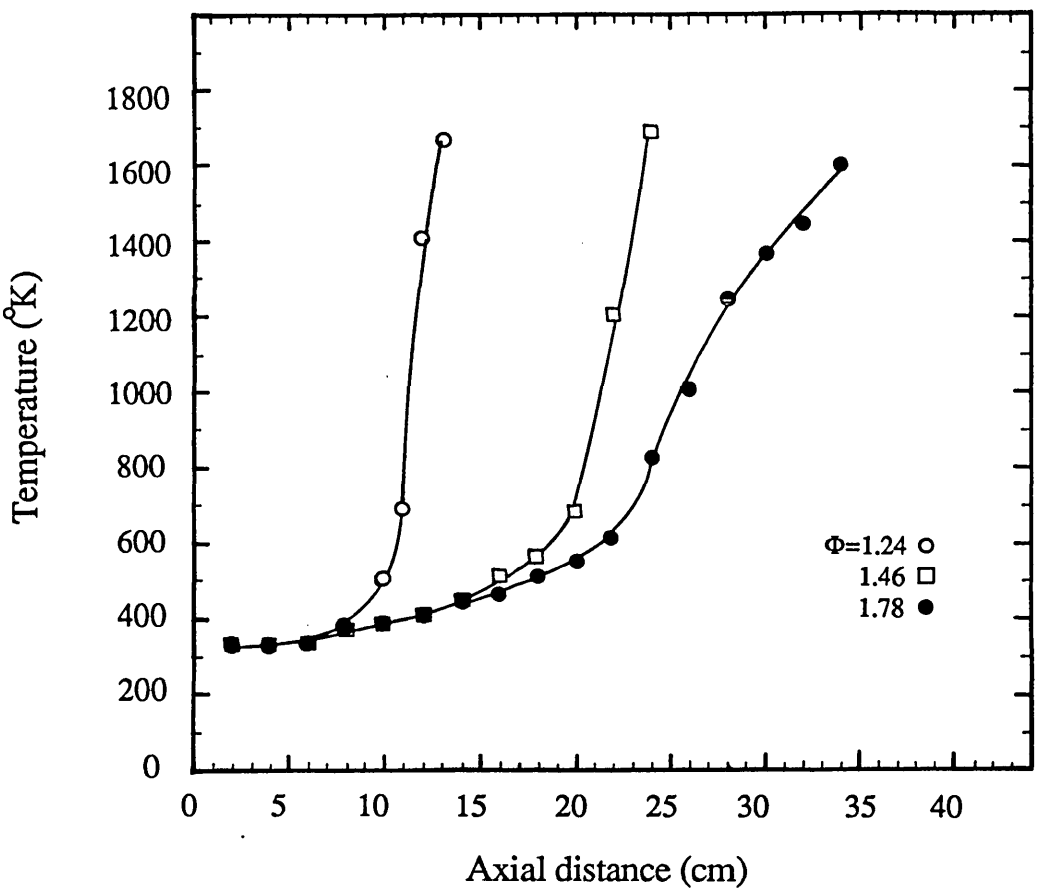

Fig. (4.4) Axial temperature profiles in the single flames for Re=14000.

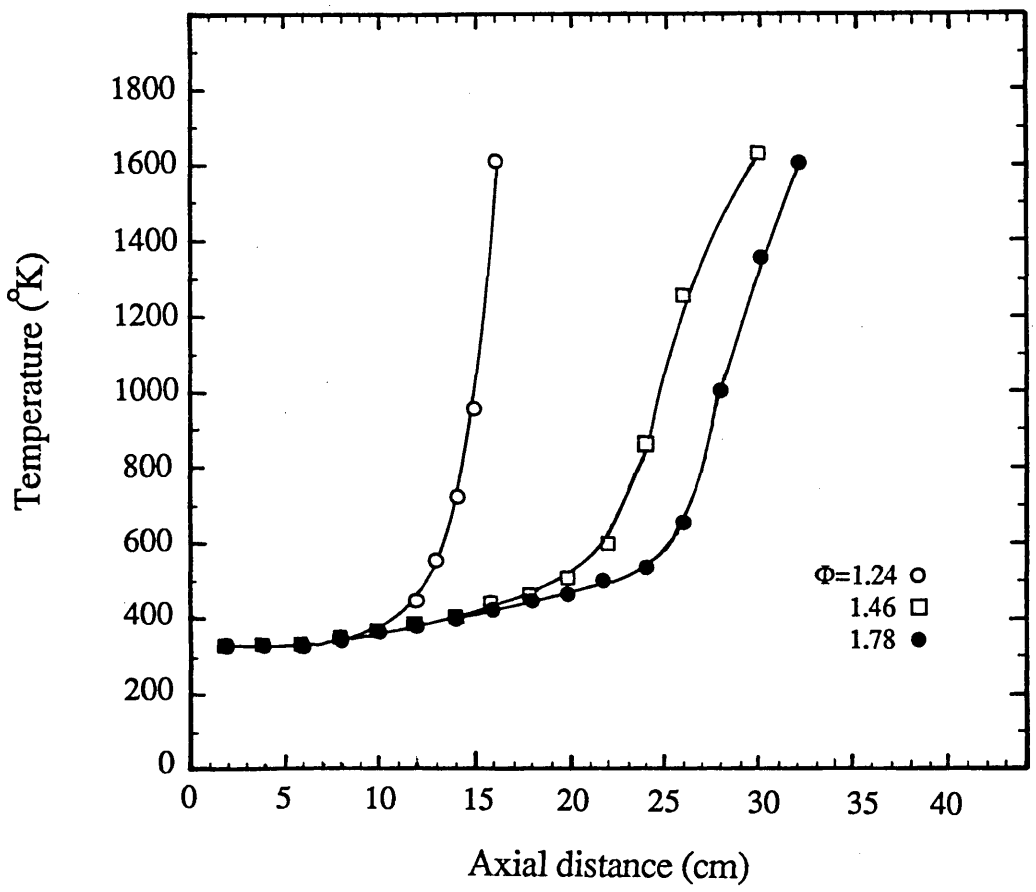

Fig. (4.5) Axial temperature profiles in the single flames for Re=20000.

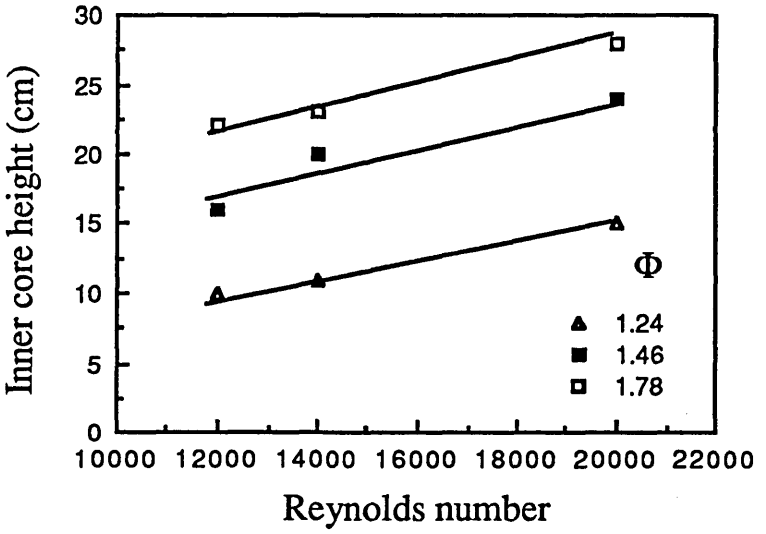

Fig. (4.6) Effect of Reynolds number on the inner core height

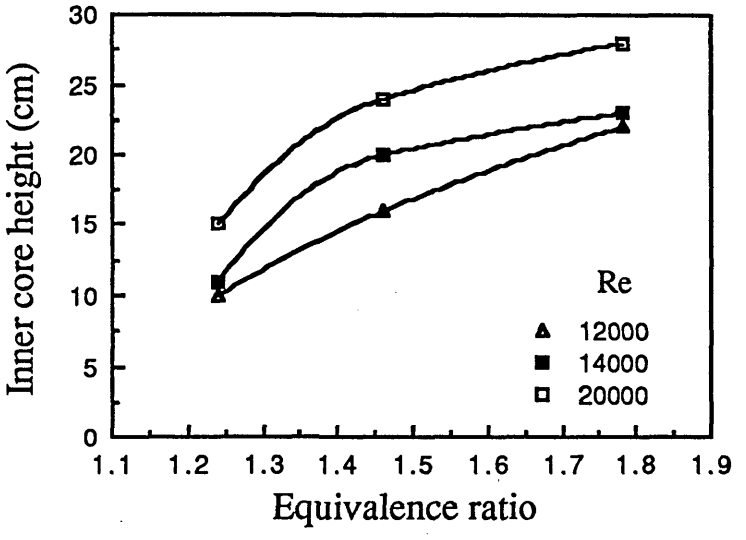

Fig. (4.7) Effect of equivalence ratio on the inner core height

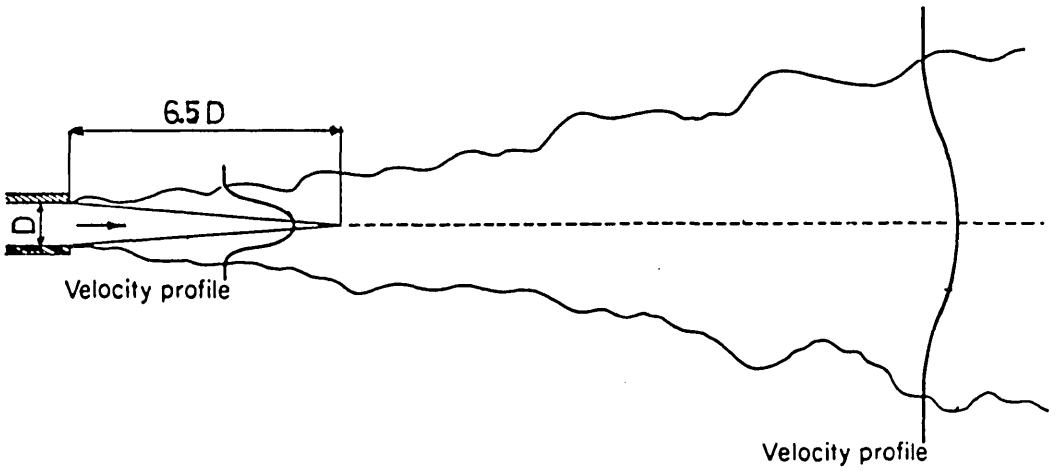

Fig. (4.8) Turbulent free jet showing typical velocity profiles, after Davies (1972).

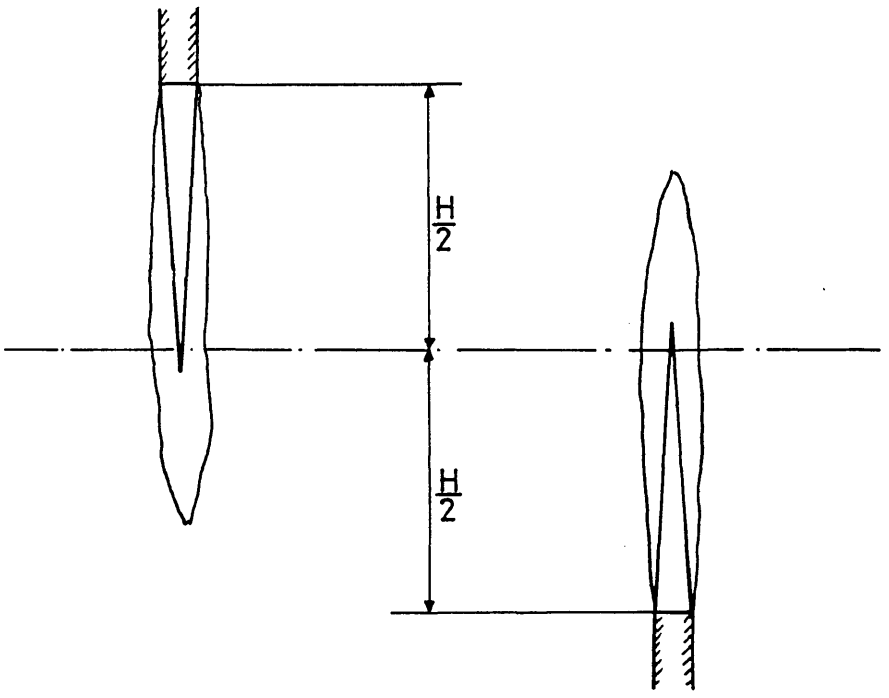

Fig. (4.9) Burner separation distance and location of physical stagnation plane.

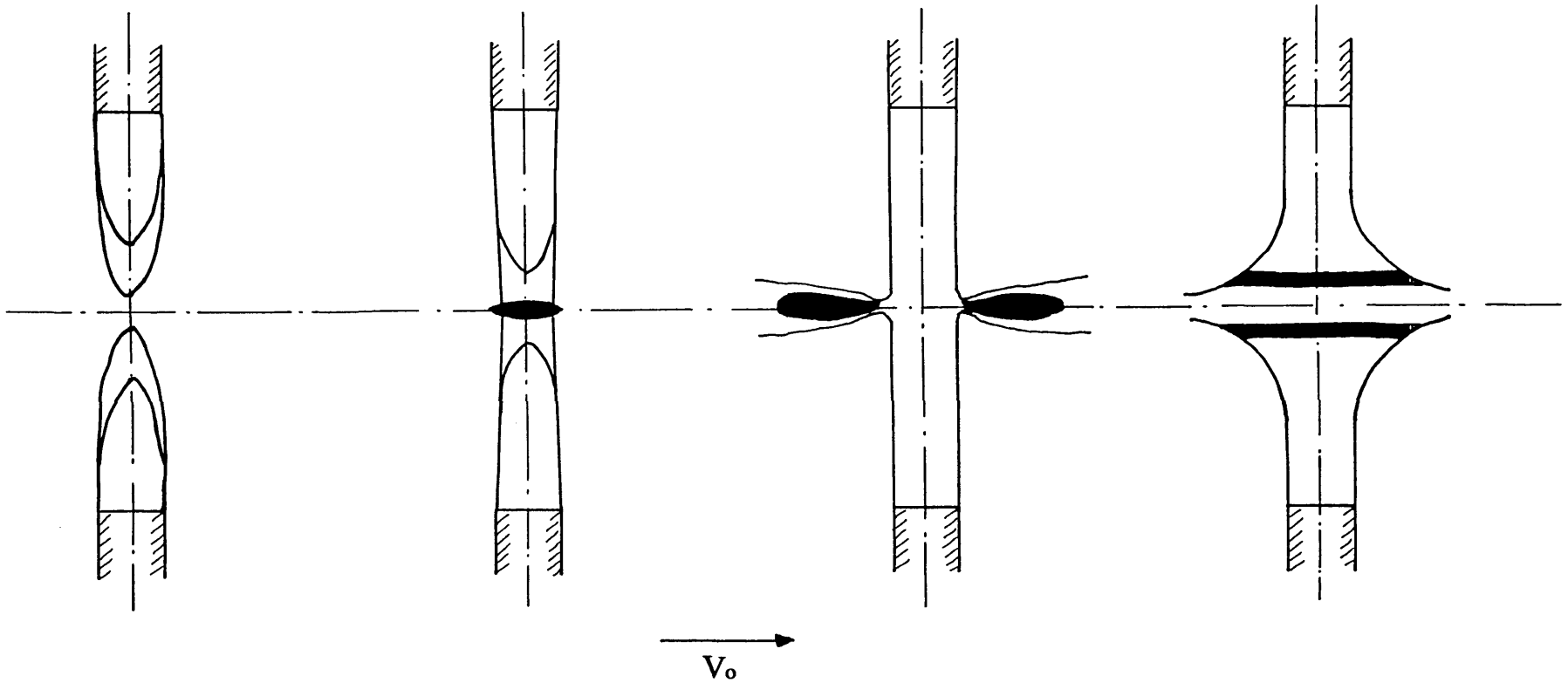

Fig. (4.10) Effect of burner exit velocity on the behaviour of two opposed premixed jets at constant equivalence ratio and burner separation distance.

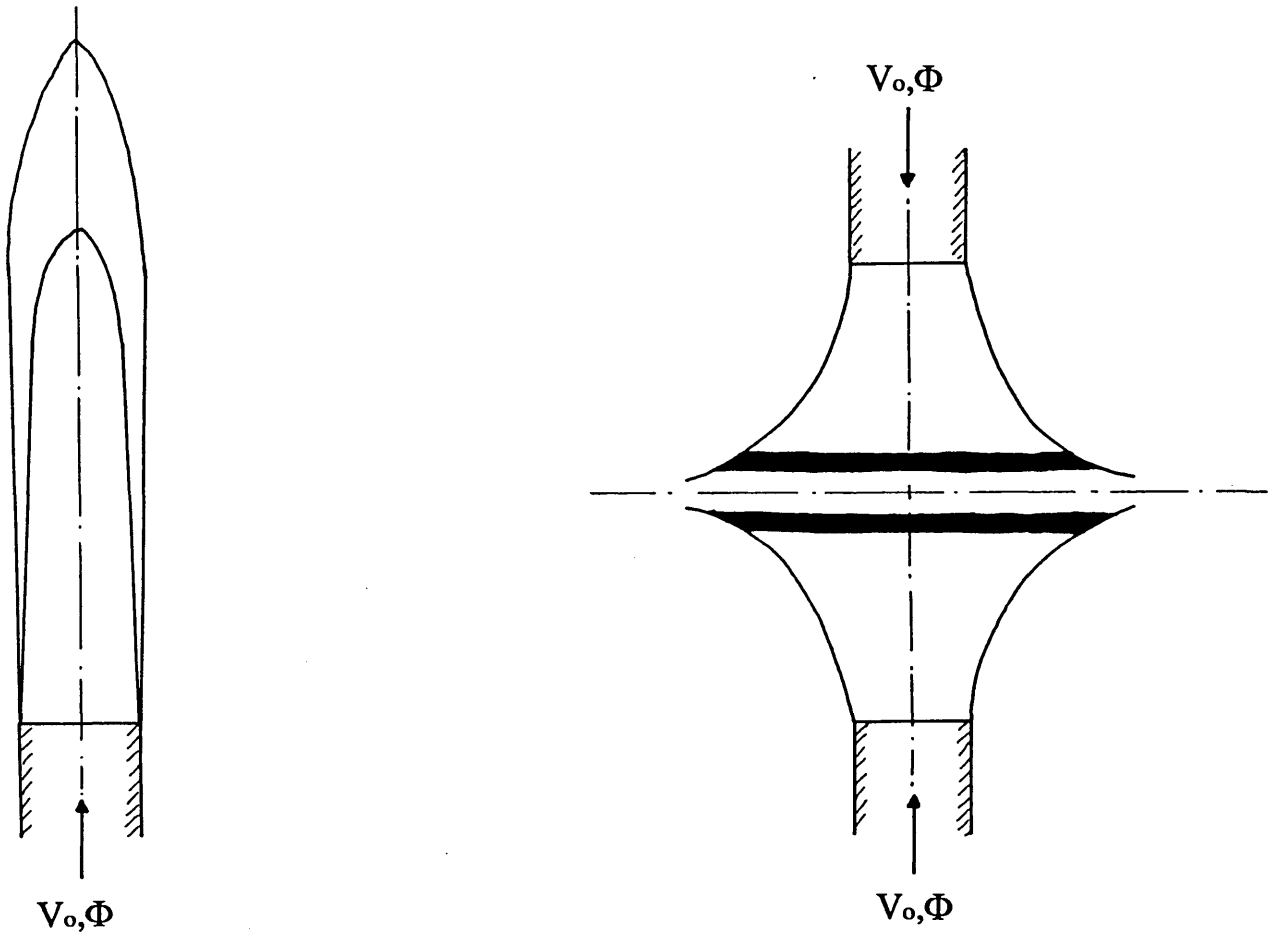

Fig. (4.11) Single flame (1) and counterflow flame, at extinction (2) for the same equivalence ratio and burner exit velocity.

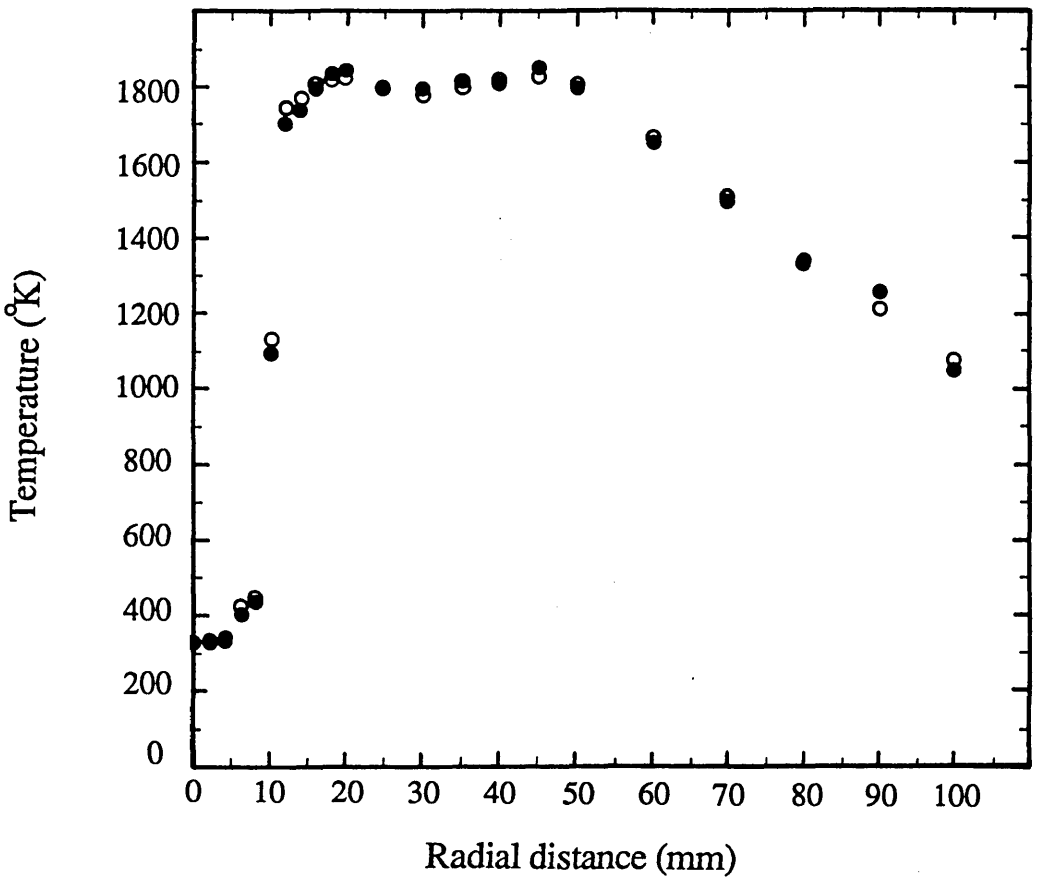

Fig. (4.12) Repeatability of the radial temperature profile in the counterflow flame for Re=20000, Φ=1.46 and H=20 cm.

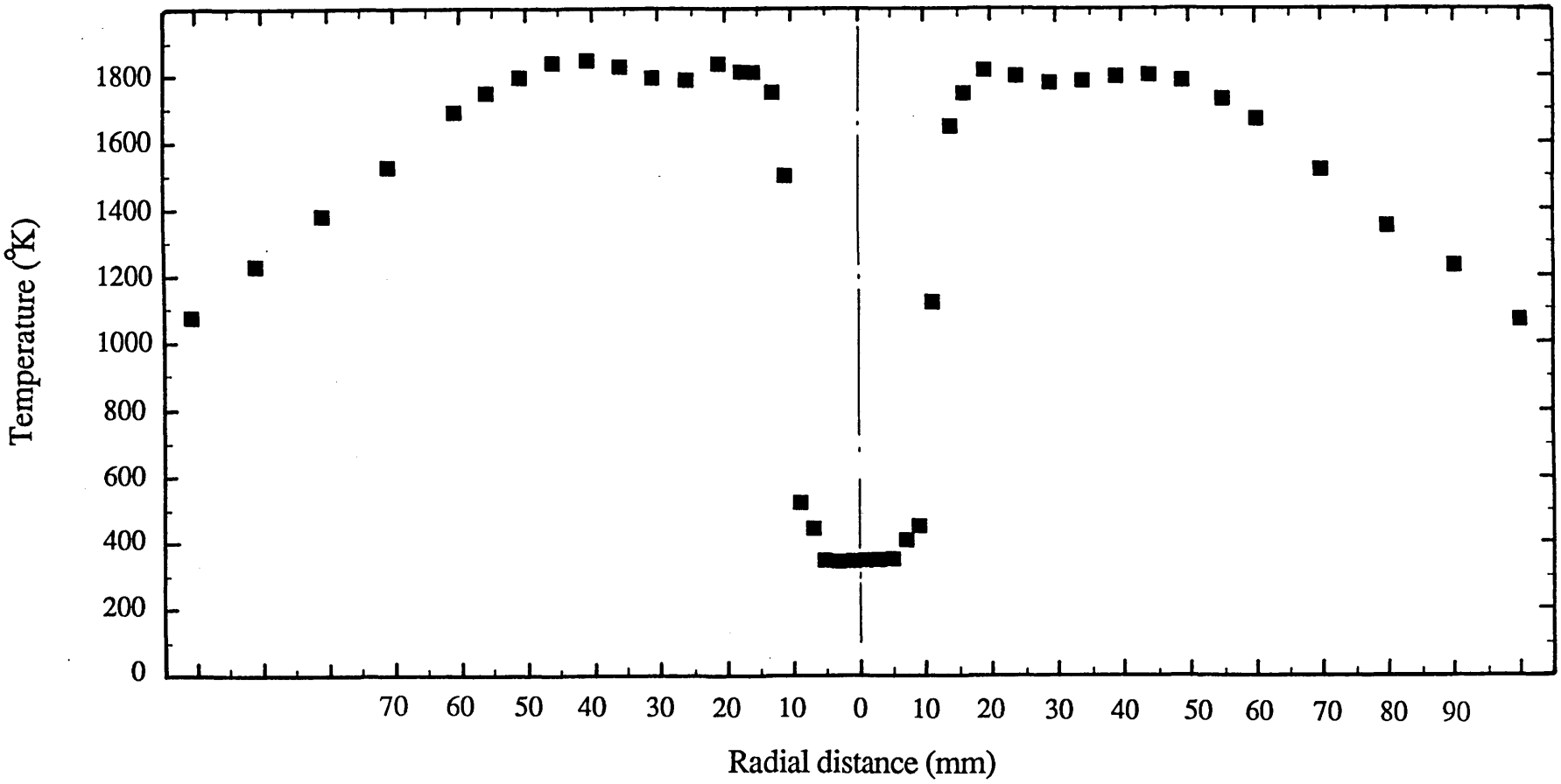

Fig. (4.13) Radial temperature profiles in two perpendicular directions in the stagnation plane of the counterflow flame for Re=20000, Φ=1.46 and H=20 cm.

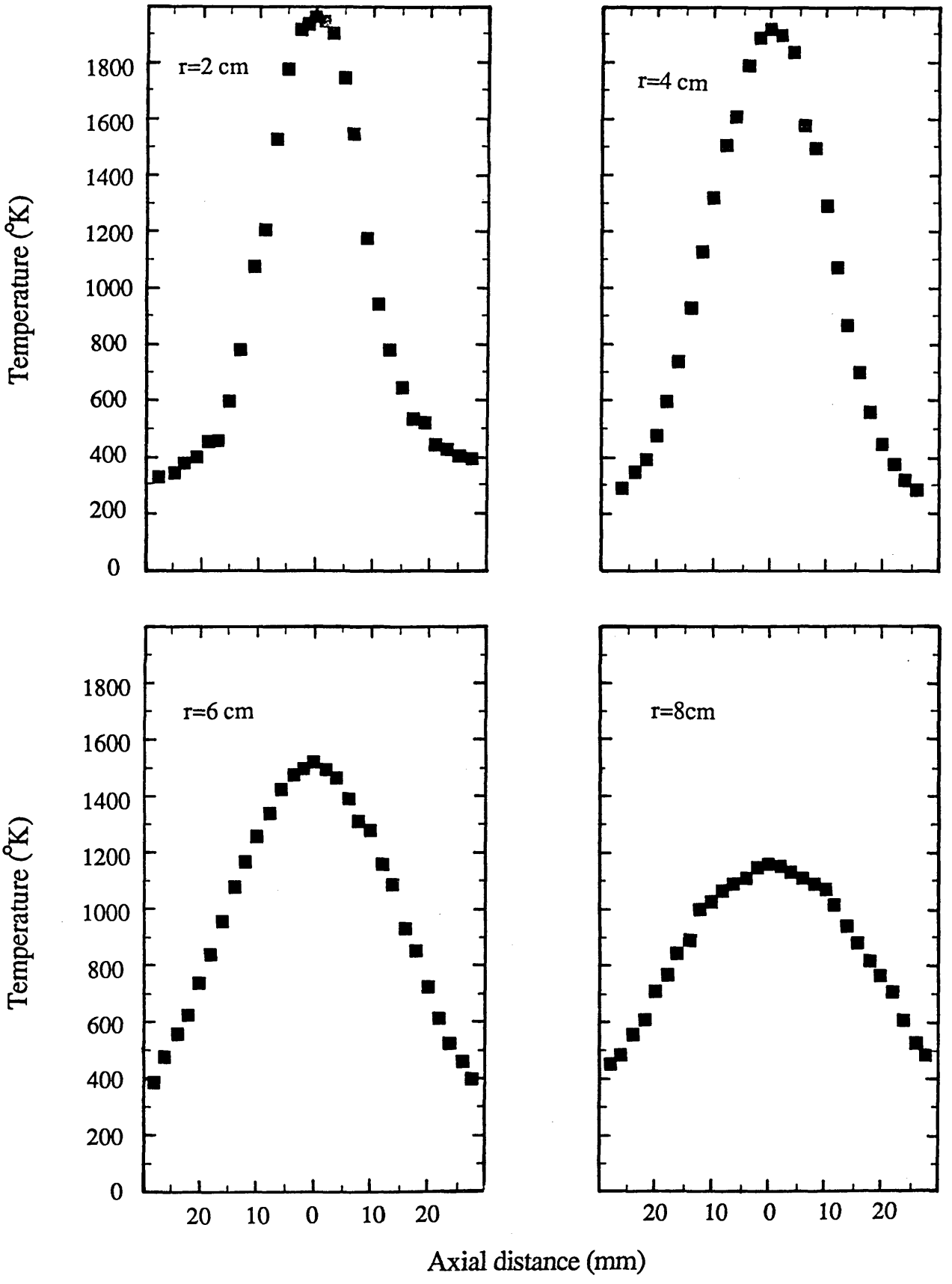

Fig. (4.14) Axial temperature profiles across the stagnation plane in the counterflow flame for Re=20000, Φ=1.24 and H=20 cm.

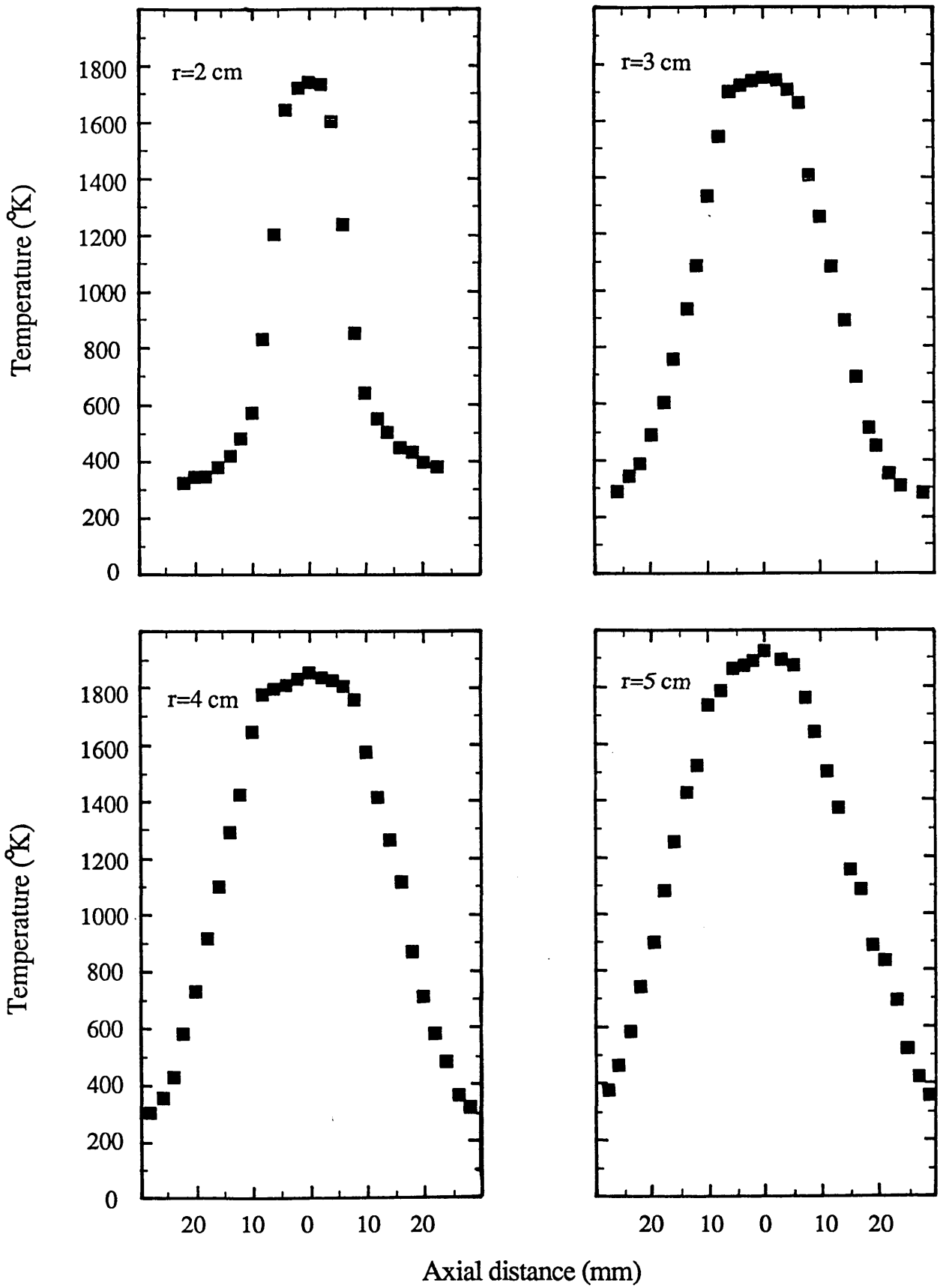

Fig. (4.15) Axial temperature profiles across the stagnation plane in the counterflow flame for Re=20000, Φ=1.78 and H=20 cm.

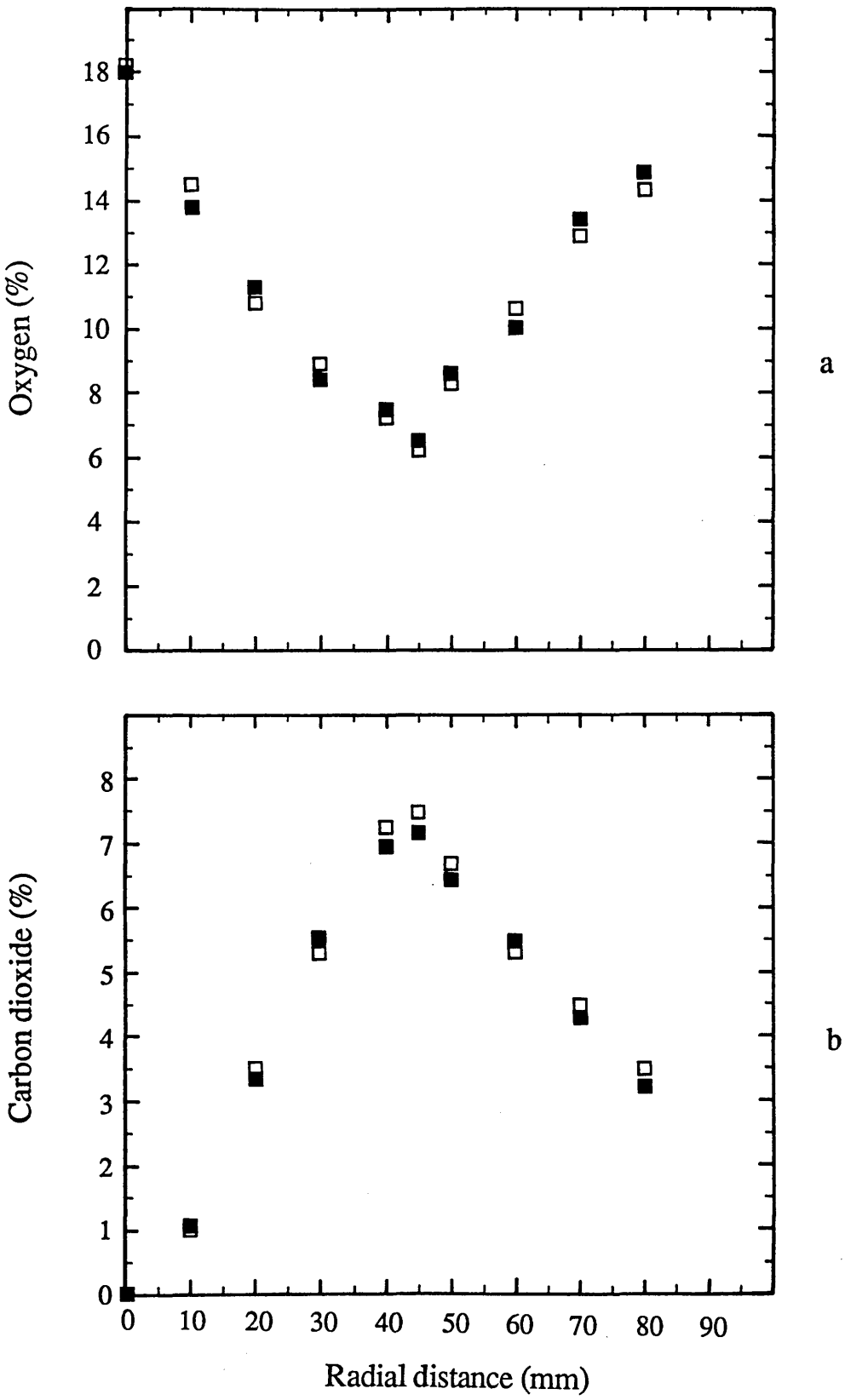

Fig. (4.16) Repeatability of the radial species concentration profiles in the counterflow flame for Re=20000, Φ=1.46 and H=20 cm.

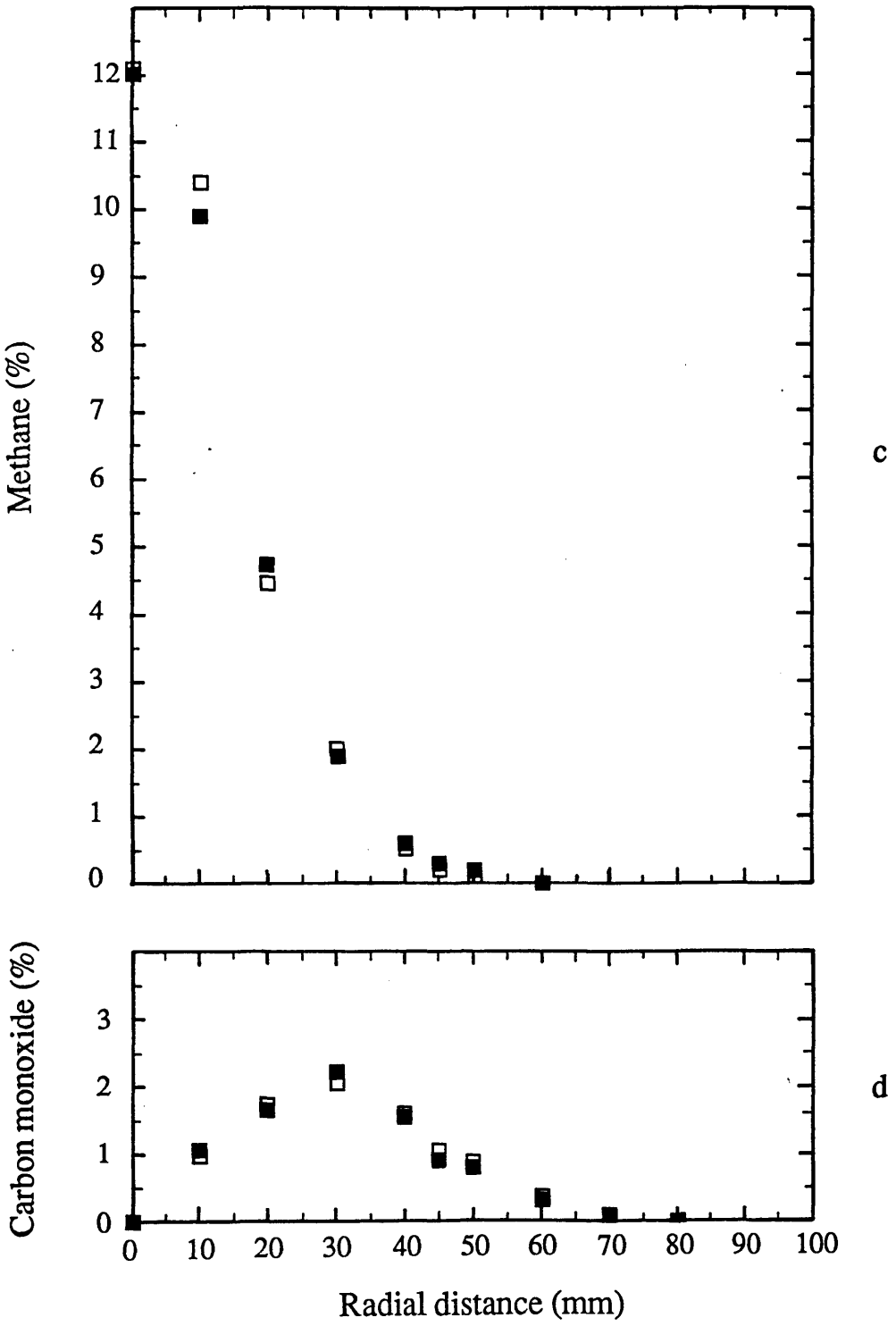
Methane (%)
0
1
2
3
4
5
6
7
8
9
10
11
12
c
Carbon monoxide (%)
0
1
2
3
d
0
10
20
30
40
50
60
70
80
90
100
Radial distance (mm)

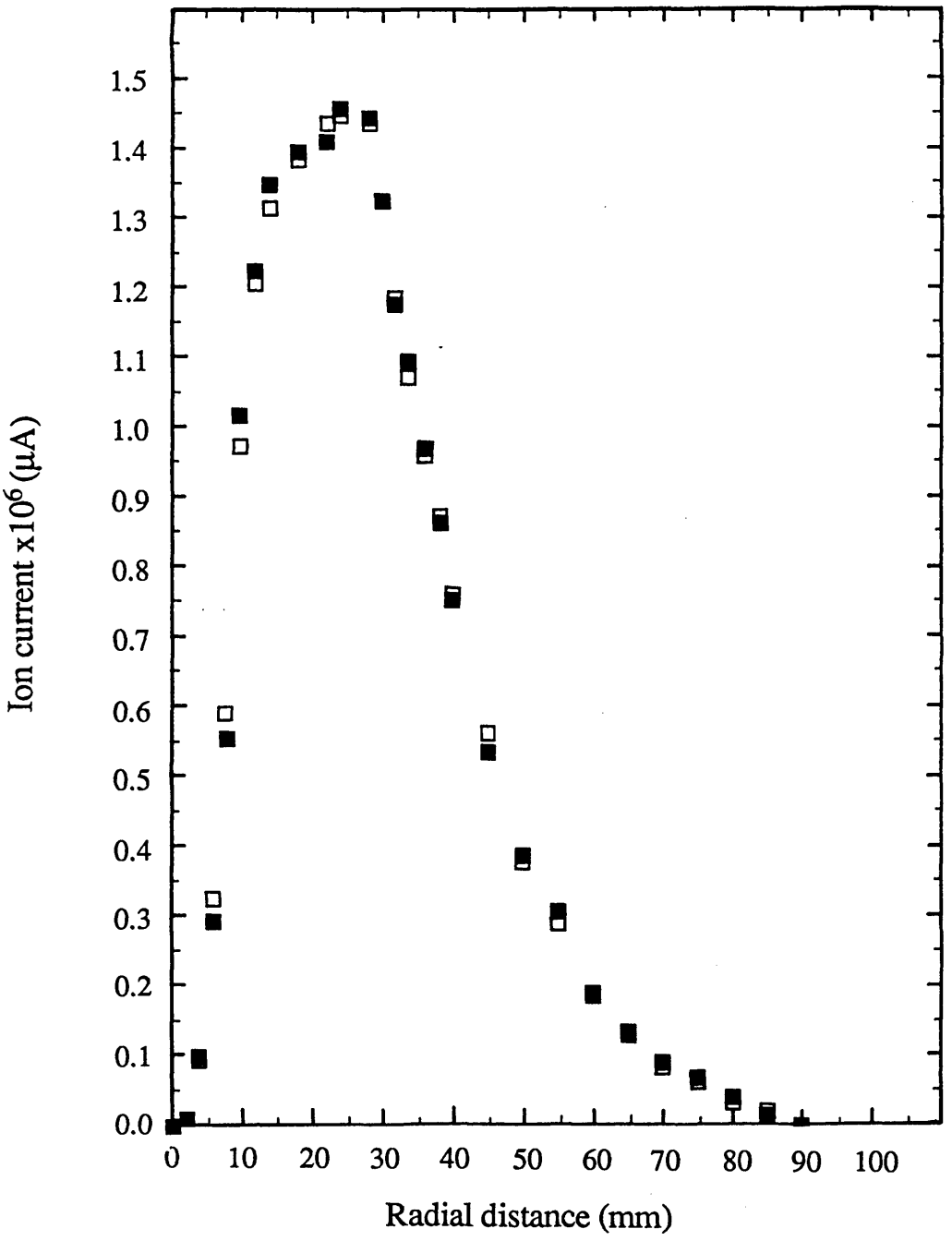

Fig. (4.17) Repeatability of the radial ion-current profile in the counterflow flame for Re=20000, Φ=1.24 and H=20 cm.

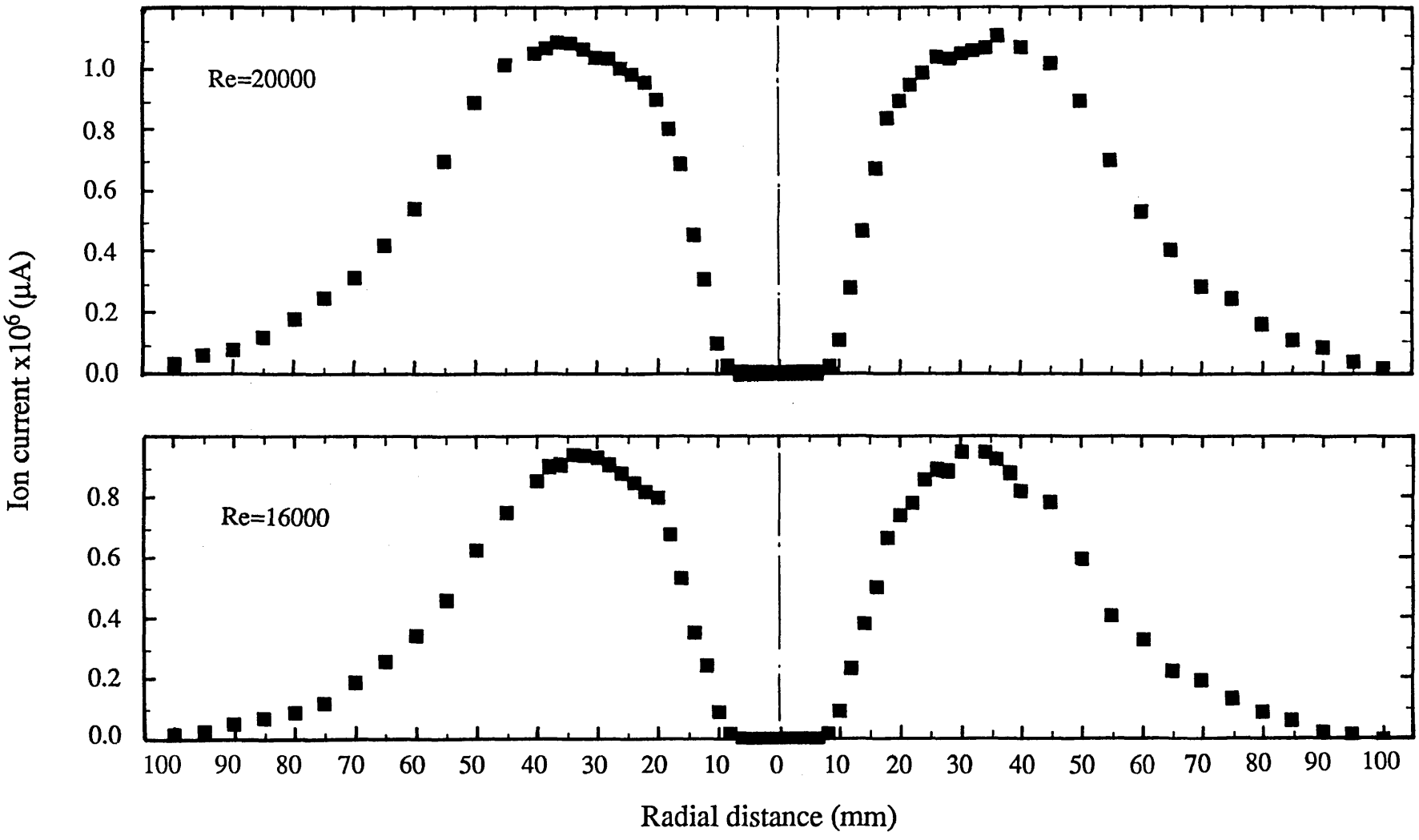

Fig. (4.18) Radial ion-current profiles in two perpendicular directions in the stagnation plane of the counterflow flame for $\Phi = 1.78$ and H=20 cm.

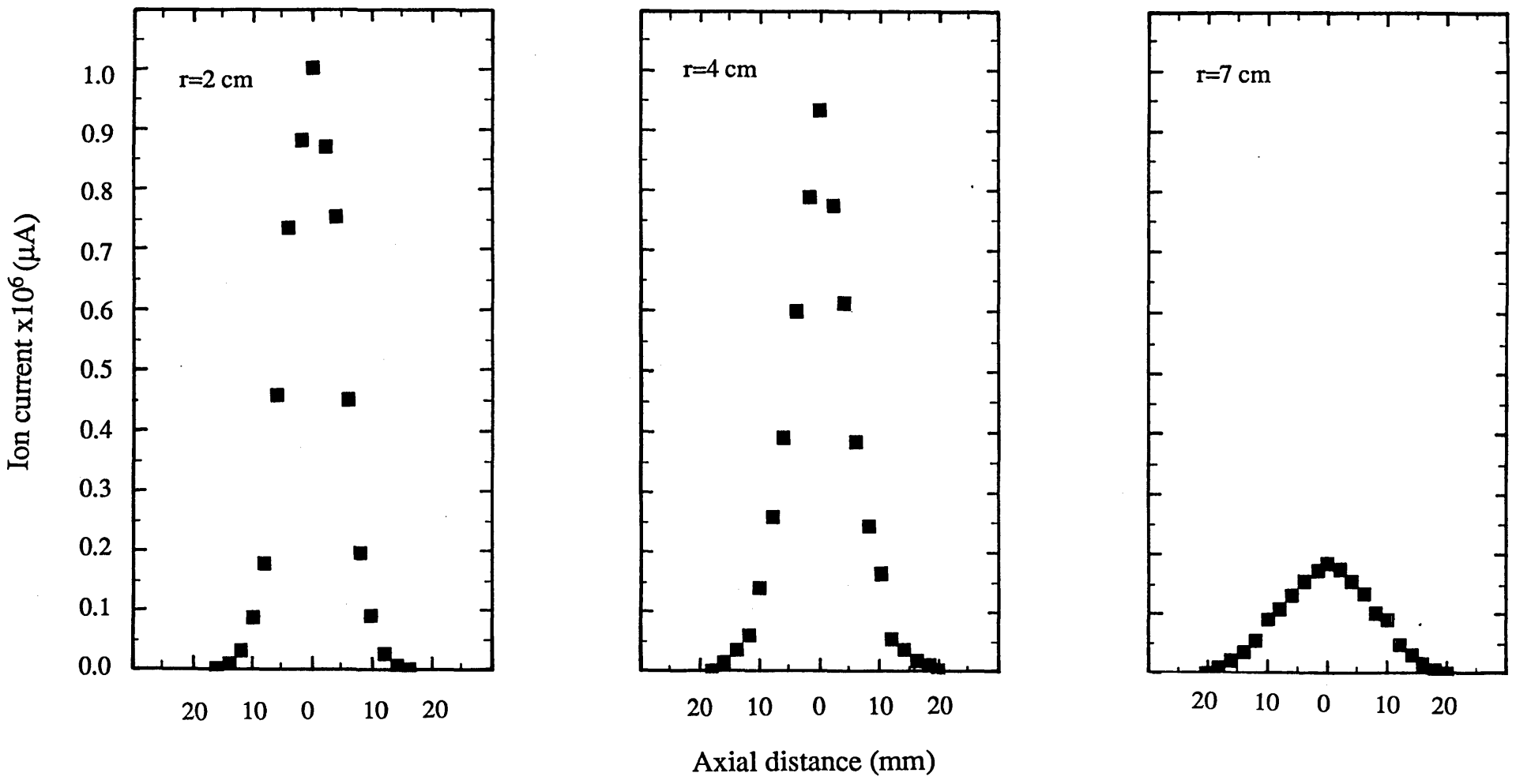

Fig. (4.19) Axial ion-current profiles across the stagnation plane in the counterflow flame for Re=20000, Φ=1.46 and H=20 cm.

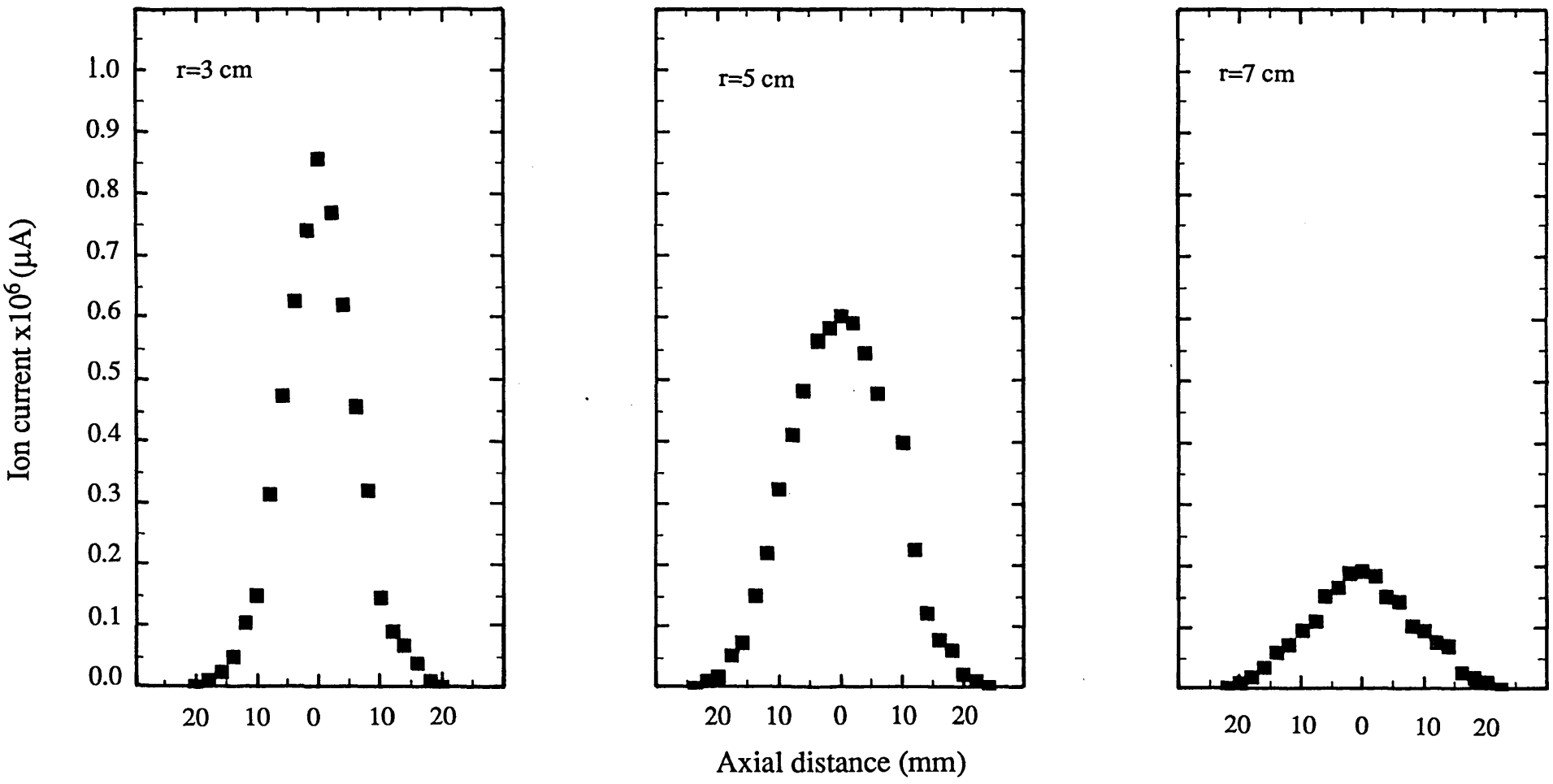

Fig. (4.20) Axial ion-current profiles across the stagnation plane in the counterflow flame for Re=16000, Φ=1.78 and H=20 cm.

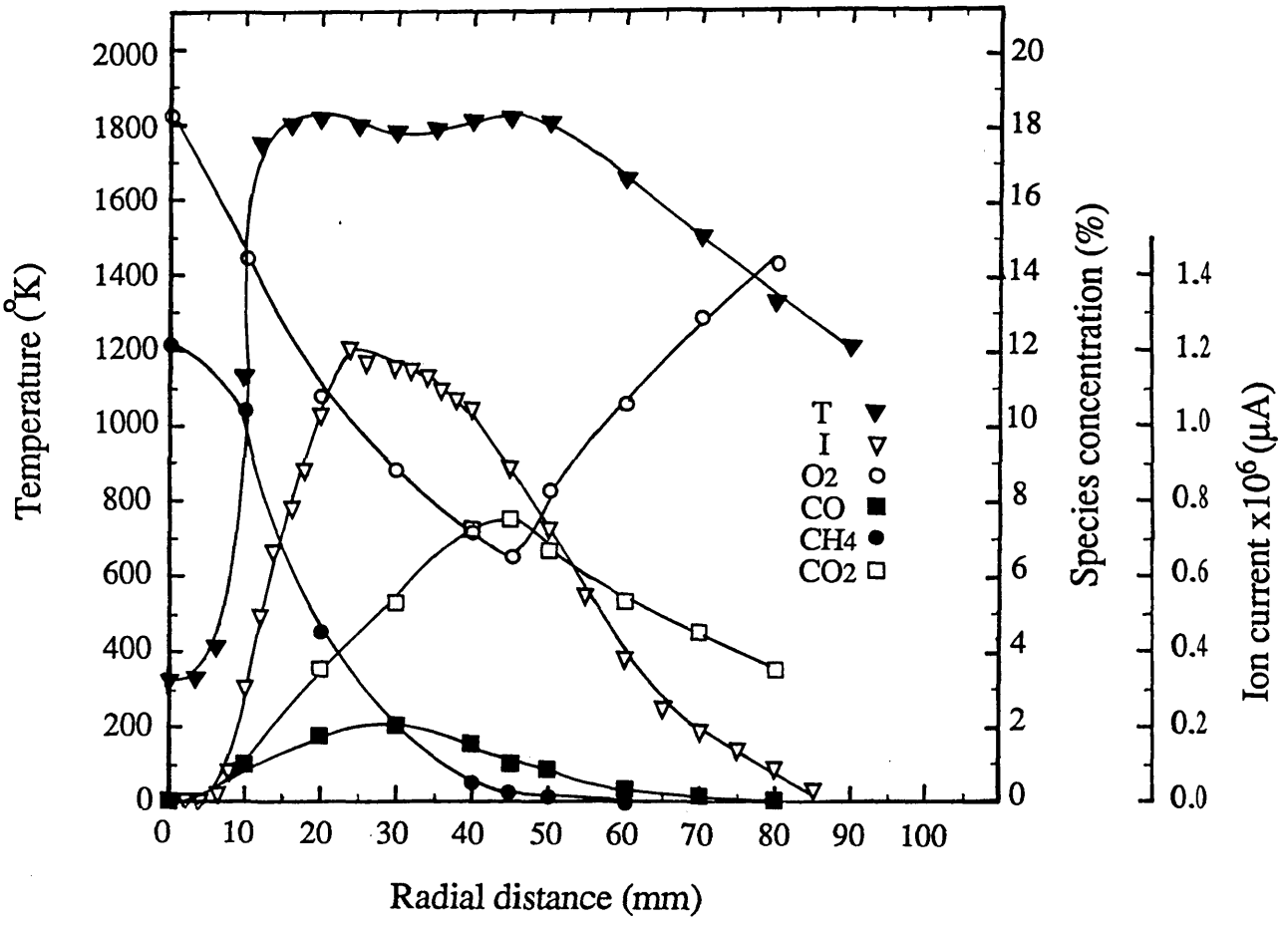

Fig. (4.21) Radial profiles of T, I, O2, CO, CH4, CO2 in the counterflow flame for Re=20000, Φ=1.46 and H=20 cm.

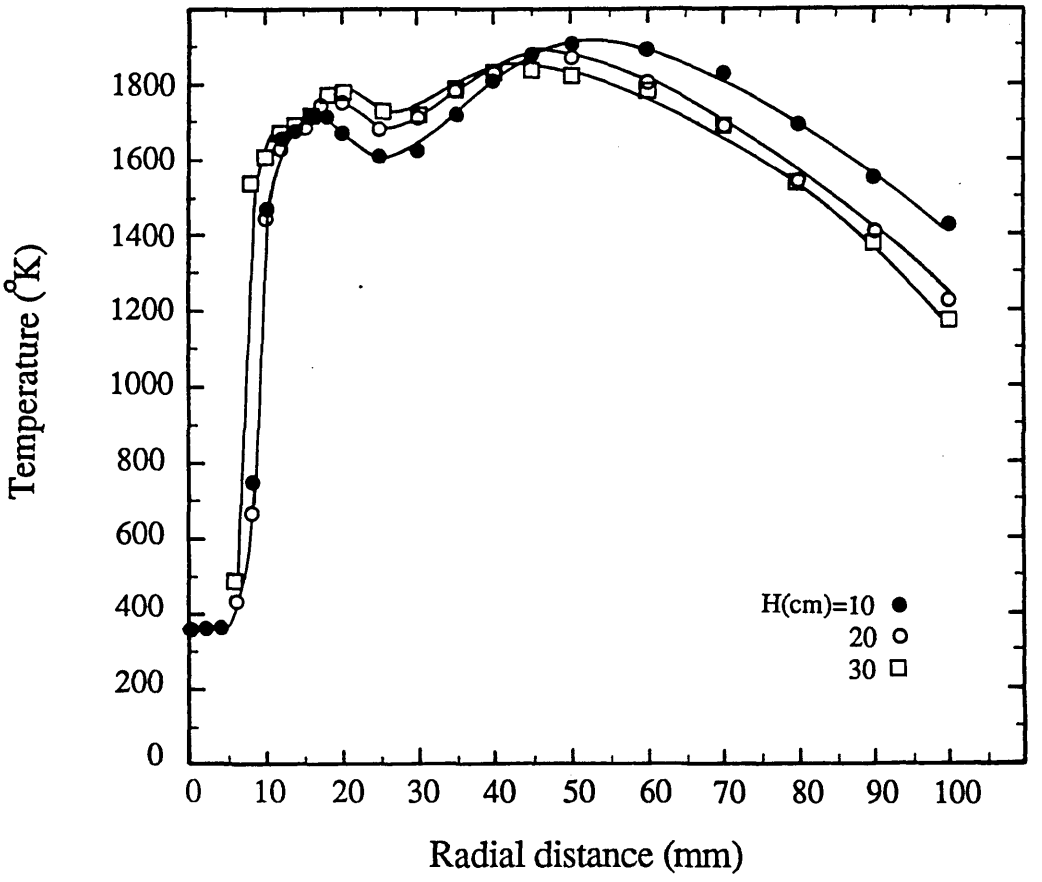

Fig. (4.22) Radial temperature profiles in counterflow flames for Re=20000 and Φ=1.78.

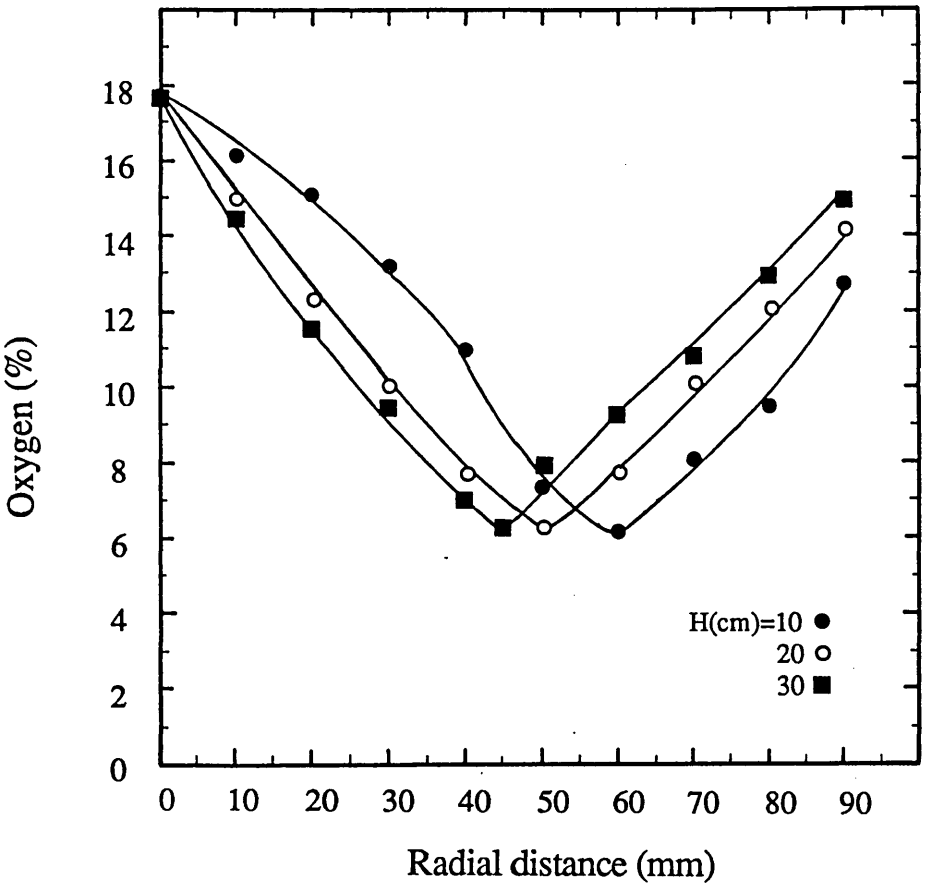

Fig. (4.23) Radial oxygen profiles in counterflow flames for Re=20000 and Φ=1.78.

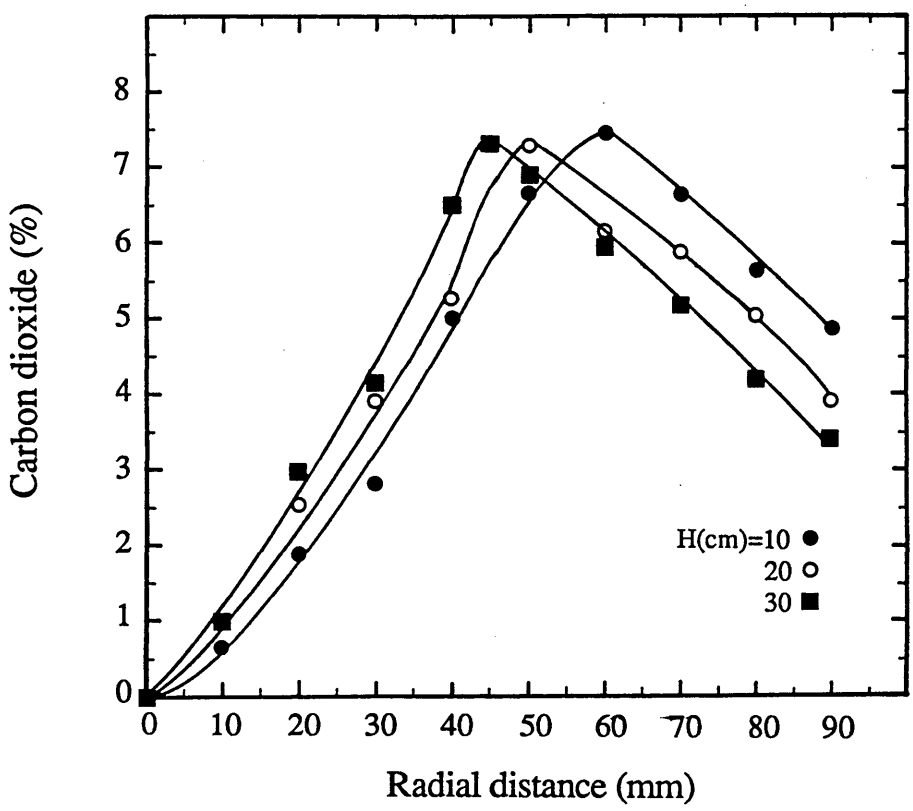

Fig. (4.24) Radial carbon dioxide profiles in counterflow flame for Re=20000 and Φ=1.78.

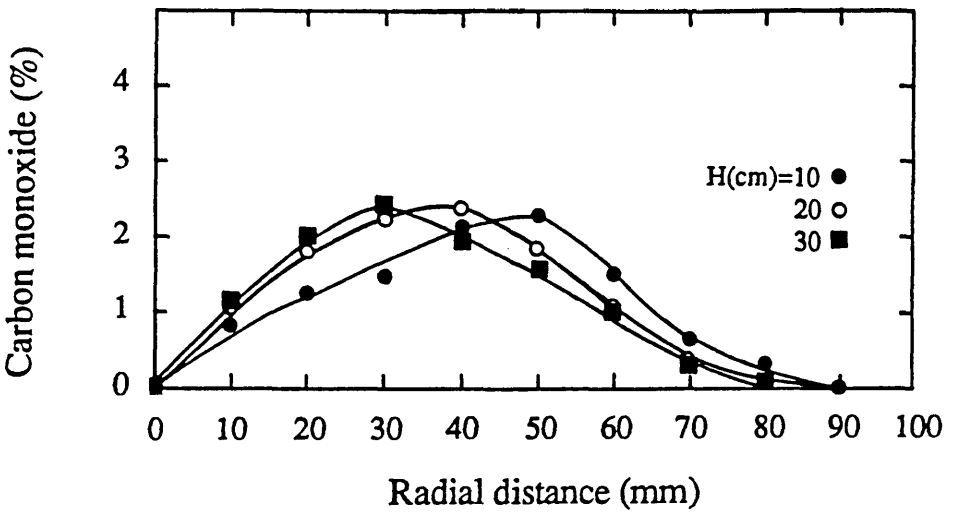

Fig. (4.25) Radial carbon monoxide profiles in counterflow flame for Re=20000 and Φ=1.78.

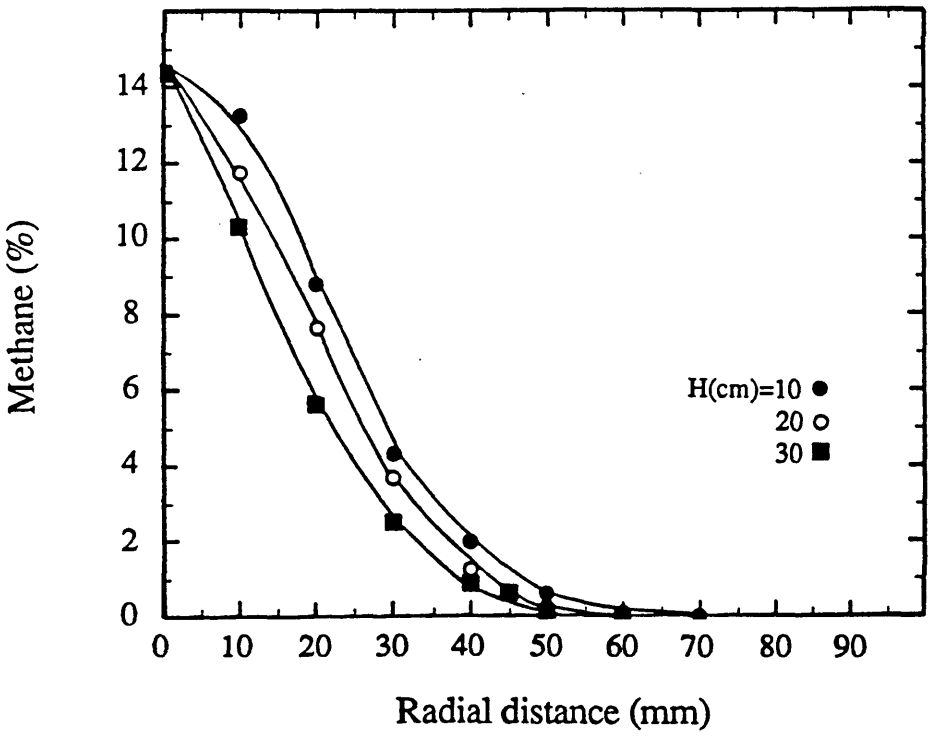

Fig. (4.26) Radial methane profiles in counterflow flames for Re=20000 and Φ=1.78.

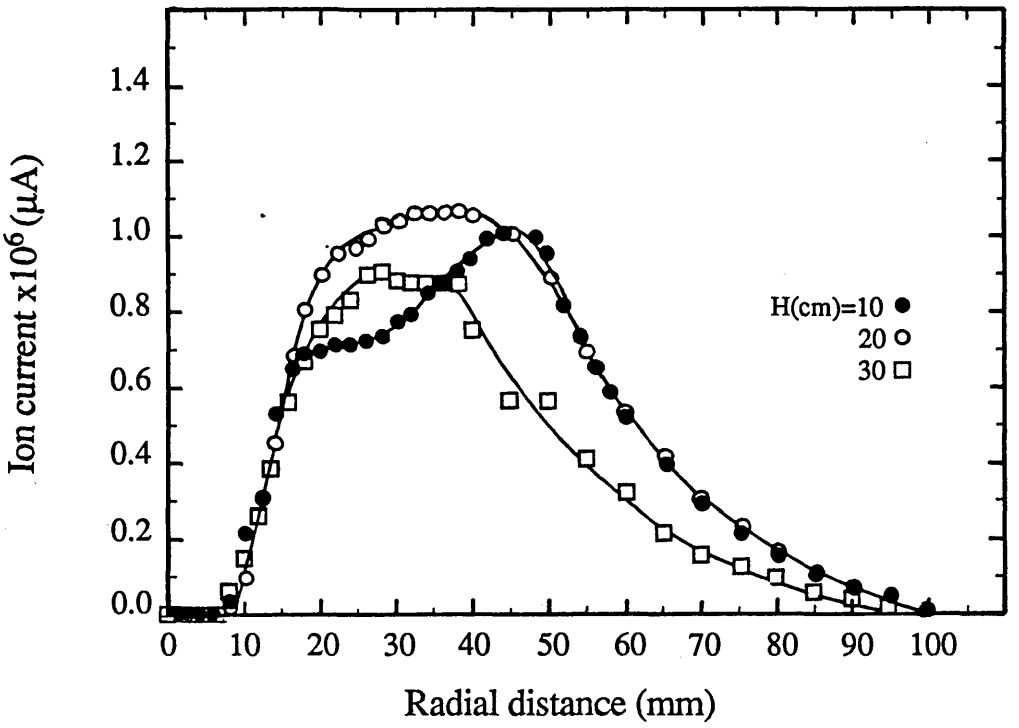

Fig. (4.27) Radial ion-current profiles in counterflow flames for Re=20000 and Φ=1.78.

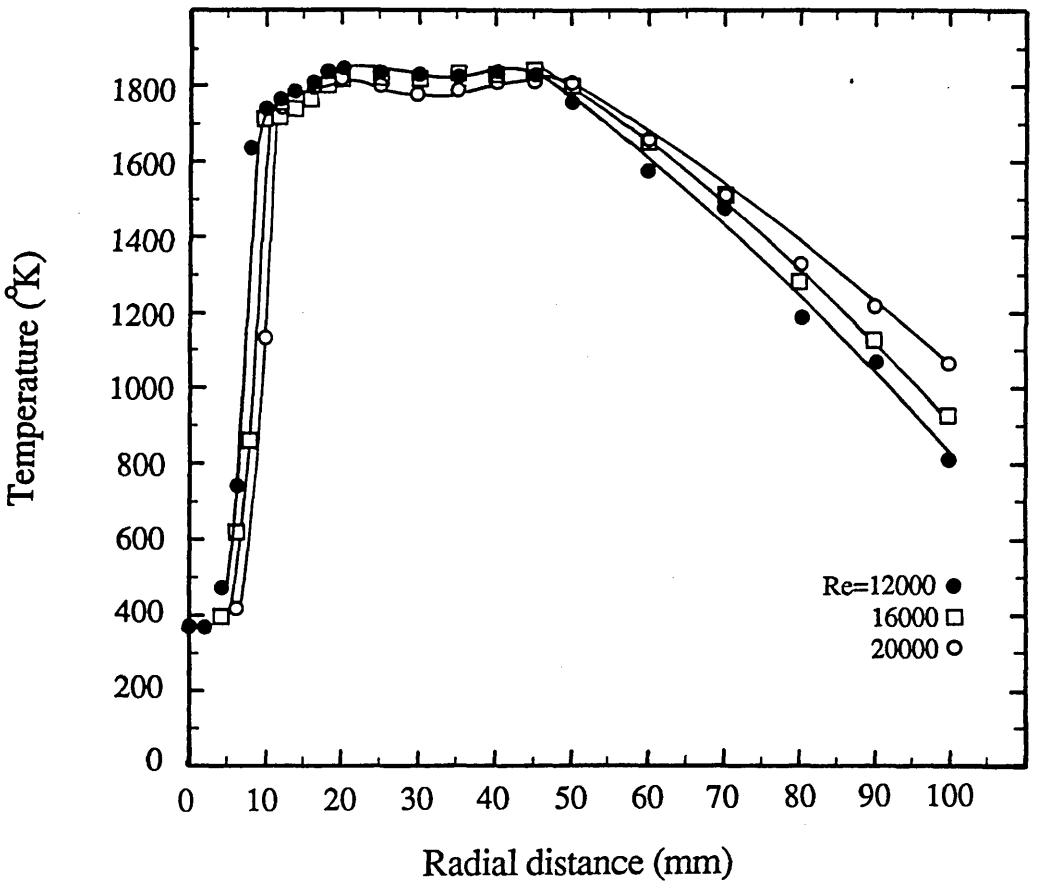

Fig. (4.28) Radial temperature profiles in counterflow flames for Φ=1.46 and H=20 cm.

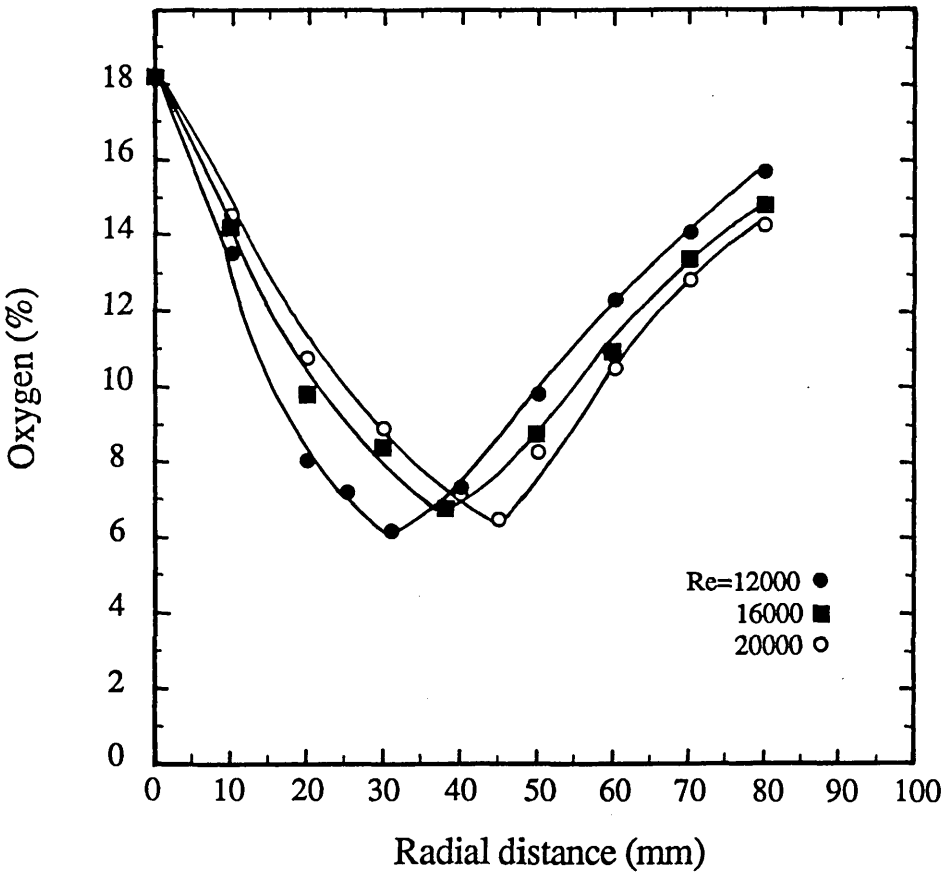

Fig. (4.29) Radial oxygen profiles in counterflow flames for Φ=1.46 and H=20 cm.

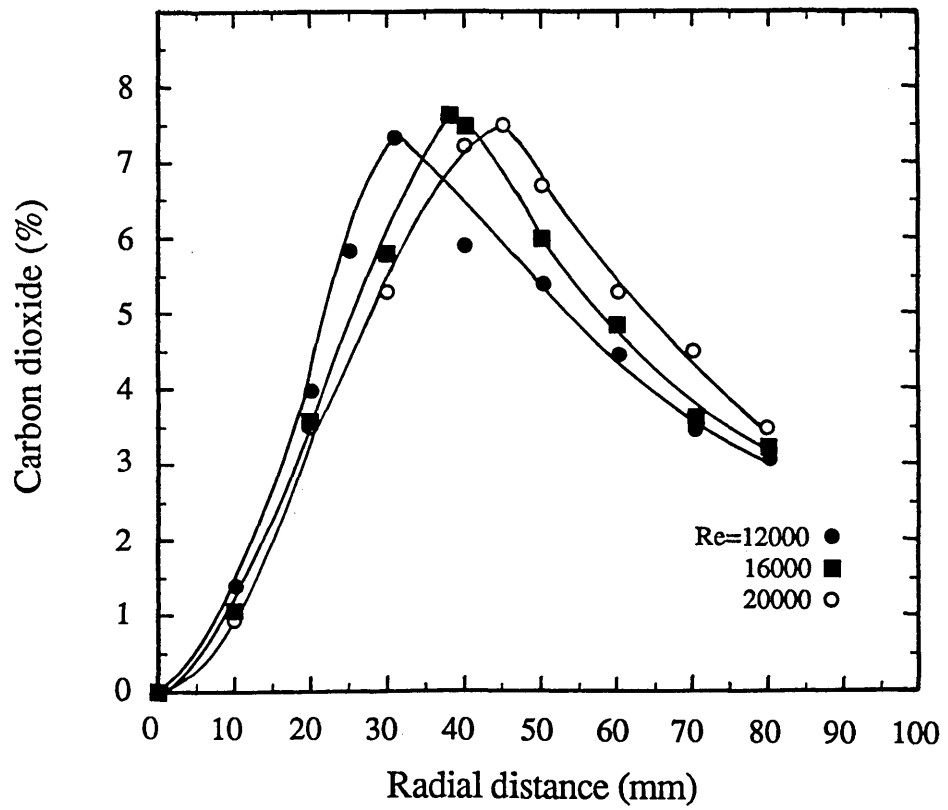

Fig. (4.30) Radial carbon dioxide profiles in counterflow flames for Φ=1.46 and H=20 cm.

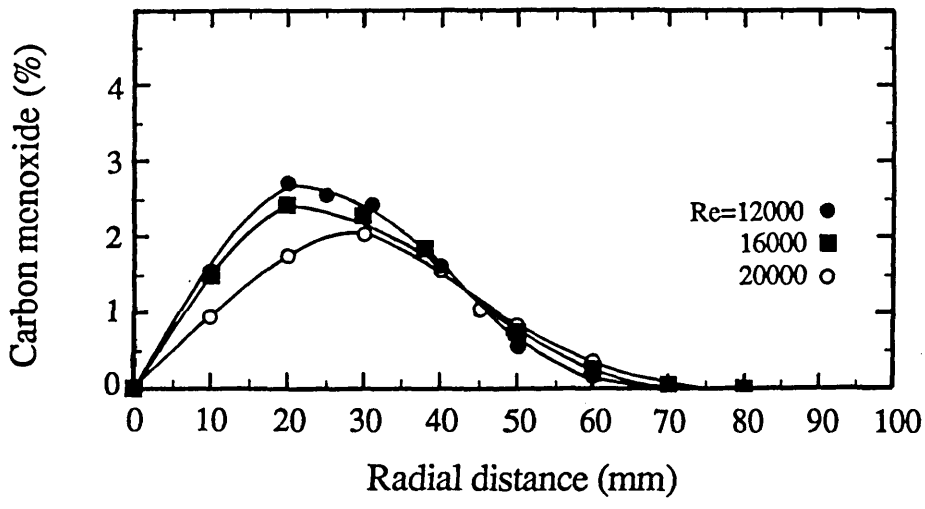

Fig. (4.31) Radial carbon monoxide profiles in counterflow flames for Φ=1.46 and H=20 cm.

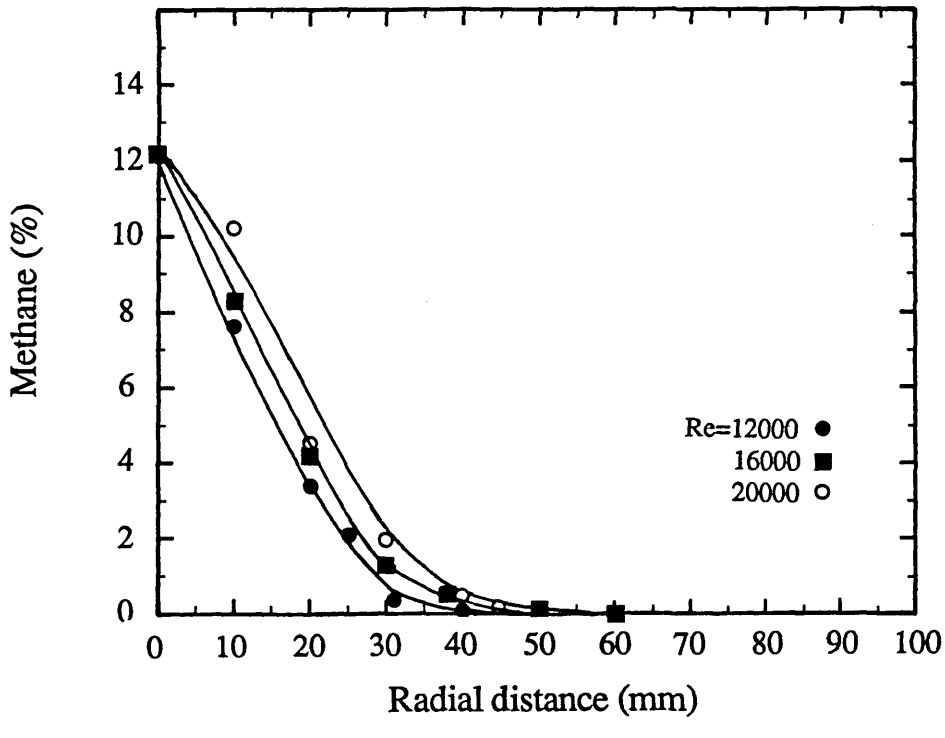

Fig. (4.32) Radial methane profiles in counterflow flames for Φ=1.46 and H=20 cm.

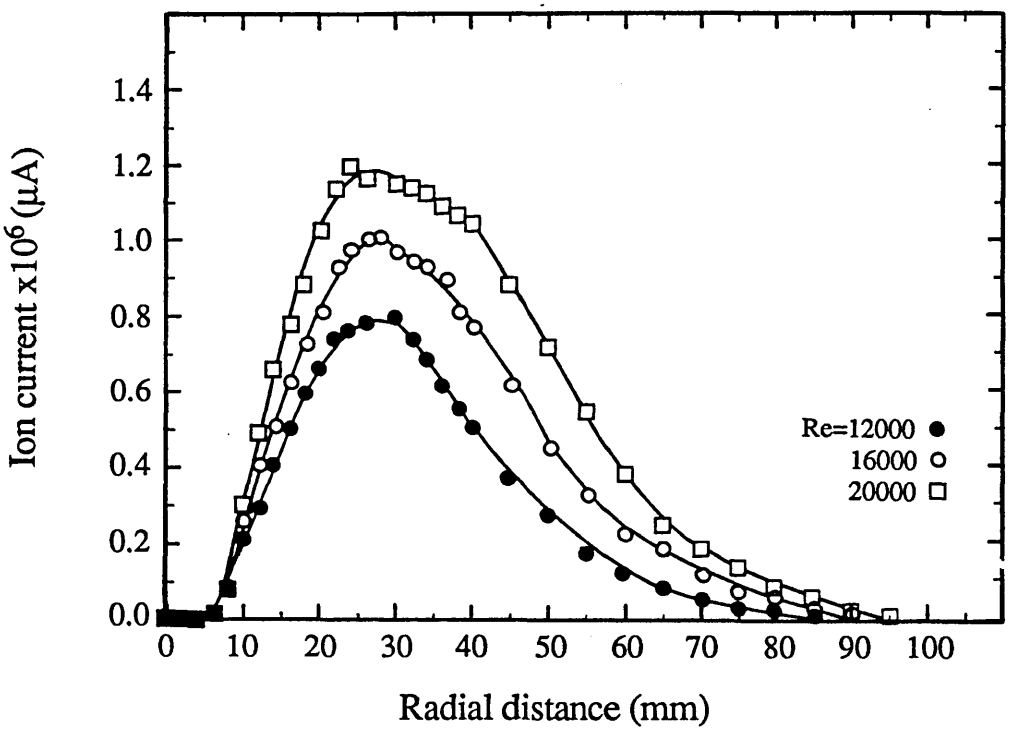

Fig. (4.33) Radial ion-current profiles in counterflow flames for Φ=1.46 and H=20 cm.

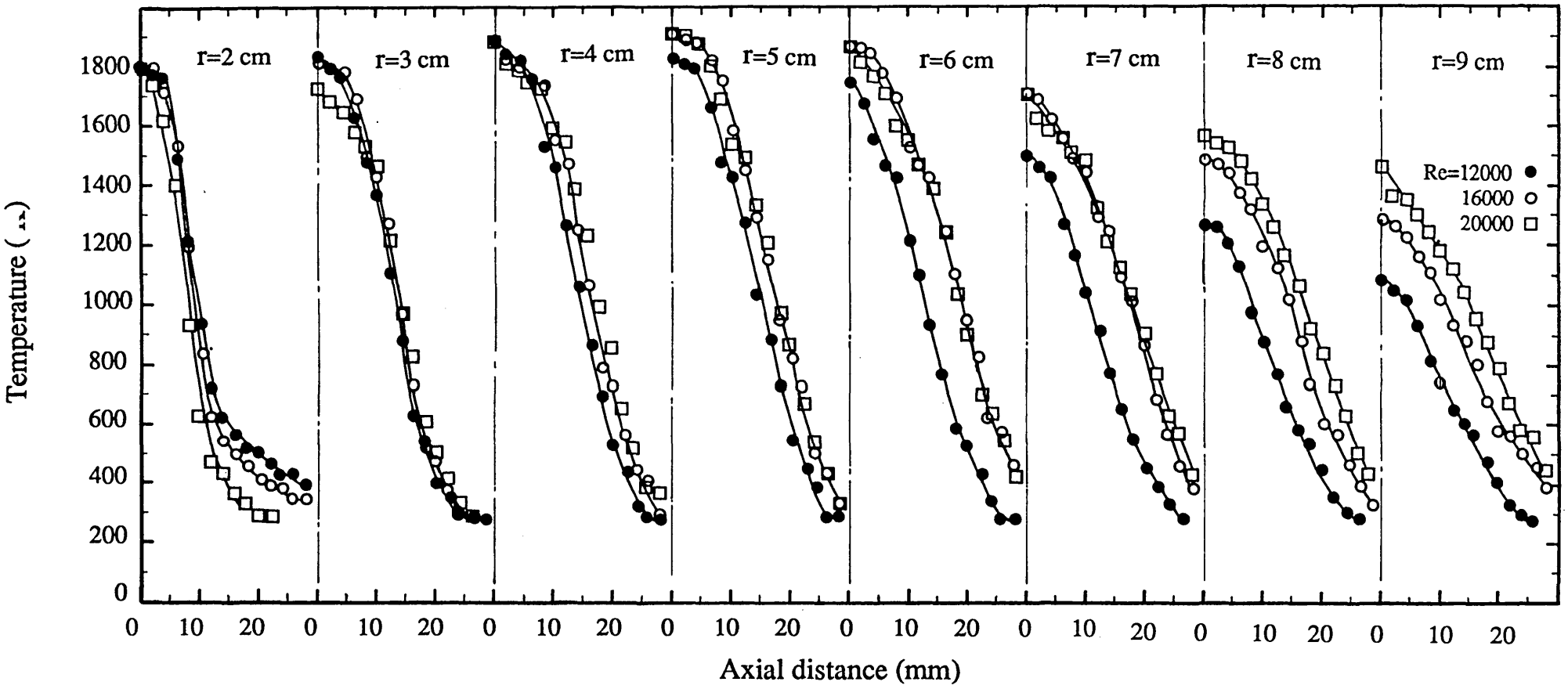

Fig. (4.34) Axial temperature profiles across the stagnation plane in counterflow flames for Φ=1.78 and H=20 cm.

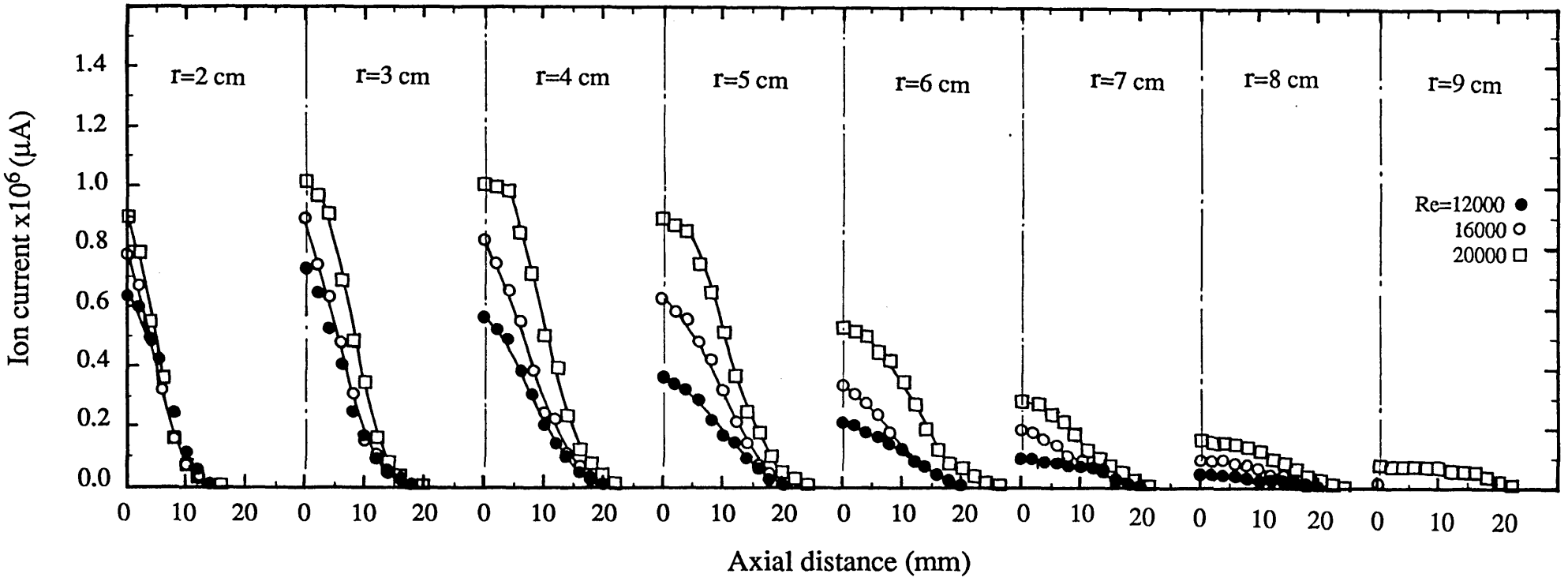

Fig. (4.35) Axial ion-current profiles across the stagnation plane in counterflow flames for Φ=1.78 and H=20 cm.

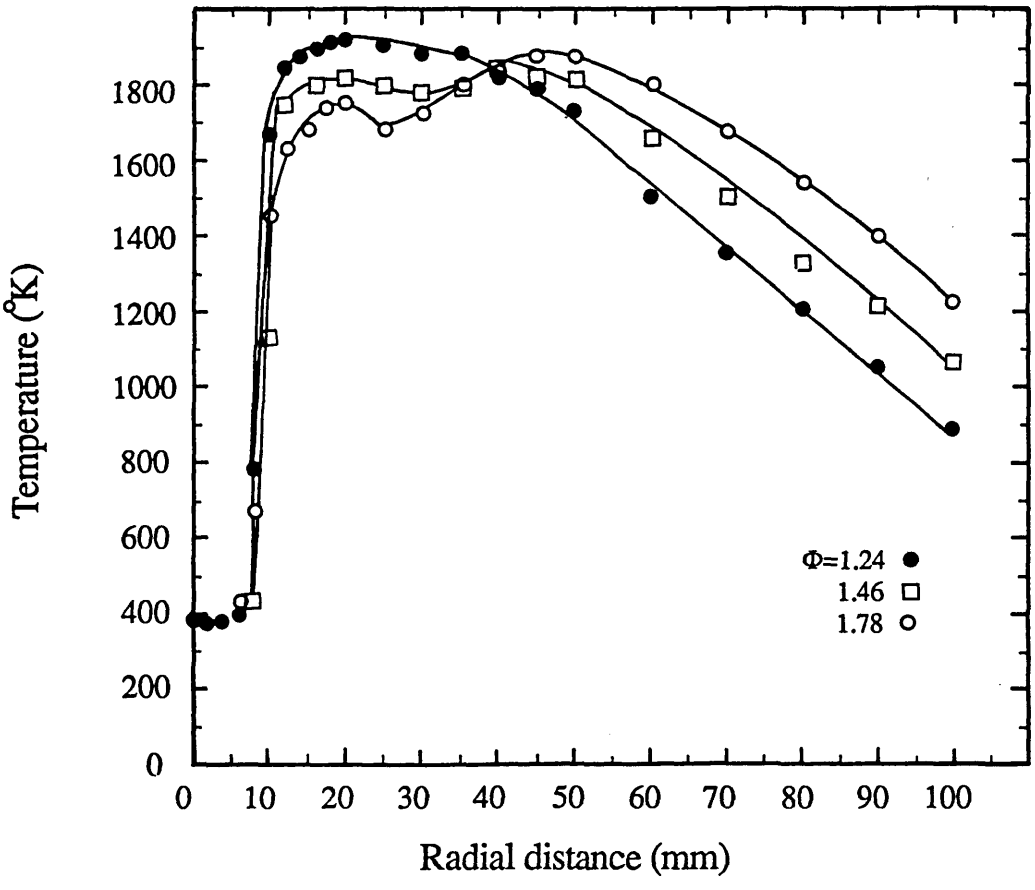

Fig. (4.36) Radial temperature profiles in counterflow flames for Re=20000 and H=20 cm.

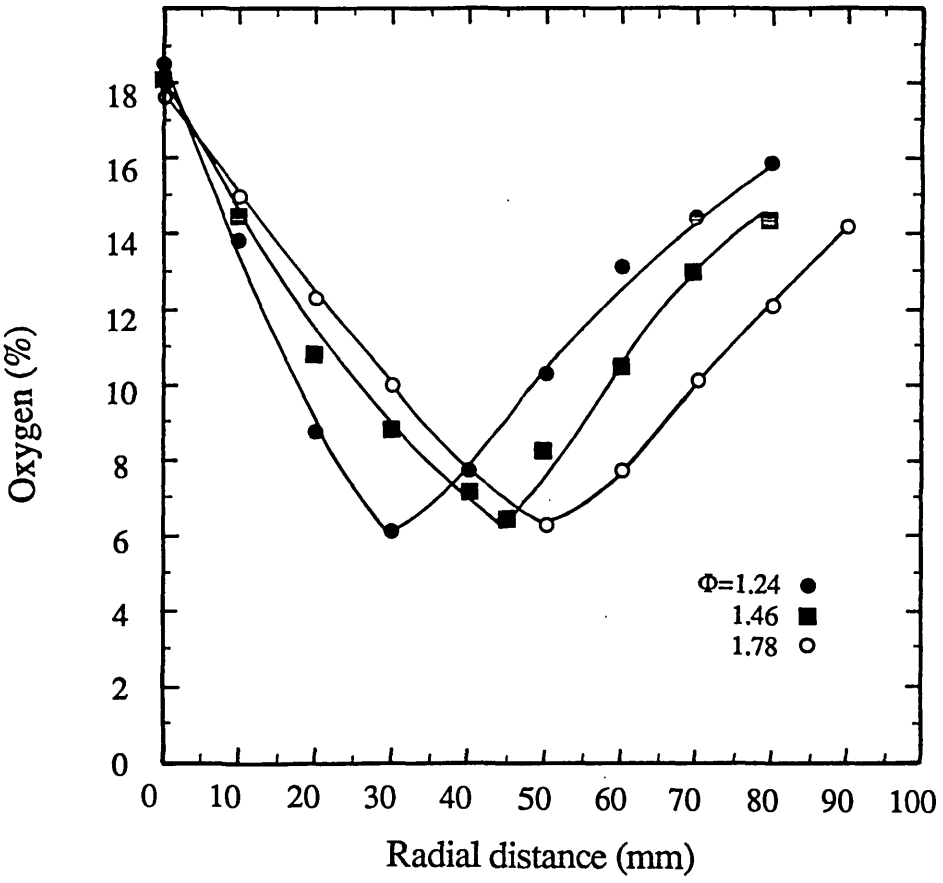

Fig. (4.37) Radial oxygen profiles in counterflow flames for Re=20000 and H=20 cm.

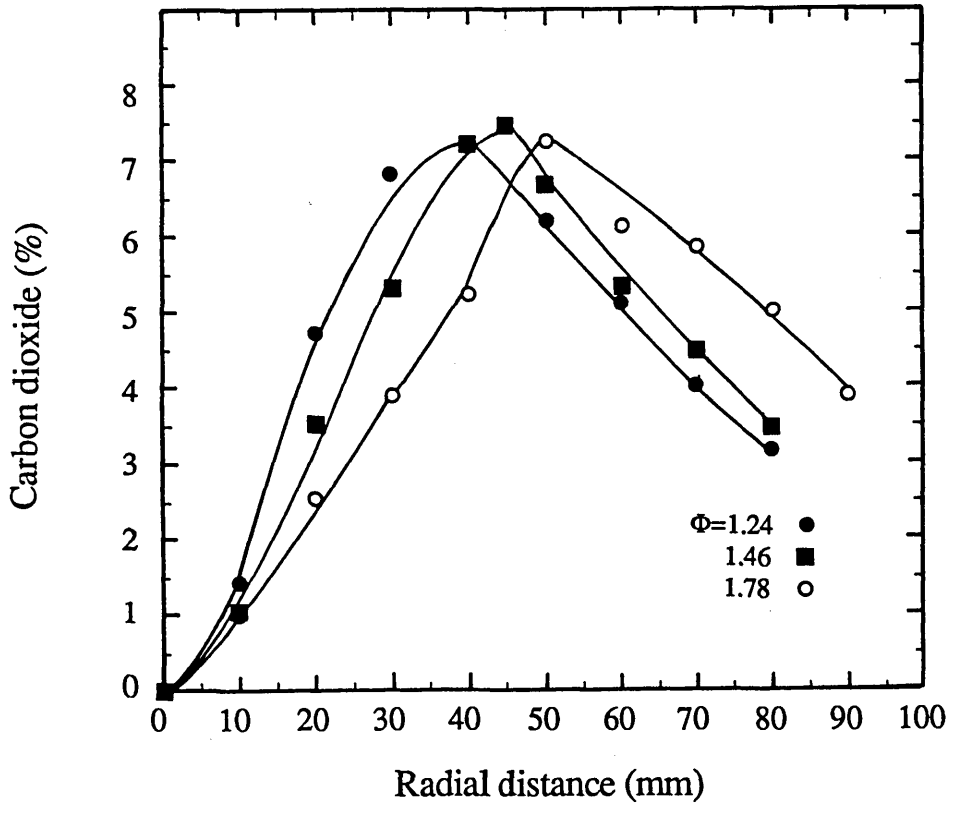

Fig. (4.38) Radial carbon dioxide profiles in counterflow flames for Re=20000 and H=20 cm.

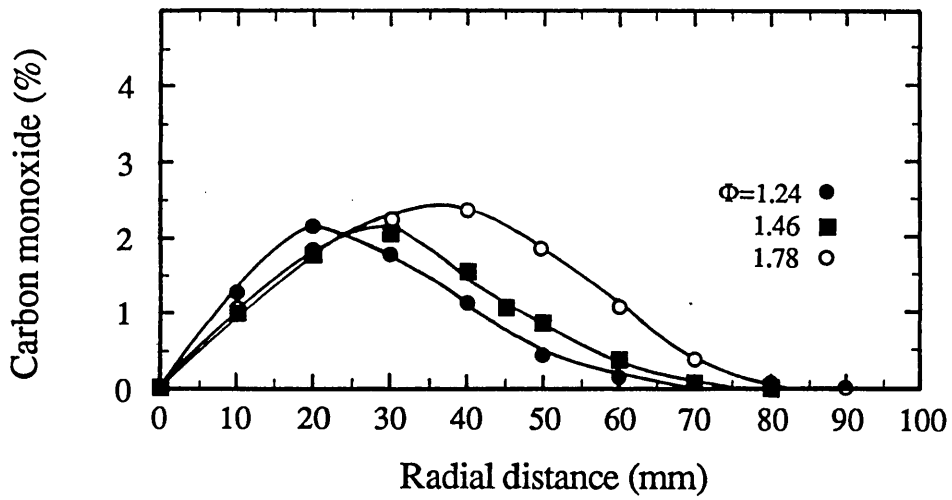

Fig. (4.39) Radial carbon monoxide profiles in counterflow flames for Re=20000 and H=20 cm.

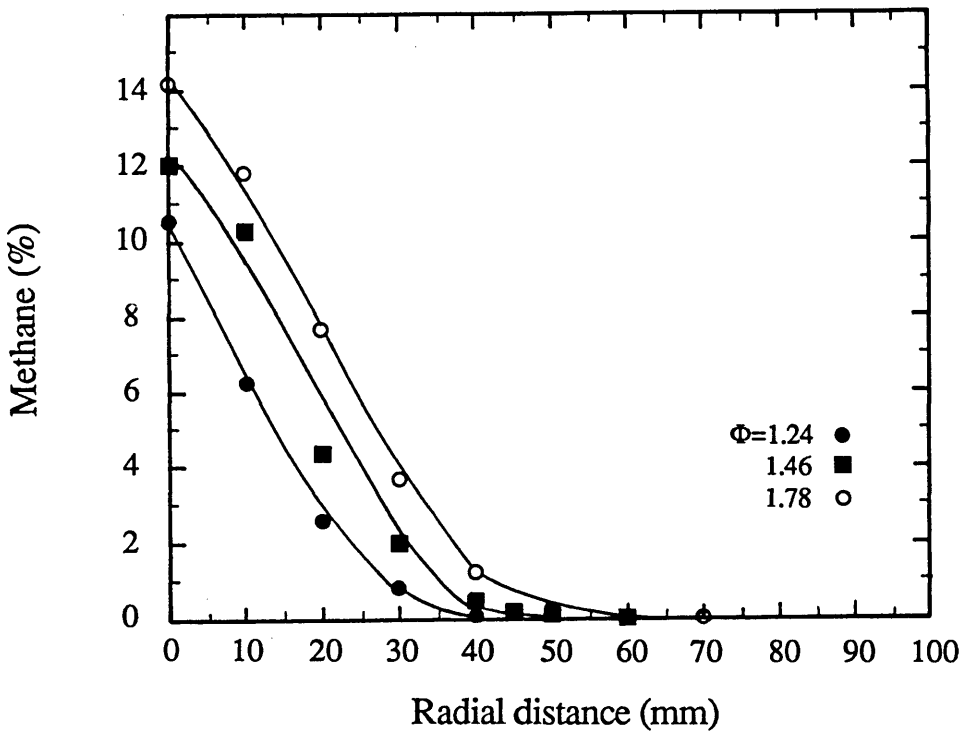

Fig. (4.40) Radial methane profiles in counterflow flames for Re=20000 and H=20 cm.

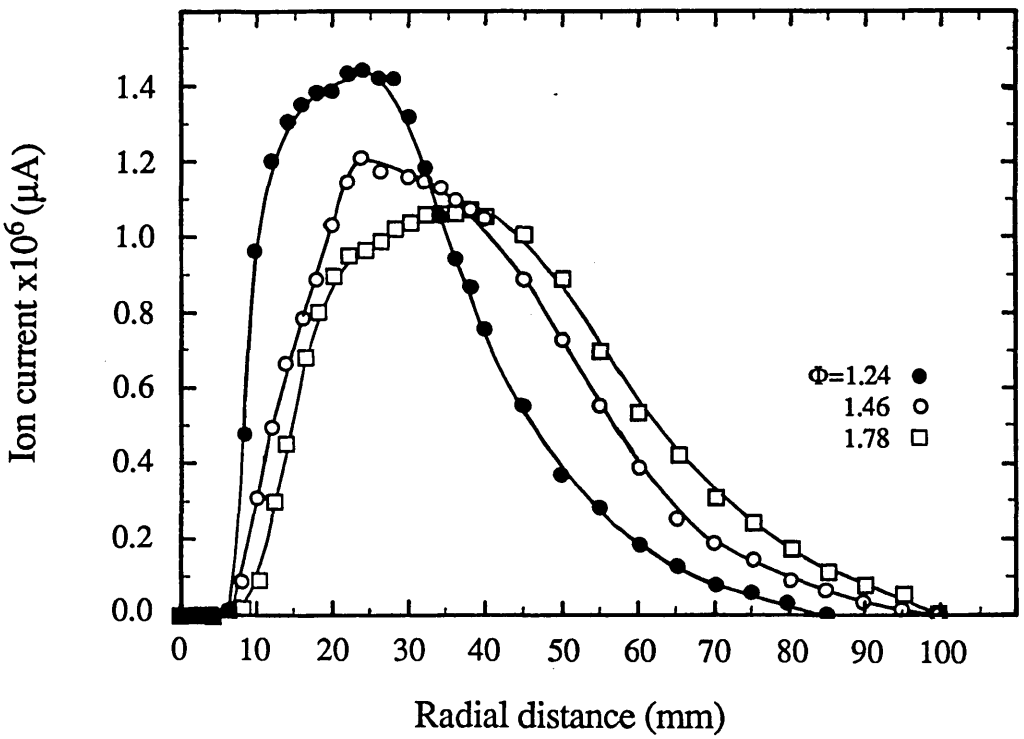

Fig. (4.41) Radial ion-current profiles in counterflow flames for Re=20000 and H=20 cm.

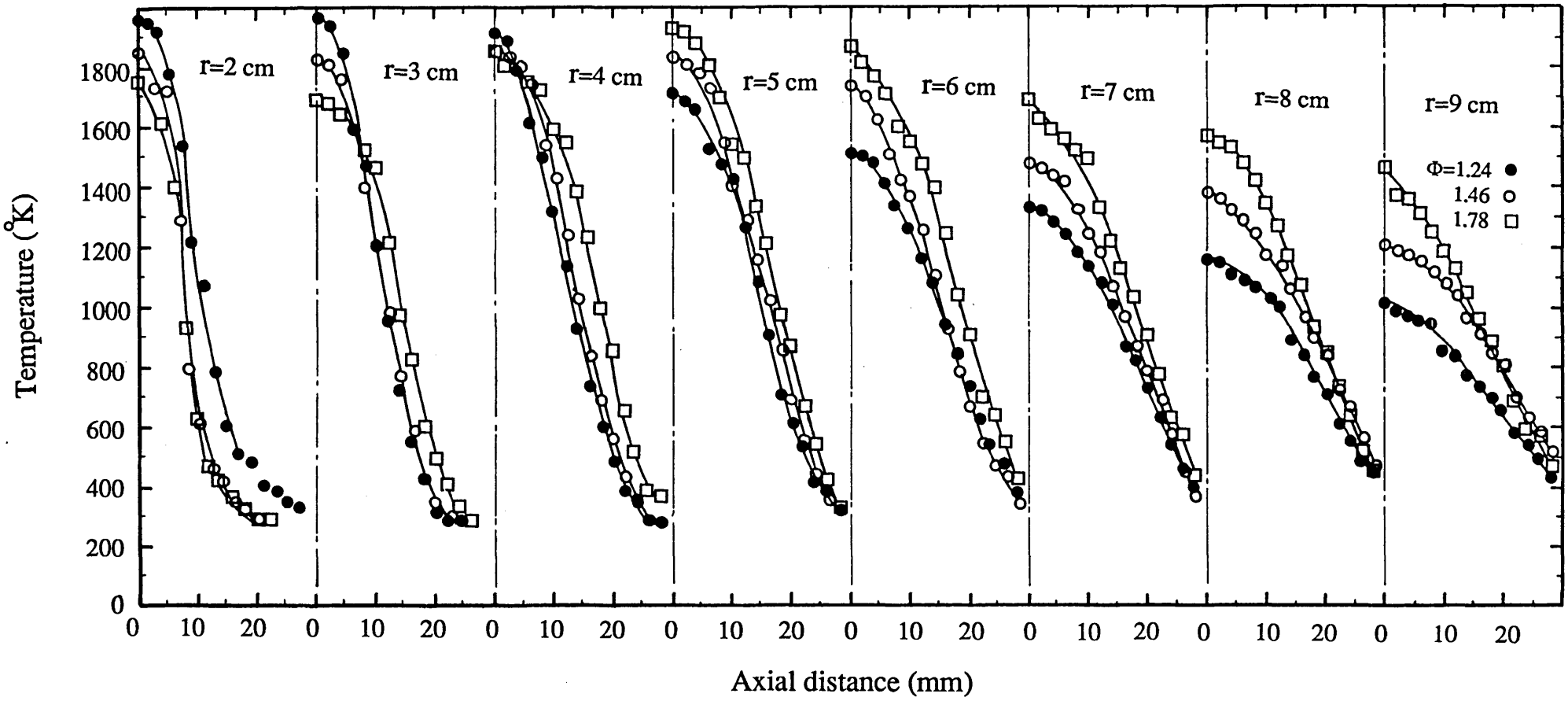

Fig. (4.42) Axial temperature profiles across the stagnation plane in counterflow flames for Re=20000 and H=20 cm.

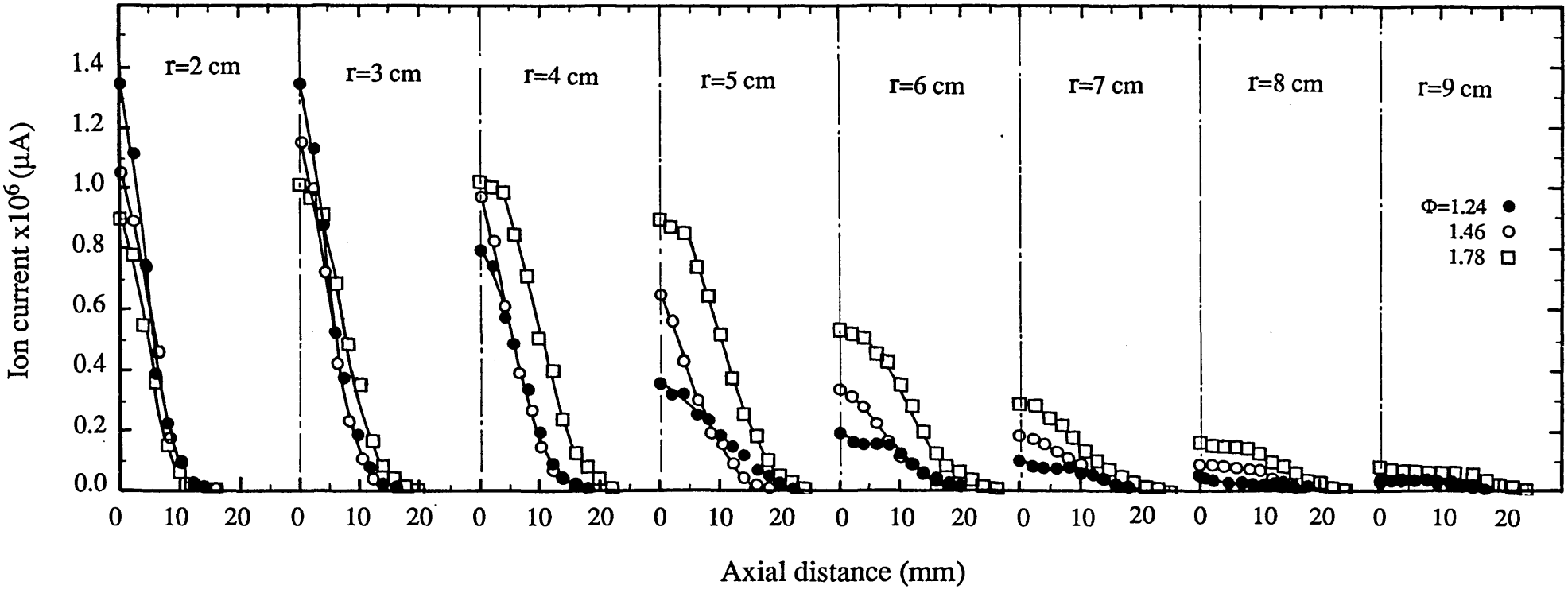

Fig. (4.43) Axial ion-current profiles across the stagnation plane in counterflow flames for Re=20000 and H=20 cm.

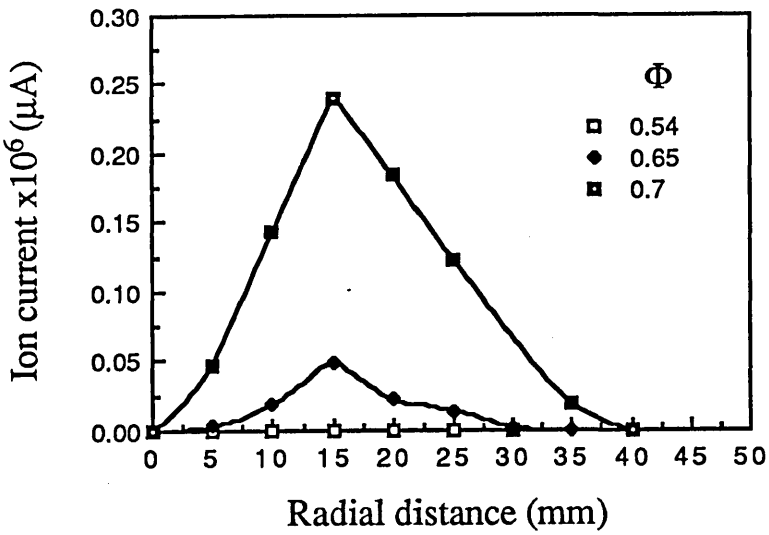

Fig. (4.44) Effect of equivalence ratio on the ion-current profiles in the stagnation plane for Re=20000 and H=7 cm.
(air and fuel are introduced from both burners)

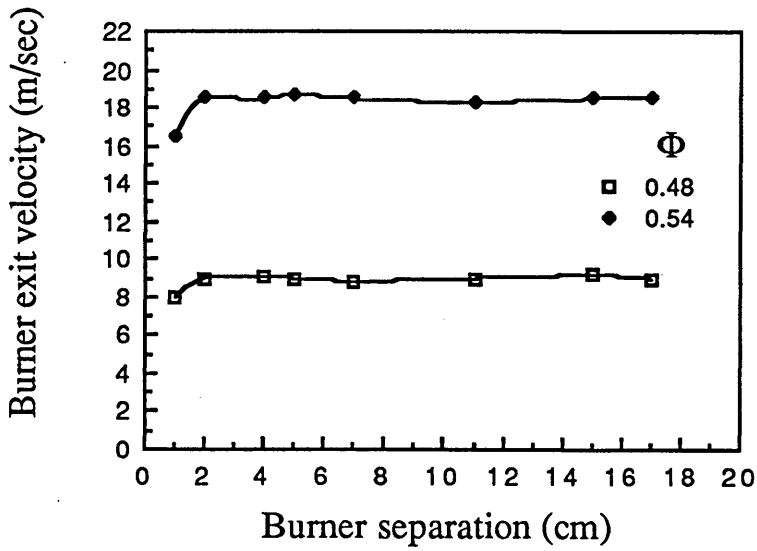

Fig. (4.45) Effect of burner separation distance on the velocity required to achieve extinction.
(air and fuel are introduced from both burners)

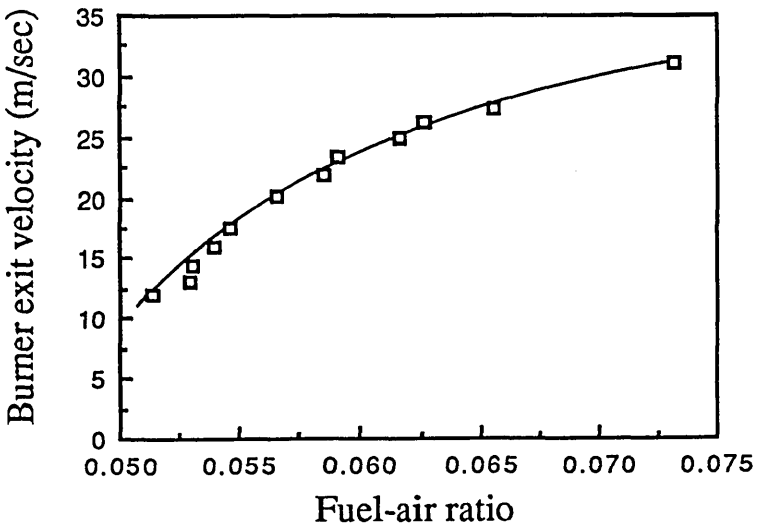

Fig. (4.46) Effect of equivalence ratio on the burner exit velocity required to achieve extinction.
(air and fuel are introduced from both burners)

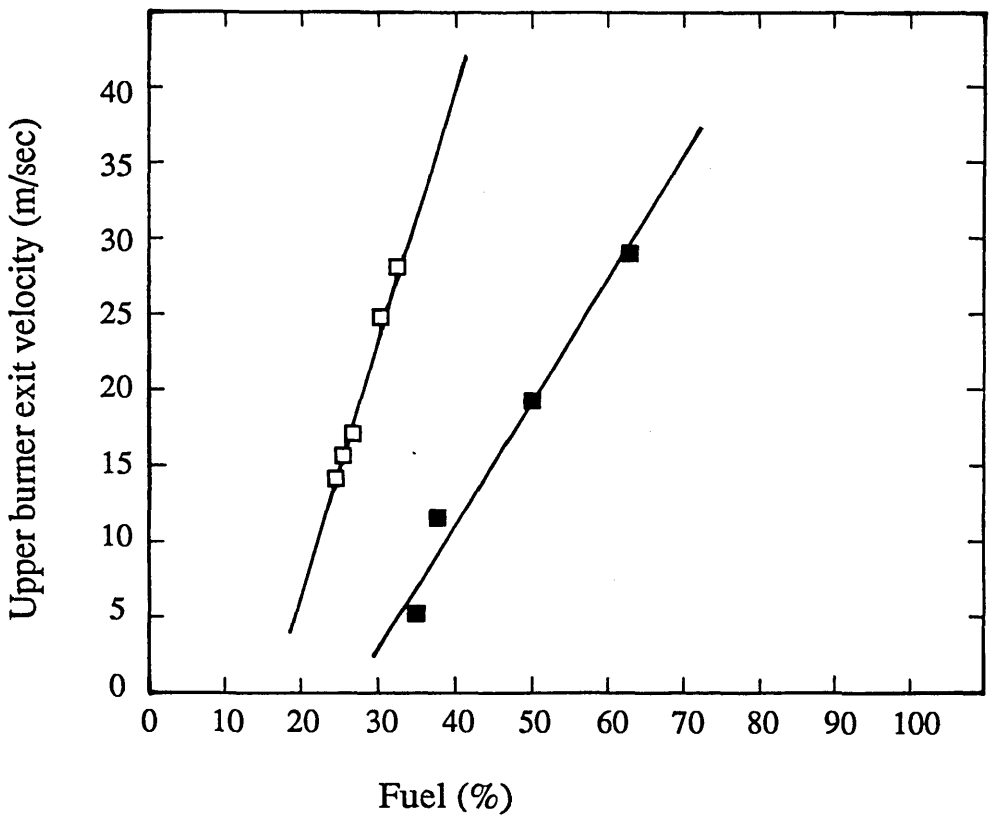

Fig. (4.47) Effect of diluting the fuel with nitrogen on the velocity required to achieve extinction.
■ air is introduced from the upper burner.
□ fuel and nitrogen are introduced from both burners.

CHAPTER 5

SUMMARY AND CONCLUSIONS

5.1 Summary

The objective of the research programme of this thesis was to provide and extend the experimental data about the turbulent counterflow flame. Axisymmetrical free vertical jets have been utilized because they are simple and well defined. The experimental programme encompassed extensive and detailed measurements of the mean temperatures, main species concentrations and mean ion currents. The measurements have been obtained using a fine-wire thermocouple for temperature, a quartz microprobe for species concentration and an ionization probe for the ion currents. A complete set of measured quantities has been obtained which show the effect of Reynolds number, burners separation distance and equivalence ratio.

Although the main objective of the present study was to provide experimental data about the counterflow flame, measurements in a single flame which were useful in delineating the run conditions were also made. In the case of the single flame, measurements of axial mean temperature were performed for a wide range of Reynolds numbers and equivalence ratios. Photographs of the single flames were also provided.

The remainder of the present chapter contains a summary of the main conclusions, section (5.2), and the recommendations for future work, section (5.3).

5.2 Conclusions

* In general, the behaviour of the present counterflow flame is similar to the single turbulent premixed flame.
* Not withstanding the previous point, a temperature drop is found to occur at a radial distance coinciding with that at which the maximum temperature occurs and the value of the temperature drop is found to increase with increasing equivalence ratio.
* The temperature measurements confirm that the stagnation plane is not an isothermal plane, it may be considered as an adiabatic plane with no heat transfer occurring across it.
* Because the equivalence ratios of the upper and lower burners were kept identical, no thermal interaction between the flames occurred.
* The radial distance where the CO_2 maximum or the O_2 minimum takes place is found to shift downstream in the radial direction with increasing Reynolds number or increasing equivalence ratio.
* Combustion is found to initiate at a radial distance of about 0.5D, independent of the Reynolds number, equivalence ratio or the

separation distance.

* The maximum temperature values are high, close to the adiabatic flame temperature, because there was little radiation loss from the present flame and most of the gases are combustion products.
* In order to achieve stable counterflow flames, the burners separation distance must be greater than 13D, twice the potential core distance.
* In the unburnt side of the flame zone, the mean ion current rises simultaneously with the mean temperature, reaching a maximum and decreasing in the burnt gas region.
* The maximum ion current is found to decrease with the distance from the burner axis resulting from the facts that, in the downstream region, the thickness of the flame zone increases and combustion is nearing completion.
* Axial temperature and ion current measurements show that the counterflow flame is symmetric across the stagnation plane.
* The thickness of the counterflow flame is found to be unaffected with increasing Reynolds number up to a radial distance of about 2.2D, while further downstream the flame thickness increases with increasing Reynolds number.
* Increasing the equivalence ratio increases the counterflow flame thickness.

5.3 Recommendations for Future Work

* Detailed information describing the behaviour of this kind of flame is useful for its modelling.
* The immediate need is to supplement the data with velocity measurements, mean and fluctuating, so that a complete record of the principal measurable quantities is available.
* Measurements of velocity with mean and fluctuating temperature is recommended in order to estimate the temperature-velocity correlation by using the two signals of temperature and velocity provided by a closely spaced fine thermocouple and laser Doppler control volume.
* Knowledge of the local and instantaneous flame front movements would be very helpful to further understanding of the characteristics of the counterflow flames. An ionization probe with two sensors can be used for this purpose. Knowing the distance between the two sensors and by comparing a pair signals of ion current the period (τ) can be determined, where τ is the time when an ion current peak is detected by one sensor to the time when almost the same peak is detected by the other sensor.

References

Abdalla, A.Y., Bradley, D., Chin, S.B. and Choilam (1982)
"Temperature fluctuations in a jet-stirred reactor and modelling implications"
19th Symp. (Int.) on Combustion, pp. 495-502

Ahlheim, M. and Gunther, R. (1979)
"Ionization measurements in free-jet diffusion flames"
Comb. and Flame, Vol. 36, pp. 117-124

Arai, M. and Hiroyasu, H. (1988)
"Measurement of soot concentration in turbulent diffusion flames"
JSME, Int. J., Vol. 31, No. 2, pp. 306-313

Attya, A.M. and Whitelaw, J.H. (1981)
"Velocity, temperature and species concentration in unconfined kerosene spray flames"
ASME Winter Annual Meeting, Nov., Paper No. 81-WA/HT-47

Ballantyne, A., Boon, D.J. and Moss, J.B. (1976)
"Measurements of fluctuating temperature in open diffusion flames employing fine wire thermocouples"
Dept. of Aeronautics and Astronautics, University of Southampton, AASU Memo. No. 36/3

Barnard, J.A. and Bradley, J.N. (1985)
"Flame and combustion"
Second edition, Chapman and Hall

Basu, P. and Bhaduri, D. (1972)
"Structure of premixed turbulent flame"
Comb. and Flame, vol. 18, pp. 303-305

Becker, H.A. and Yamazaki, S. (1978)
"Entrainment, momentum flux and temperature in vertical free turbulent diffusion flames"
Comb. and Flame, Vol. 33, pp. 123-149

Bicen, A.F., Tse, D. and Whitelaw, J.H. (1988)
"Flow and combustion characteristics of an annular combustor"
Comb. and Flame, Vol. 72, pp. 175-192

Billing, B.F. (1964)
"Thermocouples: their instrumentation, selection and use"
Mech. Eng. Dept., City & Guilds College

Boiarski, A.A., Barnes, R.H. and Kircher, J.F. (1978)
"Flame measurements utilizing raman scattering"
Comb. and Falme, Vol. 32, pp. 111-114

Boukhalfa, A. and Gokalp, I. (1988)
"Influence of the Damkohler number on the average thickness of conical turbulent premixed methane-air flames"
Comb. and Flame, Vol. 73, pp. 75-87

Bowman (1977)
AIAA Prog. in Aeronautics and Astronautics, Vol. 53, p. 3

Bradley, D. and Matthews, K.J. (1968)
"Measurement of high gas temperatures with fine wire thermocouples"
J. Mech. Eng. Sci., Vol. 10, No. 4, pp. 299-305

Bradley, J.N. (1969)
"Flame and combustion phenomena"

Brophy, J.R. and Wilbur, P.J. (1986)
"Calculation of plasma properties in ion sources"
AIAA, Vol. 24, No. 9, pp. 1516-1523

Calcote, H.F. (1957)
"Mechanisms for the formation of ions in flames"
Comb.and Flame, Vol. 1, pp. 385-403

Calcote, H.F. (1963)
"Ion and electron profiles in flames"
9th Symp. (Int.) on Combustion, pp. 622-637

Chandran, S.B.S., Komerath, N.M. and Strahle, W.C. (1984)
"Scalar-velocity correlations in a turbulent premixed flame"
20th Symp. (Int.) on Combustion, pp. 429-435

Chedalle, J. and Baud, Y. (1972)
"Measurements in flames"
Industrial Flames, Vol. 1, Edward Arnold publishers, London

Chen, Z.H., Liu, G.E. and Sohrab, S.H. (1987)
"Premixed flames in counterflow jets under rigid-body rotation"
Comb. Sci. and Tech., Vol. 51, pp. 39-50

Cho, P., Law, C.K., Hertzberg, J.R. and Cheng, R.K. (1986)
"Structrure and propagation of turbulent premixed flames stabilized in a stagnation flow"
21st Symp. (Int.) on Combustion, pp. 1493-1499

Clements, R.M. and Smy, P.R. (1969)
J. Applied Physics, Vol. 40, p. 4553

Clements, R.M. and Smy, P.R. (1969)
J. Applied Physics, Vol. 41, p. 3745

Colket, M.B., Chiappetta, L., Guile, R.M., Zabielski, M.F. and Seery, D.J. (1982)
"Internal aerodynamics of gas sampling probes"
Comb. and Flame, Vol. 44, pp. 3-14

Cowper and DeRose (1983)
"The analysis of gases by chromatography"
Pergamon Press, Oxford

Daneshyar, H., Mendes-Lopes, J.M.C. and Ludford, G.S.S (1982)
"Effect of strain fields on burning rate"
19th Symp. (Int.) on Combustion, pp. 413-421

Davies, J.T. (1972)
"Turbulent phenomena"
Academic Press, New York and London

Deckers, J. and Tiggelen, A.V. (1957)
"Extraction of ions from a flame"
Comb. and Flame, Vol. 1, pp. 281-286

Denniston, D.W., Oxendine, J.R., Knapschaefer, D.H., Burgess, D.S. and Karlovitz, B. (1957)
"Applications of the electrostatic probe to the study of turbulent flames"
J. Applied Physics, Vol. 28, pp. 70-75

Drummond, I. (1988)
"Self communication"
Chem. Eng. Dept., Imperial College

Dugger, G.L. and Heimel, S. (1952)
"Flame speed of methane-air, propane-air, and ethylene-air mixtures at low initial temperatures"
NACA, TN 2624

Eckbreth, A.C., Hall, R.J. and Shirley, J.A. (1980)
"Investigations of coherent anti-stokes raman spectroscopy (CARS) for practical combustion diagnostics"
AGARD Conference Proceedings, No. 281, Paper No. 18, pp. 1-13

Egolfopoulos, F.N., Cho, P. and Law, C.K. (1989)
"Laminar flame speeds of methane-air mixtures under reduced and elevated pressures"
Comb. and Flame, Vol. 76, pp. 375-391

Fang, M., Schmitz, R.A. and Ladd, R.G. (1971)
"Combustion of a premixed system in stagnation flow"
Comb. Sci. and Tech., Vol. 4, pp. 143-148

Fox, J.S. and Bertrand, C. (1981)
"Measurement of local saturation current in flames"
Comb. and Flame, Vol. 43, pp. 317-320

Fristrom, R.M., Prescott, R. and Grunfelder, C. (1957)
"Flame zone studies"
Comb. and Flame, Vol. 1, pp. 102-113

Fristrom, R.M. and Westinberg, A.A. (1965)
"Flame structure"
McGraw Hill, New York

Glass, M. and Kennedy, I.M. (1977)
"An improved seeding method for high temperatures laser Doppler velocimetry"
Comb. and Flame, Vol. 29, pp. 333-335

Godoy, S. (1982)
"Turbulent diffusion flames"
Ph.D. Thesis, Imperial College

Greenhalgh, D.A. (1983)
"Gas phase temperature and concentration diagnostics with lasers"
AERE Harwell, Oxfordshire, Report No. C66/83

Hall, R.J. (1979)
"CARS spectra of combustion gases"
Comb. and Flame, Vol. 35, pp. 47-60

Harris, S.J., Weiner, A.M. and Blint, R.J. (1988)
"Concentration profiles in rich and sooting ethylene flames"
21th Symp. (Int.) on Combustion, pp. 1033-1045

Hassan, M.M. (1983)
"A study of natural gas and pulverised coal diffusion flames"
Ph.D. Thesis, Imperial College

Hassan, M.M., Lockwood, F.C. and Moneib, H.A. (1983)
"Measurements in gas-fired cylindrical furnace"
Comb.and Flame, Vol. 51, pp. 249-261

Heitor, M.V., Taylor, A.M.K.P. and Whitelaw, J.H. (1985)
"Simultaneous velocity and temperature measurements in a premixed flame"
Experiments in Fluids, Vol. 3, pp. 323-339

Hinze, J.O. (1975)
"Turbulence"
2nd Eddition, McGraw Hill, New York

Hirano, T., Suzuki, T., Hashimoto, Y. and Mashiko, I. (1981)
"Basic characteristics of cylindrical, electrostatic probes for the measurements of fluctuating premixed flames"
Bulletin of the JSME, Vol.24, No. 187, pp. 168-174

Hirji, K.A. (1986)
"Combustion measurements in pulverized coal flames"
Ph.D. Thesis, Imperial College

Hirshfelder, J.O., Curtiss, C.F. and Bird, R.B. (1954)
"Molecular theory of gases and liquids" , p. 530

Ishizuka, S. and Law, C.K. (1982)
"An experimental study on extinction and stability of stretched premixed flames":
19th Symp. (Int.) on Combustion, pp. 327-335

Ishizuka, S., Miyasaka, K. and Law, C.K. (1982)
"Effect of heat loss, preferential diffusion, and flame stretch on flame- front instability and extinction of propane-air mixtures"
Comb. and Flame, Vol. 45, pp. 293-308

Ievlev, V.N. (1957)
"Combustion of a turbulent jet in burners with preliminary mixing"
6th Symp. (Int.) on Combustion, pp. 317-325

Kaiser, R.E. (1970)
"Carbon molecular sieve"

Chromatographia, Vol. 13, p. 38

Kaiser, E.W., Rothschild, W.G. and Lavoie, G.A. (1983)
"Effect of fuel-air equivalence ratio and temperature on the structure of laminar propane-air flames"
Comb. Sci. and Tech., Vol. 33, pp. 123-134

Karlovitz, B., Denniston, D.W. and Wells, F.E. (1951)
Chemical Physics, Vol. 19, p. 541

Karlovitz, B., Denniston, D.W., Knapschaefer, D.H. and Wells, F.E. (1953)
"Studies on turbulent flames"
4th Symp. (Int.) on Combustion, pp. 613-620

Katsuki, M., Mizutani, Y. and Matsumoto, Y. (1987)
"An improved thermocouple technique for measurement of fluctuating temperatures in flames"
Comb.and Flame, Vol. 67, pp. 27-36

Katsuki, M., Mizutani, Y., Yasuda, T., Kurosawa, Y., Kobayashi, K. and Takahashi, T. (1988)
"The effect of initial conditions on the propagation of a premixed flame in a mixing layer"
Comb. and Flame, Vol. 74, pp. 9-18

Kent, J.H. and Bilger, R.W. (1973)
"Turbulent diffusion flames"
14th Symp. (Int.) on Combustion, pp. 615-625

Khalil, K.L., Mahalawy, F.M. and Moneib, H.A. (1976)
"Effect of combustion air swirl on the flow pattern in a cylindrical oil furnace"
16th Symp. (Int.) on Combustion, pp. 135-143

Kilham, J.K. and Kirmani, N. (1979)
"The efect of turbulence on premixed flame noise"
17th Symp. (Int.) on Combustion, pp. 327-335

Kobayashi, H. and Kitano, M. (1989)
"Extinction characteristics of a stretched cylindrical premixed flame"
Comb. and Flame, Vol. 76, pp. 285-295

Koda, S. and Fujiwara, O. (1986)
"Silane combustion in an opposed jet diffusion flame"
21st Symp. (Int.) on Combustion, pp. 1861-1867

Kostiuk, L.W., Bray, K.N.C. and Chew, T.C. (1989)
"Premixed turbulent combustion in counterflow streams"
Comb. Sci. and Tech., Vol. 64, pp. 233-241

Kowalik, R.M. and Kruger, C. H. (1979)
"Laser fluorescence temperature measurements"
Comb. and Flame, Vol. 34, p. 135-140

Kramlich, J.C. and Malte, P.C. (1978)
"Modeling and measurement of sample probe effects on pollutant gases drawn from flame zones"
Comb. Sci. and Tech., Vol. 18, pp. 91-104

Lapp, M. and Hartley, D.L. (1976)
"Raman scattering studies of combustion"
Comb. Sci. and Tech., Vol. 13, pp. 199-210

Laurendeau, N.M. (1988)
"Temperature measurements by ligth-scattering methods"
Prog. in Energy and Combustion Science, Vol. 14, p. 147

Law, C.K., Ishizuka, S. and Mizomoto, M. (1981)
"Lean-limit extinction of propane-air mixtures in the stagnation-point flow"
18th Symp. (Int.) on Combustion, pp. 1791-1798

Law, C.K. and Sivashinsky, G.I. (1982)
"Catalytic extension of extinction limits of stretched premixed flames"
Comb. Sci. and Tech., Vol. 29, pp. 277-286

Law, C.K., Zhu, D.L. and Yu, G. (1986)
"Propagation and extinction of stretched premixed flames"
21th Symp. (Int.) on Combustion, p. 1419

Lenz, W. and Gunther, R. (1980)
"Measurements of fluctuating temperature in a free-jet diffusion flame"
Comb. and Flame, Vol. 37, pp. 63-70

Lewis, B. and Von Elbe, G. (1967)
"Combustion, flames and explosion of gases"
Academic press., New york

Lewis, G.D., David, T., Gaskell, P.H., Fukutani, S., Jinno, H., Miller, J.A., Kee, R.J., Smook, M.D., Peters, N., Effelsberg, E., Warnatz, J. and Behrendt, F. (1984)
"Calculation of the structure and extinction limit of a methane-air counterflow diffusion flame in the forward stagnation region of a porous cylinder"
20th Symp. (Int.) on Combustion, pp. 1893-1904

Lin, T.H. and Sohrab, S.H. (1987)
"Influence of vorticity on counterflow diffusion flames"
Comb. Sci. and Tech., Vol. 52, pp. 75-90

Liu, G.E., Ye, Z.Y. and Sohrab, S.H. (1986)
"On radiative cooling and temperature profiles of counterflow premixed flames"
Comb. and Flame, Vol. 64, pp. 193-201

Lockwood, F.C. and Odidi, A.O.O. (1975)
"Measurement of mean and fluctuating temperature and of ion concentration in round free-jet turbulent diffusion and premixed flames"
15th Symp. (Int.) on Combustion, pp. 561-571

Lockwood, F.C. and Moneib, H.A. (1982)
"Fluctuating temperature measurements in turbulent-jet diffusion flame"
Comb. and Flame, Vol. 47, pp. 291-314

Longwell, J.P. (1976)
"Synthetic fuels and combustion"
16th Symp. (Int.) on Combustion, pp. 1-15

Masri, A.R. and Bilger, R.W. (1984)
"Turbulent diffusion flames of hydrocarbon fuels stabilized on a bluff body"
20th Symp. (Int.) on Combustion, pp. 319-326

Masri, A.R. and Bilger, R.W. (1986)
"Turbulent non-premixed flames of hydrocarbon fuels near extinction"
21st Symp. (Int.) on Combustion, pp. 1511-1520

Matalon, M. (1983)
"On flame stretch"
Comb. Sci. and Tech., Vol. 31, pp. 169-181

Maker and Terhune (1977)
"Experimental diagnostics in gas phase combustion systems"
Prog. in Aeronautics and Astronautics, Vol. 53

Mehta, G.K., Ramachandra, M.K. and Strahle, W.C. (1981)
"Correlations between light emission, acoustic emission and ion density in premixed turbulent flames"
18th Symp. (Int.) on Combustion, pp. 1051-1059

Mendes-Lopes, J.M.C. (1983)
"Influence of strain fields on flame propagation"
Ph.D. Thesis, University of Cambridge

Michaud, P., Delfau, J.L. and Barassin, A. (1981)
"The positive ion chemistry in the post-combustion zone of sooting premixed acetylene low pressure flat flames"
18th Symp. (Int.) on Combustion, pp. 443-451

Moneib, H.A. (1980)
"Experimental study of the fluctuating temperature in inert and reacting turbulent jets"
Ph.D. thesis, Imperial college

Pindera, M.Z. and Talbot, L. (1988)
"Some fluid dynamic considerations in the modeling of flames"
Comb. and Flame, Vol. 73, pp. 111-125

Odidi, A.O.O. (1974)
"The influence of turbulence on the time-mean rate of chemical reactions"
Ph.D. thesis, Imperial College

Olson, D.B. and Calcote, H.F. (1981)
"Ions in fuel-rich and sooting acetylene and benzene flames"
18th Symp. (Int.) on Combustion, pp.453-464

Peters, N. (1986)
"Laminar flamelet concepts in turbulent combustion"
21st Symp. (Int.) on Combustion, pp. 1231-1250

Potter, A.E. (1960)
Prog. Combustion Sci. Tech., Vol. 1, p. 145

Puri, I.K. and Seshadri, K. (1986)
"Extinction of diffusion flames burning diluted methane and diluted propane in diluted air"
Comb. and Flame, Vol. 65, pp. 137-150

Puri,I.K., Seshadri, K., Smook, M.D. andKeyes, D.E. (1987)
"A comparison between numerical calculations and experimental measurements of the structure of a counterflow methane-air diffusion flame"
Comb. Sci. and Tech., Vol. 56, pp. 1-22

Richmond, J.K., Singer, J.M., Cook, E.B., Oxendine, J.R., Grumer, J. and Burgess, D.S. (1957)
"Turbulent burning velocities of natural gas-air flames with pipe-flow turbulence"
6th Symp. (Int.) on Combustion, pp. 303-311

Rogg, B. (1988)
"Response and flamelet structure of stretched premixed methane-air flames"
Comb. and Flame, Vol. 73, pp. 45-65

Rose, J.W. and Cooper, J.R. (1977)
"Technical data of fuel"
Seventh Eddition, British National Committee

Sato, J. (1982)
"Effects of Lewis number on extinction behavior of premixed flames in a stagnation flow"
19th Symp. (Int.) on Combustion, pp. 1541-1548

Schaefer, B.A. (1984)
"The calculation of ion currents in hydrocarbon flames"
Comb. and Flame, Vol. 56, pp. 43-49

Schichting, H. (1968)
"Boundary layer theory"
McGraw Hill Book Co.

Schoenung, S.M. and Hanson, R.K. (1981)
"CO and temperature measurements in a flat flame by laser absorption spectroscopy and probe technique"
Comb. Sci. and Tech., Vol. 24, pp. 227-237

Sochet, L.R., Lucqiun, M., Bridoux, M., Crunelle-Cras, M., Grase, F. and Delhaye, M. (1979)
"Use of multichannel pulsed raman spectroscopy as a diagnostic technique in flames"
Comb. and Flame, Vol. 36, pp.109-116

Sohrab, S.H. and Law, C.K. (1984)
"Extinction of premixed flames by stretch and radiative loss"
Int. J. Heat Mass Transfer, Vol. 27, No. 2, pp. 291-300

Sohrab, S.H., Ye, Z.Y. and Law, C.K. (1984)
"An experimental investigation on flame interaction and the existence of negative flame speed"
20th Symp. (Int.) on combustion, pp. 1957-1965

Sohrab, S.H., Ye, Z.Y. and Law, C.K. (1986)
"Theory of interactive combustion of counterflow premixed flames"
Comb. Sci. and Tech., Vol. 45, pp. 27-45

Starner, S.H. and Bilger, R.W. (1985)
"Characteristics of a piloted diffusion flame designed for study of combustion turbulence interactions"
Comb. and Flame, Vol. 61, pp. 29-38

Suzuki, T., Hashimoto, Y. and Mashiko, I. (1979)
"Ion-current fluctuations recorded with a cylindrical electrostatic probe passing premixed flames"
Comb. and Flame, Vol. 36, pp. 179-191

Suzuki, T., Hirano, T. and Tsuji, H. (1979)
"Flame front movements of a turbulent premixed flame"
17th Symp. (Int) on Combustion, pp. 289-297

Suzuki, T. and Hirano, T. (1982)
"Ion-current correlation measurements in a turbulent premixed flame"

Tine (1961)
"Gas sampling and chemical analysis in combustion processes"
Pergamon Press, New York

Travers, B.E.L. and Williams, H. (1965)
"The use of electrical probes in flame plasmas"
10th Symp. (Int.) on Combustion, pp. 657-672

Tsuji, H. and Hirano, T. (1970)
"Ion-concentration distributions in two-dimensional nozzle burner flames at atmospheric pressure"

Comb. and Flame, Vol. 15, No. 1, pp. 47-56

Tsuji, H. and Yamaoka, I. (1982)
"Structure and extinction of near-limit flames in a stagnation flow"
19th Symp. (Int.) on Combustion, pp. 1533-1540

Van Wylen, G.J. and Sonntag, R.E. (1985)
"Fundamentals of classical thermodynamics"
3rd Eddition

Ventura, J.M.P., Suzuki, T., Yule, A.J., Ralph, S. and Chigier, N.A. (1981)
"The investigation of time dependent flame structure by ionizatio
probes"
18th Symp. (Int.) on Combustion, pp. 1543-1551

Ventura, J.M.P., Yule, A.J. and Chigier, N.A. (1982)
"Ionization and concentration measurements in the transitional region of partially premixed flames"
19th Symp. (Int.) on Combustion, pp. 469-475

Vranos, A., Faucher, J.E. and Curtis, W.E. (1969)
"Turbulent mass transport and rates of reaction in a confined hydrogen-air diffusion flame"
12th Symp. (Int.) on Combustion, pp. 1051-1057

Westenberg, A.A., Raezer, S.D. and Fristrom, R.M. (1957)
"Interpretation of the sample taken by a probe in a laminar concentration gradient"
Comb. and Flame, Vol. 1, pp. 467-478

Williams, F. A. (1984)
"Some aspects of the interactions between turbulent flows and combustion

proccesses"
Ref. Comb. Sci. and Tech., Vol. 51, pp. 39-50

Yanagi, T. (1972)
"Effect of concentration gradient on composition of sampled gas.II. Experimental verification"
Comb. and Flame, Vol. 19, pp. 1-9

Yanagi, T. and Mimura, Y. (1972)
"Effect of concentration gradient on composition of sampled gas.I. Theoretical analysis"
Comb. and Flame, Vol. 18, pp. 347-356

Yanagi, T. (1977)
"Effects of probe sampling rates on sample composition"
Comb.and Flame, Vol. 28, pp. 33-44

Yoshida, A. and Gunther, R. (1981)
"An experimental study of structure and reaction rate in turbulent premixed flames"
Comb. Sci. and Tech. , Vol. 26, pp. 43-50

Zinn, B.T. (1977)
"Experimental diagnostics in gas phase combustion systems"
Prog. in Aeronautics and Astronautics, Vol. 53, AIAA

APPENDIX I

MIXTURE CALCULATIONS

The calculations of the equivalence ratio and the Reynolds number as a function of the air and gas flow rates are presented in this Appendix. Where:

$V_{a,at}$ = air volume flow rate at the atm. conditions

V_a = air volume flow rate at the workong conditions

m_a = air mass flow rate

P = working pressure

$V_{g,at}$ = gas volume flow rate at the atm. conditions

V_g = gas volume flow rate at the workong conditions

m_g = gas mass flow rate

ρ_a = air density

ρ_a = gas density

μ_a = air viscosity

μ_g = gas viscosity

***Air**

$$V_{a,at} = (V_a)\,(P / p_{at})^{0.5} \quad \text{L/min} \qquad \text{(A1.1)}$$

$$m_a = (V_{a,at})\,(\rho_{a,at})$$

$$= (V_a)\,(\rho_{a,at})\,(P / p_{at})^{0.5}$$

$$= (V_a)\,(10^{-3})\,(1.22)\,(P / 1.013)^{0.5}$$

$$= (1.2121)\ (10^{-3})\ (V_a)\ (p)^{0.5} \qquad \text{kg/min} \qquad \text{(A1.2)}$$

***Gas**

$$V_{g,at} = (V_g)\ (p / p_{at})^{0.5} \qquad \text{L/min} \qquad \text{(A1.3)}$$

$$m_g = (V_{g,at})\ (\rho_{g,at})$$

$$= (V_g)\ (\rho_{g,at})\ (p / p_{at})^{0.5}$$

$$= (V_g)\ (10^{-3})\ (0.7283)\ (p / 1.013)^{0.5}$$

$$= (0.7236)\ (10^{-3})\ (V_g)\ (p)^{0.5} \qquad \text{kg/min} \qquad \text{(A1.4)}$$

***Air/fuel ratio (A/F)**

$$(A/F)_m = m_a / m_g \qquad \text{(A1.5)}$$

$$= [(1.2121)\ (V_a)] / [(0.7236)\ (V_g)]$$

$$= (1.68)\ (V_a / V_g) \qquad \text{(A1.6)}$$

$$(A/F)_v = V_a / V_g \qquad \text{(A1.7)}$$

***Stoichiometric air/fuel ratio $(A/F)_{st}$**

According to gas compositions, table (2.1), the stoichiometric air/fuel ratio can be calculated;

Fuel + Air ——— Products

$$[\ 0.9363\ CH_4 + 0.0325\ C_2H_6 + 0.0178\ N_2 + 0.0069\ C_3H_8 + 0.0027\ C_4H_{10} + 0.0013\ CO_2 + 0.0009\ C_5H_{12}\ ] + [\ X\ (\ O_2 + (79/21)\ N_2)] \text{ ———}$$

$A\ CO_2 + B\ CO + [\ 0.0178 + (79/21)\ X\ ]\ N_2$

Carbon balance (C):

$$A = 0.9363 + 2\ (0.0325) + 3\ (0.0069) + 4\ (0.0027) + 0.0013 + 5\ (0.0009)$$

$$A = 1.0386 \qquad \text{(A1.8)}$$

Hydrogen balance (H):

$$2\ (B) = 4\ (0.9363) + 6\ (0.0325) + 8\ (0.0069) + 10\ (0.0027) + 12\ (0.0009)$$

$$B = 2.0166 \qquad \text{(A1.9)}$$

Oxygen balance (O):

$$2\ (0.0013) + 2\ (X) = 2\ (A) + B$$

From (A1.8) and (A1.9):

$$2\ (0.0013) + 2\ (X) = 2\ (1.0386) + 2.0166$$

$$X = 2.04 \qquad \text{(A1.10)}$$

$$(A/F)_{st,v} = (X)\ (100/21)$$

From (A1.10):

$$(A/F)_{st,} = (2.04)\ (100/21)$$

$$= 9.71 \qquad \text{(A1.11)}$$

$$(A/F)_{st,m} = ((A/F)_{st,v})\ (M_a / M_g)$$

$$= 16.35 \qquad \text{(A1.12)}$$

***Equivalence ratio (Φ)**

$$\Phi = (F/A)_v / (F/A)_{st,v} \qquad \text{(A1.13)}$$

$$= (F/A)_v / (1/9.71)$$

$$= (9.71)\ (F/A)_v \qquad \text{(A1.14)}$$

Or $\Phi = (F/A)_m / (F/A)_{st,m}$ (A1.15)

$$= (F/A)_m / (1 / 16.35)$$

$$= (16.35)\ (F/A)_m \qquad \text{(A1.16)}$$

***Mixture density (ρ_m)**

$$\rho_m = [\rho_a / (1+(F/A)_v)] + [\rho_g / (1+(A/F)_v)]: \qquad \text{(A1.17)}$$

Gordon et al (1985), from (A1.14):

$$\rho_m = [^{1.22} / (1+(\Phi/9.71))] + [^{0.7283} / (1+(9.71/\Phi))] \qquad \text{(A1.18)}$$

Fig. (A1.1) shows the effect of equivalence ratio on the mixture density.

***Mixture viscosity (μ_m)**

$$^1 / (\mu_m)^{0.5} = [^{x_a} / ((\mu_a)^{0.5})] + [^{x_g} / ((\mu_g)^{0.5})]: \qquad \text{(A1.19)}$$

Hirshfelder et al (1954)

where:

$$x_a = ^A / (A+F) = ^1 / (1+(F/A)_v)$$

$$x_g = ^F / (A+F) = ^1 / ((A/F)_v+1)$$

$$^1 / (\mu_m)^{0.5} = \{^1 / [(1+(F/A)_v)(\mu_a)^{0.5}]\} +$$

$$\{^1 / [((A/F)_v+1)(\mu_g)^{0.5}]\} \qquad \text{(A1.20)}$$

From (A1.14):

$$1 / (\mu_m)^{0.5} = \{ {}^{1} / [(1+(\Phi/9.71))(1.81\text{x}10^{-5})^{0.5}] \} +$$
$$\{ {}^{1} / [((9.71/\Phi)+1)(1.087\text{x}10^{-5})^{0.5}] \}$$
$$= \{235.1 / (1+(\Phi/9.71))\} +$$
$$\{303.3 / ((9.71/\Phi)+1)\} \qquad \text{(A1.21)}$$

Fig. (A1.2) shows the effect of equivalence ratio on the mixture viscosity.

***Burner exit velocity (V_o)**

V_o = total mass flow rate /(area x mixture density)

$= (m_a+m_g) / [(2)(\pi/4)(D)^2(\rho_m)(60)]$ m/sec

$= (m_a+m_g) / [(2)(\pi/4)(0.0137)^2(\rho_m)(60)]$

$= (m_a+m_g) / [(0.0177)(\rho_m)]$

$= m_a [(1+(F/A)_m) / ((0.0177)(\rho_m))]$ (A1.22)

From (A1.16)

$V_o = [(1+(\Phi/16.35)) / 0.0177] ({}^{m_a}/_{\rho_m})$ m/sec (A1.23)

Or $= m_g [((A/F)_m+1) / ((0.0177)(\rho_m))]$

From (A1.16):

$V_o = [((16.35/\Phi)+1) / 0.0177] ({}^{m_g}/_{\rho_m})$ m/sec (A1.24)

***Reynolds number (Re)**

$Re = [(V_o)(\rho_m)(D)] / \mu_m$

$$= [(m_a+m_g) / ((0.0177) (\rho_m))] \times [((\rho_m) (0.0137)) / \mu_m]$$

$$= (0.774) (m_a+m_g) / \mu_m$$

$$= (0.774) (1+(F/A)_m) (^{m}a / \mu_m)$$

From (A1.16):

$$Re = (0.774) (1+(\Phi/16.35)) (^{m}a / 5y\mu_m) \qquad (A1.25)$$

Or

$$= (0.774) ((A/F)_m+1) (^{m}g / \mu_m)$$

From (A1.16)

$$= (0.774) ((16.35/\Phi)+1) (^{m}g / \mu_m) \qquad (A1.26)$$

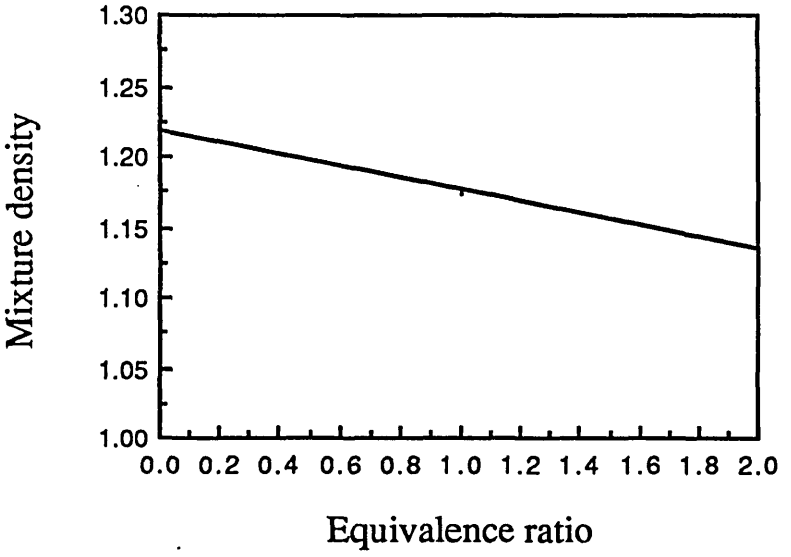

Fig. (A1.1) Effect of equivalence ratio on the mixture density.

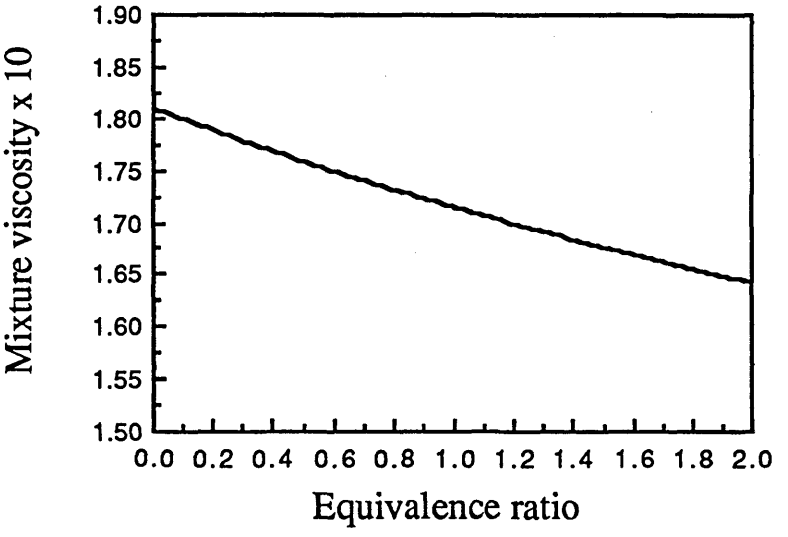

Fig. (A1.2) Effect of equivalence ratio on the mixture viscosity.

APPENDIX II

IONIZATION CIRCUIT

Fig. (A2.1) shows a schematic diagram of the ionization circuit used in the present study. The circuit mainly consists of 1 MΩ resistance and a total voltage of _ 15 v. The resistance is incorporated in order to convert the current into voltege, while the applied voltage is used for ions attraction.

The relationship between mean ion current and mean temperature is shown in Fig. (A2.2) in a genaral form of I/I_{max} and $\Delta T/\Delta T_{max}$, where ΔT is taken to be the difference between the sensed and ambient temperature. Although the data are scattering, a roughly linear relation can be found.

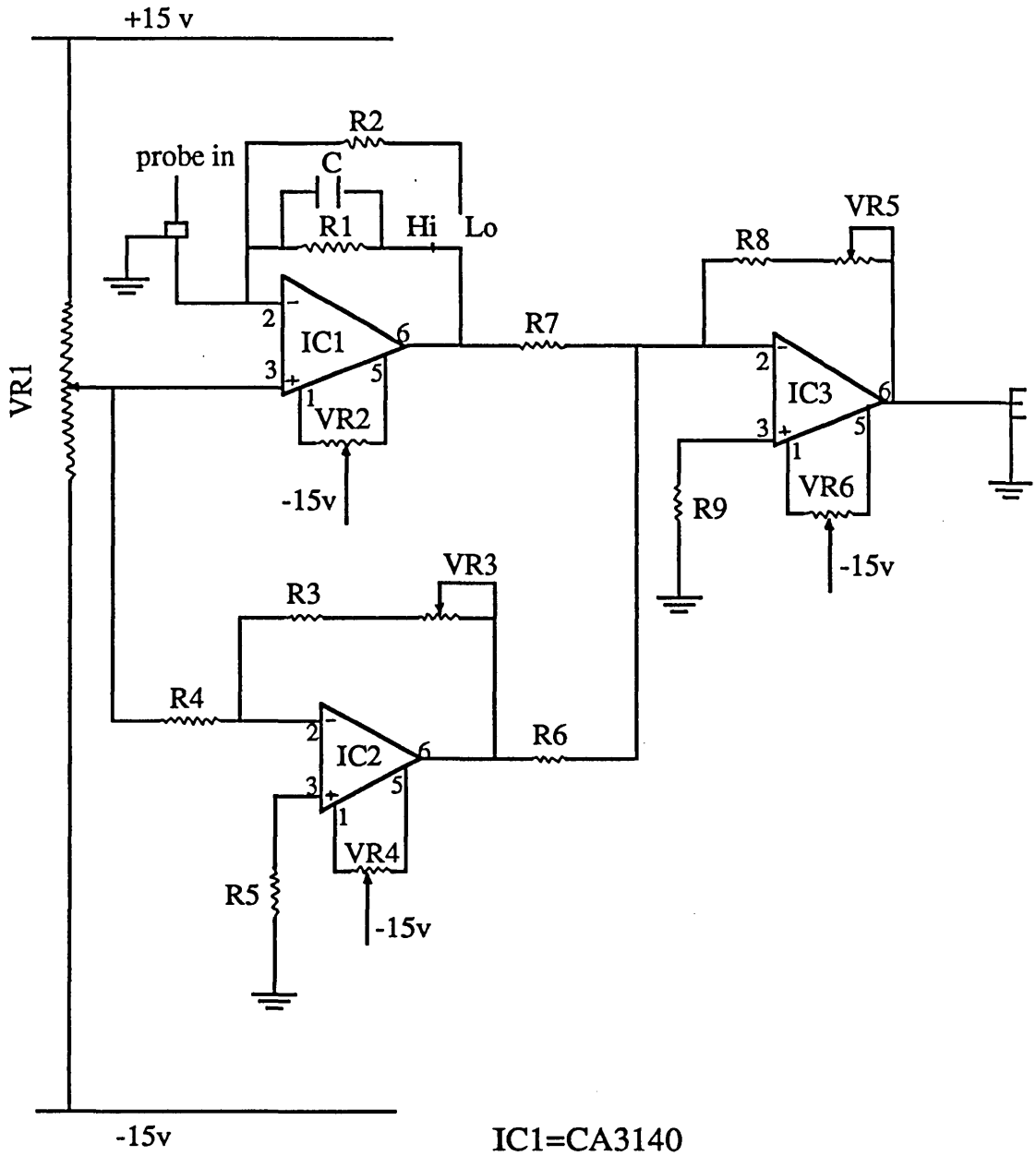

IC1=CA3140
IC2=IC4=741
C=8.2 PF
R1=1 MΩ
R2=100 KΩ
R3=R4=R6=R7=10 KΩ
R5=R8=R9=4.7 KΩ
VR1=20 K
VR2=VR3=VR4=VR5=VR6=10 K

Fig. (A2.1) Ionization circuit diagram.

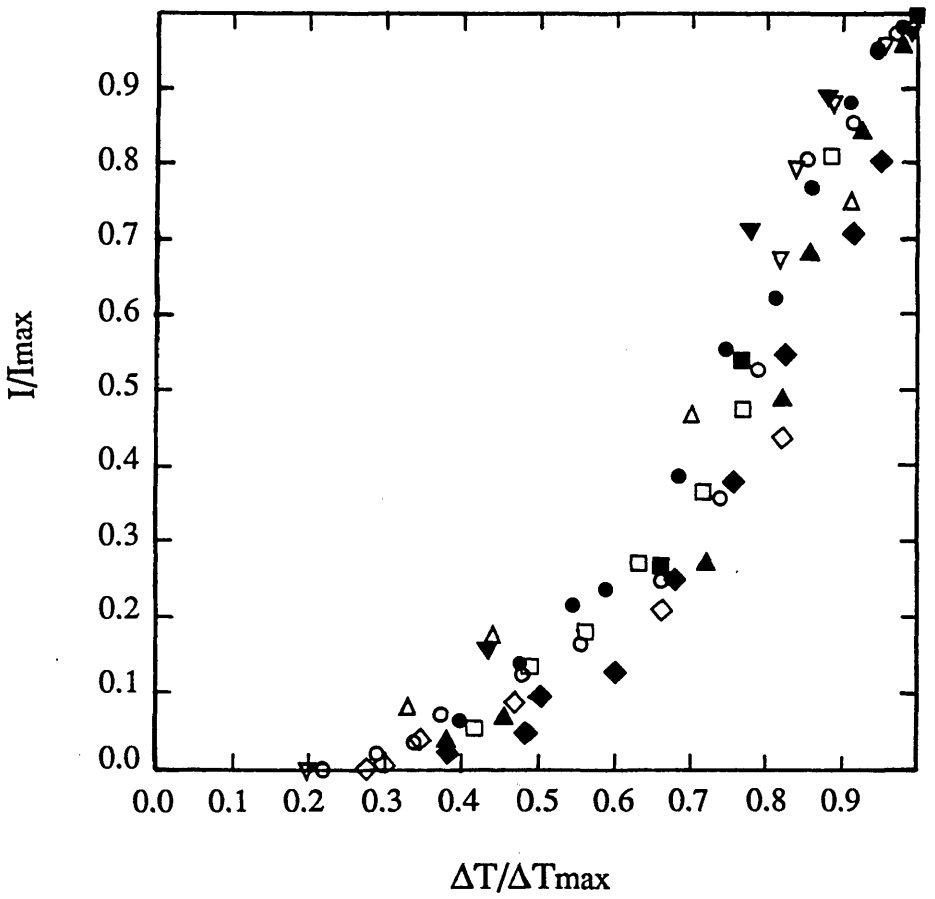

Fig. (A2.2) Relationship between I/Imax and ΔT/ΔTmax.